AFWAL-TR-80-2117

SMALL LAMINATED AXIAL TURBINE DESIGN AND TEST PROGRAM

R. W. Vershure, Jr. and L. J. Meyer

AiResearch Manufacturing Company of Arizona
A Division of the Garrett Corporation
P. O. Box 5217
Phoenix, Arizona 85010

DECEMBER 1980

TECHNICAL REPORT AFWAL-TR-80-2117

Final Report for Period 15 September 1976 - 29 February 1980

Approved for Public Release; Distribution Unlimited

AERO PROPULSION LABORATORY
AIR FORCE WRIGHT AERONAUTICAL LABORATORIES
AIR FORCE SYSTEMS COMMAND
WRIGHT-PATTERSON AIR FORCE BASE, OHIO 45433
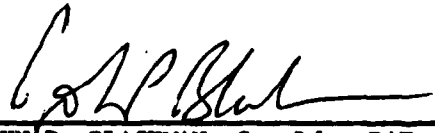
82   04   20   014

NOTICE

When Government drawings, specifications, or other data are used for any purpose other than in connection with a definitely related Government procurement operation, the United States Government thereby incurs no responsibility nor any obligation whatsoever; and the fact that the government may have formulated, furnished, or in any way supplied the said drawings, specifications, or other data, is not to be regarded by implication or otherwise as in any manner licensing the holder or any other person or corporation, or conveying any rights or permission to manufacture, use, or sell any patented invention that may in any way be related thereto.

This report has been reviewed by the Office of Public Affairs (ASD/PA) and is releasable to the National Technical Information Service (NTIS). At NTIS, it will be available to the general public including foreign nations.

This technical report has been reviewed and is approved for publication.

DONALD W. ZABIEREK
Project Engineer, Components Branch
Turbine Engine Division
For the Commander

JOHN P. BLACKMAN, Sqn Ldr, RAF
Acting Chief, Components Branch
Turbine Engine Division

JAMES M. SHIPMAN, Major, USAF
Acting Director
Turbine Engine Division

AIR FORCE/56780/6 April 1982 — 70

REPORT DOCUMENTATION PAGE		READ INSTRUCTIONS BEFORE COMPLETING FORM
1. REPORT NUMBER AFWAL-TR-80-2117	2. GOVT ACCESSION NO. AD-A113 600	3. RECIPIENT'S CATALOG NUMBER
4. TITLE (and Subtitle) SMALL LAMINATED AXIAL TURBINE DESIGN AND TEST PROGRAM		5. TYPE OF REPORT & PERIOD COVERED FINAL 15 SEPT '76-29 FEB '80
		6. PERFORMING ORG. REPORT NUMBER 21-3413-A
7. AUTHOR(s) R.W. Vershure, Jr. and L. J. Meyer		8. CONTRACT OR GRANT NUMBER(s) F33615-76-C-2176
9. PERFORMING ORGANIZATION NAME AND ADDRESS AiResearch Mfg. Co. of Arizona P.O. Box 5217 Phoenix, Arizona 85010		10. PROGRAM ELEMENT, PROJECT, TASK AREA & WORK UNIT NUMBERS 3066-06-23
11. CONTROLLING OFFICE NAME AND ADDRESS Aero Propulsion Laboratory(AFWAL/POTC) Air Force Wright Aeronautical Labs. Wright-Patterson AFB, Ohio 45433		12. REPORT DATE December, 1980
		13. NUMBER OF PAGES 126
14. MONITORING AGENCY NAME & ADDRESS(if different from Controlling Office)		15. SECURITY CLASS. (of this report) Unclassified
		15a. DECLASSIFICATION/DOWNGRADING SCHEDULE

16. DISTRIBUTION STATEMENT (of this Report)

Approved for public release; distribution unlimited

17. DISTRIBUTION STATEMENT (of the abstract entered in Block 20, if different from Report)

18. SUPPLEMENTARY NOTES

19. KEY WORDS (Continue on reverse side if necessary and identify by block number)

Laminated-Turbine
Axial-Turbine
Rig-Test Program

20. ABSTRACT (Continue on reverse side if necessary and identify by block number)

In September, 1976, AiResearch Manufacturing Company of Arizona initiated a program for the Aero Propulsion Laboratory to hot-rig test TFE731-3 Axial Laminated Turbine Rotors and verify their heat-transfer performance and mechanical integrity. The testing was to be conducted in the AiResearch High Temperature Turbine Test —> and

(CONT'D)

DD FORM 1473 EDITION OF 1 NOV 65 IS OBSOLETE

Facility, and three major tests were planned - a heat-transfer performance test, an accelerated stress-rupture test, and a thermal cyclic test. This final report describes the progress to date on the Hot-Rig Program, including the redirection in accordance with contract modification, P00003. This redirection concluded the hot-rig activities. The redirected test program tested one of the laminated turbine wheels directly in the Model 1131-1 Advanced Gas Generator. Also, a small laminated axial turbine rotor suitable for cruise-missile application was designed during this program.

Accession For

NTIS CRA&I	☑
DTIC TAB	☐
Unannounced	☐
Justification	

By
Distribution/
Availability Codes

Dist	Avail and/or Special
A	

DTIC
COPY
INSPECTED
2

PREFACE

TABLE OF CONTENTS

LIST OF ILLUSTRATIONS

LIST OF ILLUSTRATIONS (CONTD)

LIST OF ILLUSTRATIONS (CONTD)

LIST OF ILLUSTRATIONS. (CONTD)

LIST OF ILLUSTRATIONS (CONTD)

LIST OF TABLES

SUMMARY

In September 1976, AiResearch Manufacturing Company of Arizona initiated a program for the United States Air Force Aero Propulsion Laboratory to demonstration test the TFE731 cooled axial laminated turbine rotor and to design a small axial turbine rotor suitable for cruise-missile-engine application. In February 1978, this program was redirected to test the laminated wheel in an advanced gas generator, the Model 1131-1, rather than the hot-rig facility as originally planned. The engine demonstration test was successfully completed in October 1978 with the following test results:

o   Twenty cycles were successfully completed with a total operating time of 20 hours and 45 minutes, including 2 hours at a maximum turbine inlet temperature of 2030°F.

o   Pyrometer temperature measurements accurately recorded the blade temperature and verified the repeatability of the laminated cooling scheme by indicating ±1.5-percent blade-to-blade temperature variation.

o   A high blade cooling effectiveness was verified – the measured effectiveness was 0.52 versus a predicted value of 0.53.

o   Post-test inspection of the laminated turbine indicated the turbine wheel was in excellent condition after the engine test.

Following the engine demonstration test a small, cooled, axial, laminated turbine was designed for cruise-missile application based on the test and process fabrication experience. This design utilizes the Low Aspect Ratio Turbine (LART) aerodynamic

design scaled to a 6.65-inch diameter with 46 cooled blades to match a cruise-missile engine configuration. The cooling design includes a side-entry configuration to an air cavity in the disk rim which supplies the blades with cooling air for a one-pass, two-cavity cooling scheme using pin fins for heat-transfer enhancement. A total of 4.90-percent core airflow is utilized which results in a bulk average metal temperature of 1500°F and a cooling effectiveness of 0.50. The creep life at a maximum inlet temperature of 2300°F was calculated to be 12 hours, which is equivalent to 142 mission hours based on a typical cruise-missile cycle.

SECTION I - ENGINE DEMONSTRATION TESTING

INTRODUCTION

This document is submitted by the AiResearch Manufacturing Company of Arizona, a division of The Garrett Corporation, and presents the Final Technical Report on "The Small Laminated Axial Turbine Design and Test Program", conducted for the USAF Aero Propulsion Laboratory, Wright-Patterson Air Force Base, Ohio. The Program was authorized under Air Force Systems Command Contract No. F33615-76-C-2176, Project No. 3066. This final report summarizes the engine demonstration and component testing of an 11-inch-diameter, cooled, laminated, axial turbine rotor and the design of a small (6.65-inch-diameter) cooled axial laminated turbine rotor suitable for a cruise-missile engine application.

A redirection in accordance with Contract Modification P00003 occurred on February 2, 1978, and changed the emphasis and overall objectives of the program from a hot-rig test program to the present engine demonstration test and cruise-missile engine rotor design.

Over the past five years, AiResearch has been developing the laminate manufacturing process, under Air Force sponsorship, to fabricate a low-cost, high-temperature, cooled, axial turbine wheel suitable for operation at 2600°F. References 1 and 2, describe the early design and manufacturing process development efforts that led to the manufacture of a small, integral, cooled turbine using photoetched laminates bonded together to form a complete wheel.

1. Vershure, R. W., Jr., H. R. Fisk and J. A. Vonada, "Demonstration of a Cooled Laminated Integral Axial Turbine," AIAA Paper 77-949. Reprinted in Journal of Aircraft, Vol. 15, No. 11, pp 735-742, 1978.

2. Furst, D.G., R.W. Vershure, J.A. Pyne, and J.J. Clark, "Integral, Low-Cost, High-Temperature Turbine Feasibility Demonstrator (Small Laminated Axial Turbine Program)" AFAPL-TR-77-2, February 1977.

The original objective of this program prior to the contract modification was to verify the heat-transfer performance and mechanical integrity of the laminated turbine wheel in a hot dynamic environment, and correlate the results with design predictions.

The testing planned was to be conducted in the AiResearch company-sponsored high-temperature turbine test facility, which was specifically developed to permit evaluation of cooled components for gas turbine engines.

Four TFE731-3 Laminated Turbine Wheels were to be bailed to the test program from the AFML Laminated Wheel Fabrication Development Program (Contract F33615-75-C-5211). Two Waspaloy wheels were to be used in the airflow and component testing, and in the heat-transfer performance test in the high-temperature rotating rig. Two Astroloy wheels were to be used in the life tests, which were the accelerated stress rupture, and the thermal cycling tests in the hot rig.

In summary, the three major tests planned were:

1) <u>A heat-transfer performance test</u> to determine turbine blade and disk metal temperatures of the Waspaloy wheel over a range of turbine inlet temperatures, cooling airflow rates, and airflow temperature conditions.

2) <u>An accelerated stress-rupture test</u> of about 10 hours duration at steady-state conditions, using the Astroloy wheel, and testing to the limit of the rotors predicted two-percent creep life.

3) <u>A thermal cyclic test</u> to be conducted with the second Astroloy wheel. The thermal cycle would have been accomplished by varying the mainstream gas temperature

2

and periodically inspecting the rotor every 10 cycles, up to a total of 50 thermal cycles.

The following paragraphs describe the progress on the Hot-Rig Test Program prior to the modification and including the design analysis, advanced instrumentation, fabrication, and air-flow testing of the laminated rotors. This analysis and component testing was in general directly applicable to the engine demonstration test of the cooled laminated rotor. Following the engine demonstration test a new, small, cooled, axial, laminated, turbine rotor was designed for cruise-missile application based on the cooled laminated turbine test and process fabrication experience. A final program objective was to design and fabricate Photochemical Machining Tooling (PCM) for the small diameter laminated rotor.

DESIGN ANALYSIS

Heat-Transfer Performance Predictions

The expected metal temperature levels for the laminated
Waspaloy turbine blade and disk were predicted based on the test
conditions selected for the hot-rig and the test data obtained
from the airflow bench testing of the turbine blades. In 1974, a
company-sponsored, high-temperature rotating rig was tested with
the TFE731-3 high-pressure turbine rotor. The results from this
test became the basis for the planned hot-rig test with the
TFE731 laminated high-pressure turbine rotor (P/N 3551198-1).

TFE731-3 Test Data Comparison -- The company-sponsored high-
temperature rotating rig at AiResearch was utilized to test the
first-stage turbine blades of the TFE731-3. During these tests,
the rig was operated to an inlet temperature of 2057°F, an inlet
pressure of 119.5 psia, a main flow of 18.4 lb/sec, a speed of
30,223 rpm, and a power level of 1378 hp. A total of 14 test
points was obtained. For each point, all pertinent parameters
were measured, including a radiation pyrometer metal temperature
scan of all the blades on the rotor. A schematic of the test
section is shown in Figure 1, including the instrumentation and
pyrometer installation and with a typical set of data from the
TFE731-3 rig test. These results were considered in establishing
heat-transfer performance predictions for the laminated turbine
blade.

Heat-Transfer Verification Test - The overall objective of this
program was to verify the heat-transfer performance of the lami-
nated turbine wheel in a hot, dynamic environment; and to corre-
late the results with design predictions. To accomplish this
objective, the original intent was to test the wheel in the
AiResearch high-temperature rotating rig, with sufficient
instrumentation to establish a correlation between measured ver-
sus predicted temperatures. In the redirected program, the wheel

4

POINT 1-11-9
TIME: 15:37:41

$W_1 + W_2 + W_3 = 3.39\%$

HP = 684 HP

| W_2 1008°F 52.2 PSIA | 1.73% 638°F 56.1 PSIA | W_1 989°F 50.9 PSIA |

1413°F

$P_s = 50.1$ PSIA

7.28 LB/SEC

1848°F

W_3 1071°F 50.0 PSIA

0.039 IN.
0.027 IN.
0.038 IN.
0.030 IN.

$P_s = 25.4$ PSIA

1615°F MAX.

$P_R = 1.98$

1475°F AVG.

$P_s = 25.3$ PSIA

$T_{CB} = 772°F$

0.43%

| 0.50% 643°F 32.5 PSIA | 0.22% 565°F 39.1 PSIA | 2.62% 780°F 72.2 PSIA | 0.29% 600°F 40.2 PSIA | 0.23% 548°F 32.7 PSIA |

36.1 PSIA | 35.6 PSIA | 37.8 PSIA

7.68°F

2.62%

N = 28,998 RPM

0.72%

VANE

1218°F 1143°F
1284°F 1284°F
1351°F
1241°F 1245°F 1298°F

BLADE

1313°F 1237°F
1160°F 1220°F
1272°F
1512°F 144°F
1347°F 1287°F
1383°F

$T_{TR} = 1500°F$ AT 30% SPAN, 1549°F AT 50% SPAN, 1504°F AT 70% SPAN

$T_{AVG} = 1351°F$

1 10 20 30 40 50 60 62 1
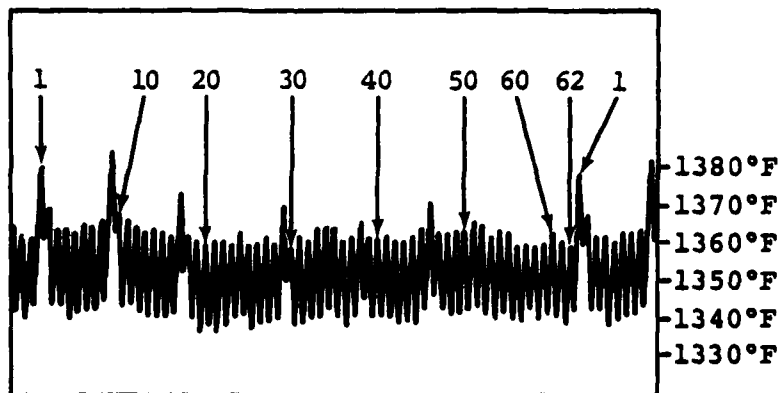
1380°F
1370°F
1360°F
1350°F
1340°F
1330°F
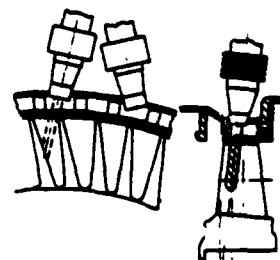
PYROMETER TEMPERATURE DISTRIBUTION, °F, FOR 62 BLADES MEASURED ON THE BLADE PRESSURE SIDE

Figure 1. Typical Test Results from TFE731-3 Hot-Rig Testing.

5

was tested in a realistic engine environment in the Model 1131-1 Advanced Gas Generator. The objectives were to verify the heat-transfer performance as related to cooling effectiveness by measuring the blade trailing-edge metal temperature with an optical pyrometer, and to demonstrate the mechanical integrity and durability of the wheel in an engine environment.

A test matrix was established for the rig testing with a total of 18 test points defined to permit a significant variation in basic parameters and to provide a data base for confirmation of prediction techniques. The test matrix is shown in Table 1. Note that the matrix includes three turbine inlet temperatures (1800, 1900, and 2000°F), three cooling flow rates (1.25. 2.0, and 3.0 percent of gas flow), and two coolant temperatures (800 and 1000°F). All other parameters remained constant.

Blade Thermal Analysis - The laminated turbine blade was analyzed for a reduced turbine inlet temperature of 2000°F. All other parameters remain unchanged from the TFE731-3 design. A reevaluation was made, based on the changed external boundary conditions, with a turbine inlet temperature of 2000°F and the internal cooling flow conditions. Figures 2 and 3 are cross sections of the airfoil showing the predicted flow splits. The critical blade section was previously determined to be at a radius of 4.6095 inches. A two-dimensional thermal analysis was made at the critical section to determine metal temperatures under combined effects of convection and conduction. Figure 4 shows the element and nodal layout of the critical section grid model. The outside heat-transfer coefficients and adiabatic wall temperatures are shown in Figures 5 and 6, respectively. The resulting steady-state metal temperatures are shown in Figure 7. These temperatures were then used in the stress and life analyses described below.

TABLE 1. TEST MATRIX FOR THE HEAT-TRANSFER VERIFICATION TEST IN THE HIGH-TEMPERATURE TURBINE RIG.

T_{gas} (°F)	Cooling Flow (% W_{gas})	Cooling Air Temp (°F)
1800	8.0	800
	6.0	
	4.0	
	8.0	1000
	6.0	
	4.0	
1900	8.0	800
	6.0	
	4.0	
	8.0	1000
	6.0	
	4.0	
2000	8.0	800
	6.0	
	4.0	
	8.0	1000
	6.0	
	4.0	

All other parameters remained constant.

7

RADIUS = 4.6095

RADIAL

RADIAL

Figure 2.   Laminated Blade Chordwise Flow Patterns.

8

NOTE:
0.XXX - FRACTIONS
OF TOTAL PASSAGE
INLET FLOW

3.38% OF W$_3$ 2.5% OF W$_3$
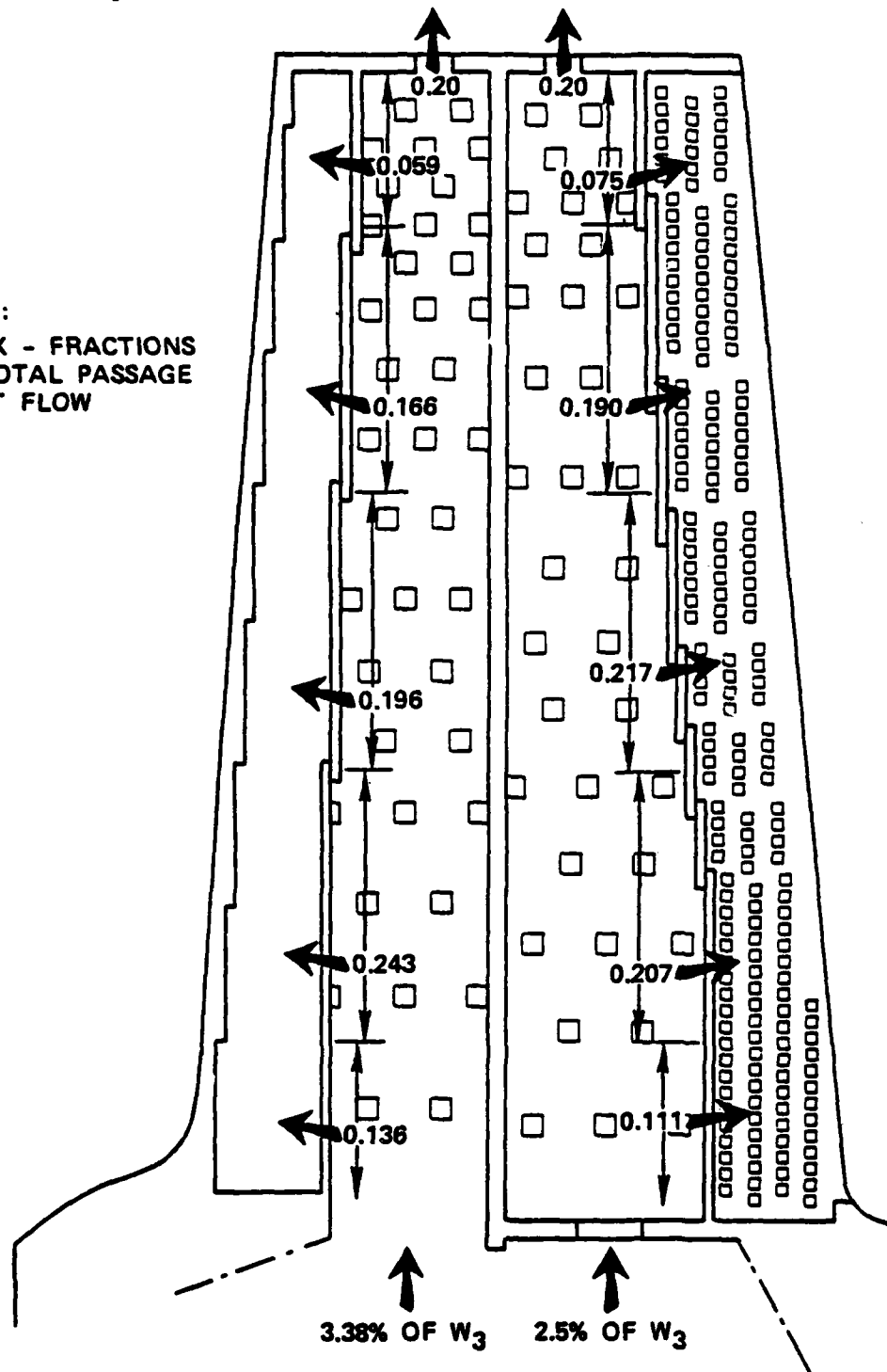
TOTAL COOLANT FLOW = 5.88 PERCENT OF COMPRESSOR FLOW (W$_3$)

Figure 3.   Laminated Blade Cooling-Flow Split and
Radial Distribution.

9

ELEMENTS

NODES

RADIUS = 4.6095 INCHES
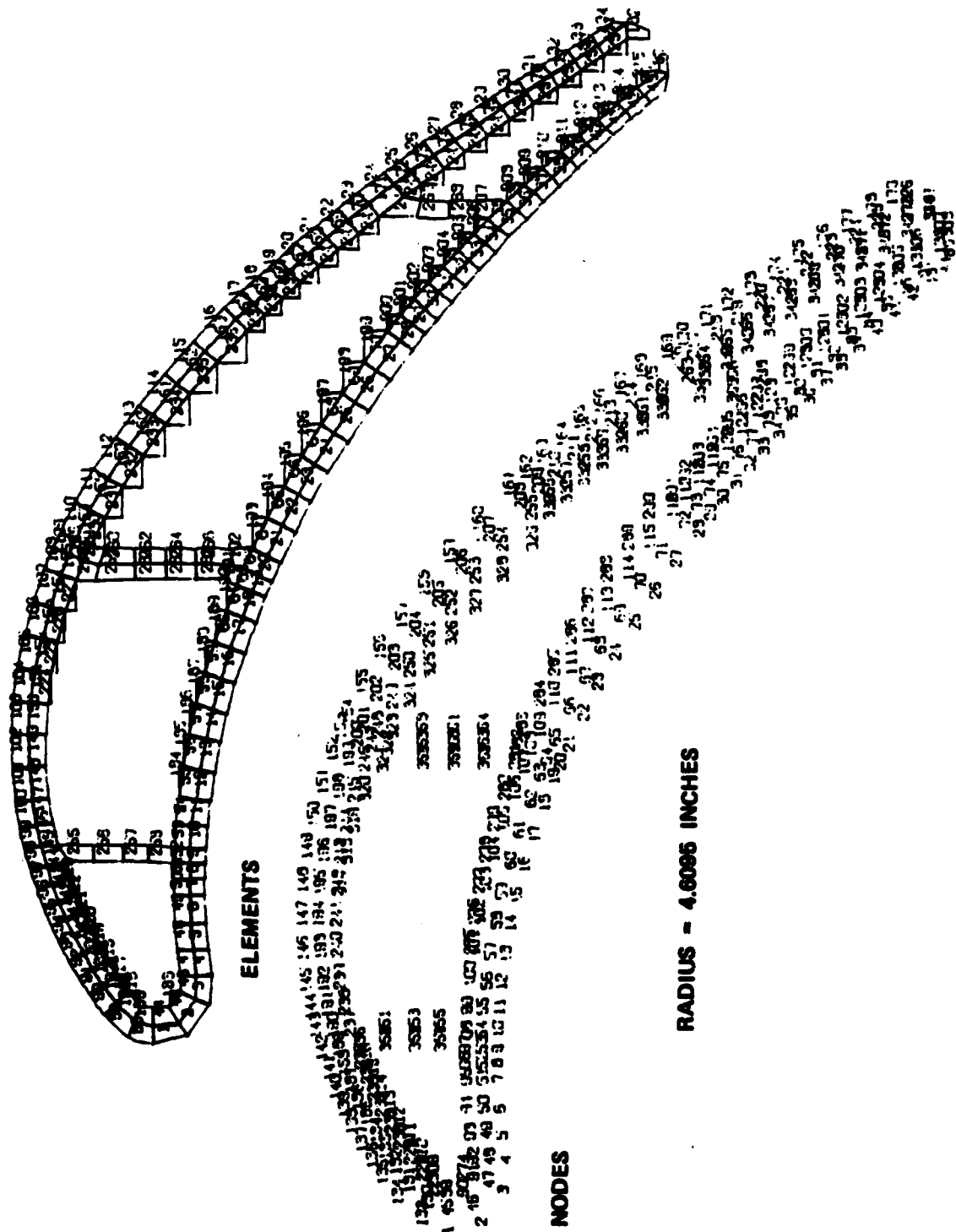
Figure 4. Laminated Turbine Blade Critical Section Grid Model.

10
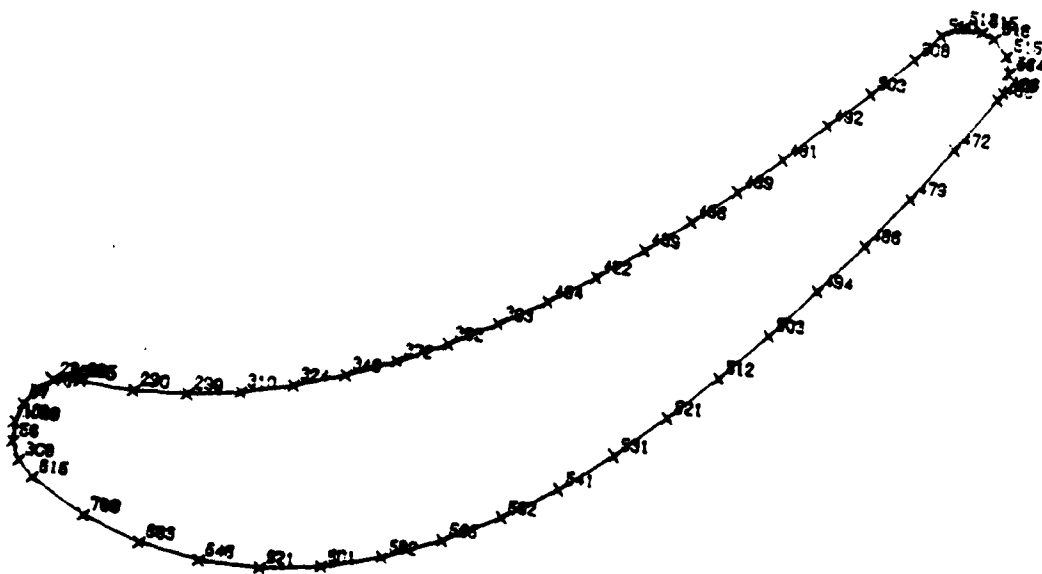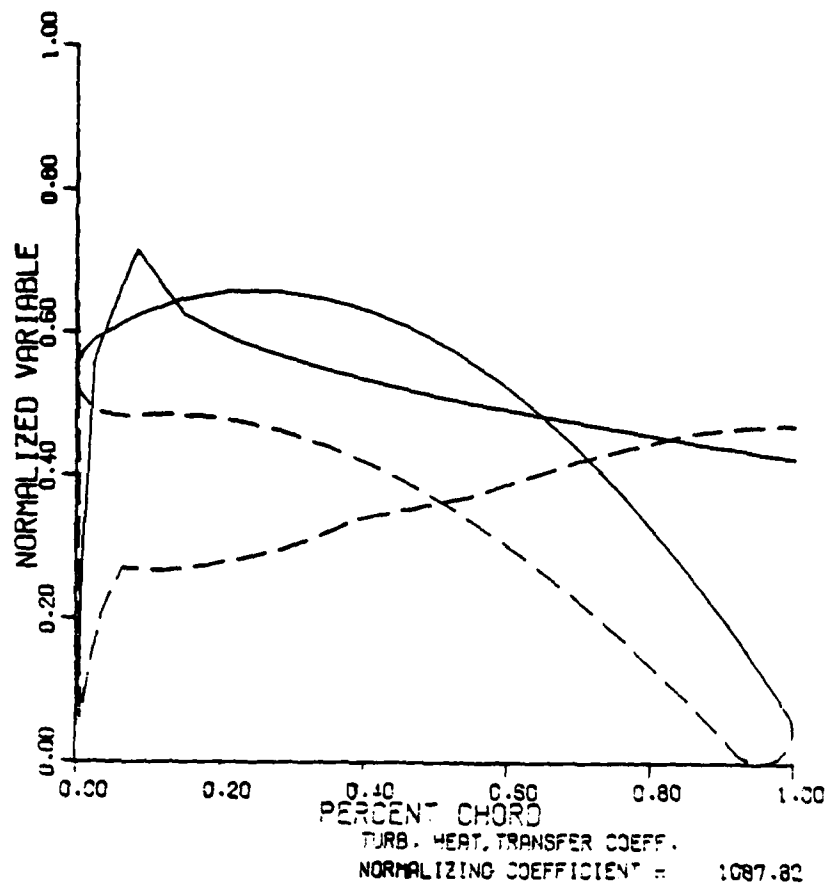
Figure 5. Laminated Turbine Blade Outside Heat
Transfer Coefficients at 2000°F T.I.T.

11
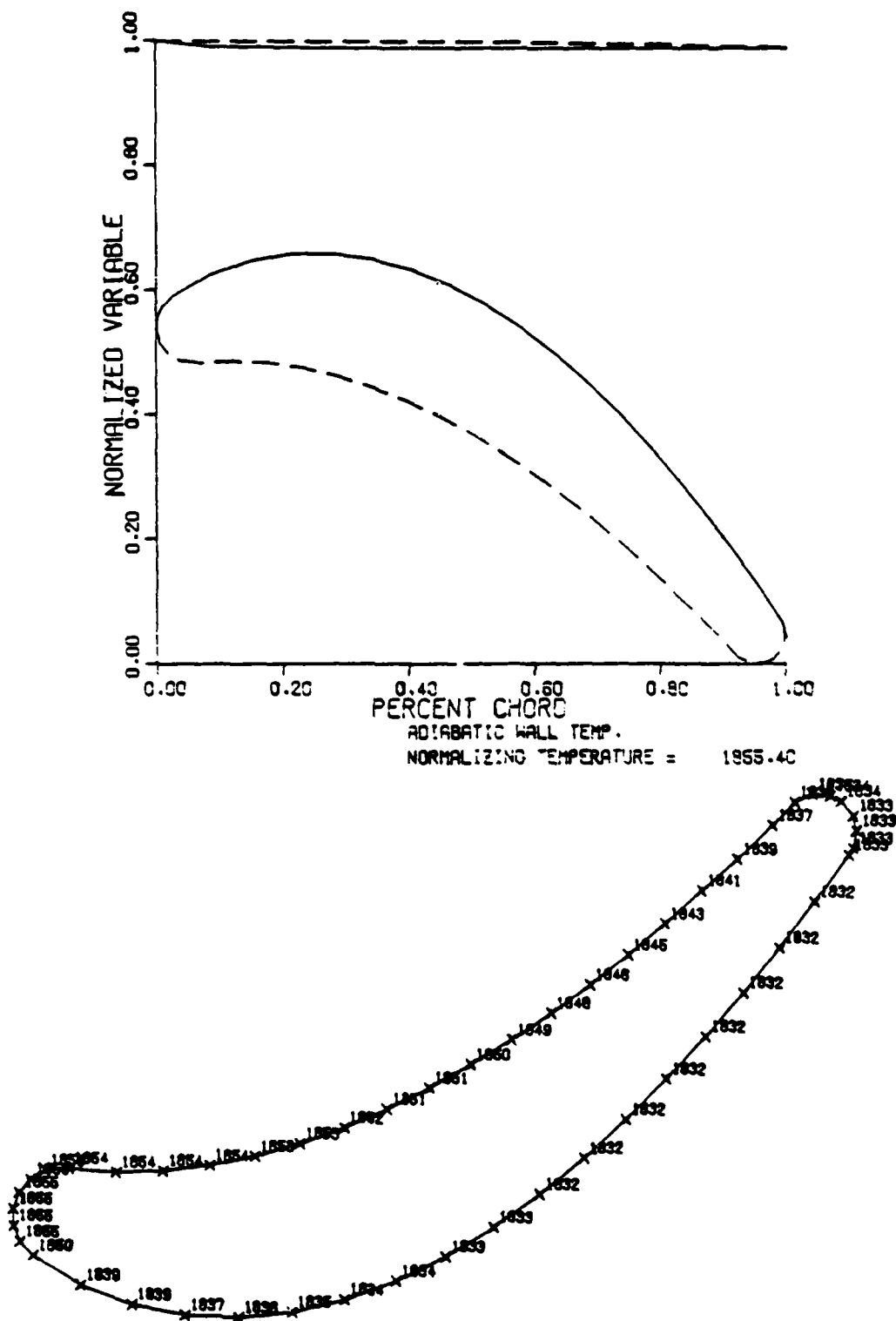
Figure 6. Laminated Turbine Blade Adiabatic
Wall Temperatures at 2000°F T.I.T.

12
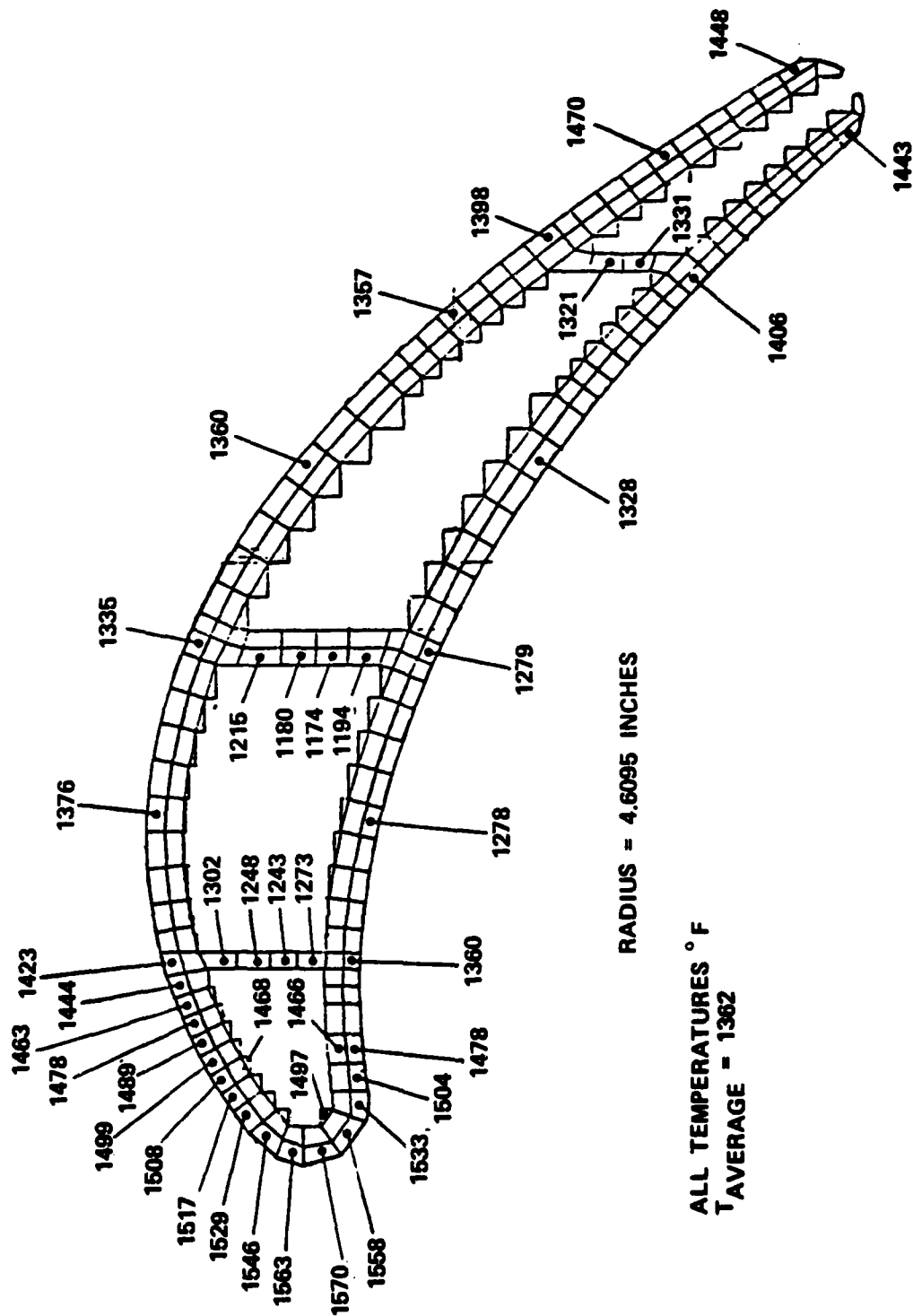
Figure 7. Laminated Turbine Blade Critical Section Steady-State Temperature Distribution (TIT Average = 2000°F, and $W_{coolant}$ = 5.9 Percent).

RADIUS = 4.6095 INCHES

ALL TEMPERATURES °F
$T_{AVERAGE}$ = 1362

13

Stress and Life Analysis -

1) <u>Laminated Waspaloy-A Creep Properties</u> - A two-percent creep design curve for the laminated turbine of Waspaloy-A was developed from AiResearch test data and from consideration of the parent material stress-rupture properties. This curve is shown in Figure 8.

2) <u>Blade Stress Analysis</u> - The steady-state stress solution for the critical solution was computed with the completion of the two-dimensional thermal analysis of the blade critical section, and the calculated radial load and moments acting on this section due to gas-bending loads and centrifugal loading. This program combines thermal stresses and mechanically generated stresses to describe a steady-state, two-dimensional, uniaxial stress field. This solution for an average TIT of 2000°F and with a 5.9-percent cooling flow is shown in Figure 9.

In additon to the steady-state stress calculation, a creep analysis of the blade was also performed. The critical section creep behavior occurs over a finite radial length of the blade. The blade stress distribution was recalculated after each increment of creep strain, using the steady-state temperature distribution. Calculated creep strains and stress values were continued until some element in the blade reached the creep-strain limit of two percent.

The two-percent creep life at an average TIT of 2000°F, with a 5.9-percent cooling flow, using calculated metal temperature, was 700 hours. The failure or maximum strain location was along the suction wall of the forward center cavity. The creep distribution at

14
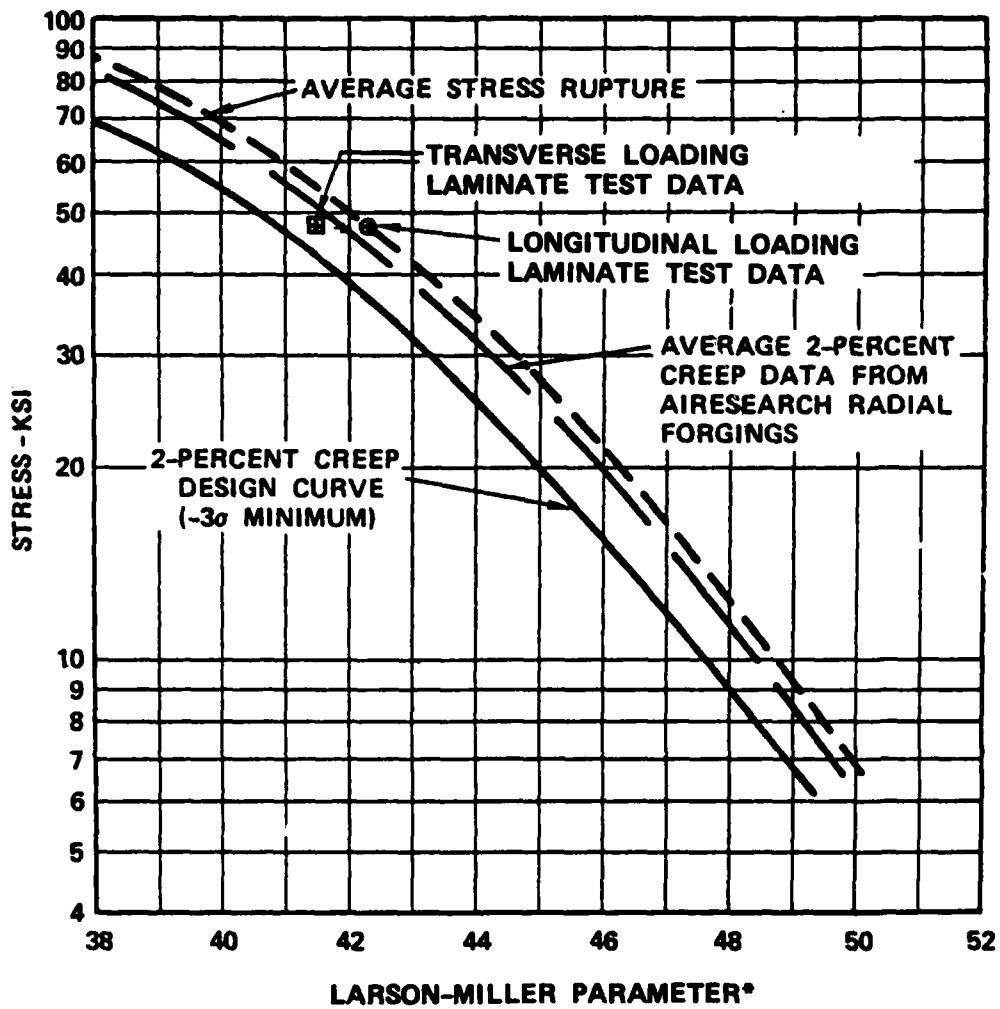
Figure 8.   Laminate Waspaloy-A 2-Percent Creep
Design Curve.

15
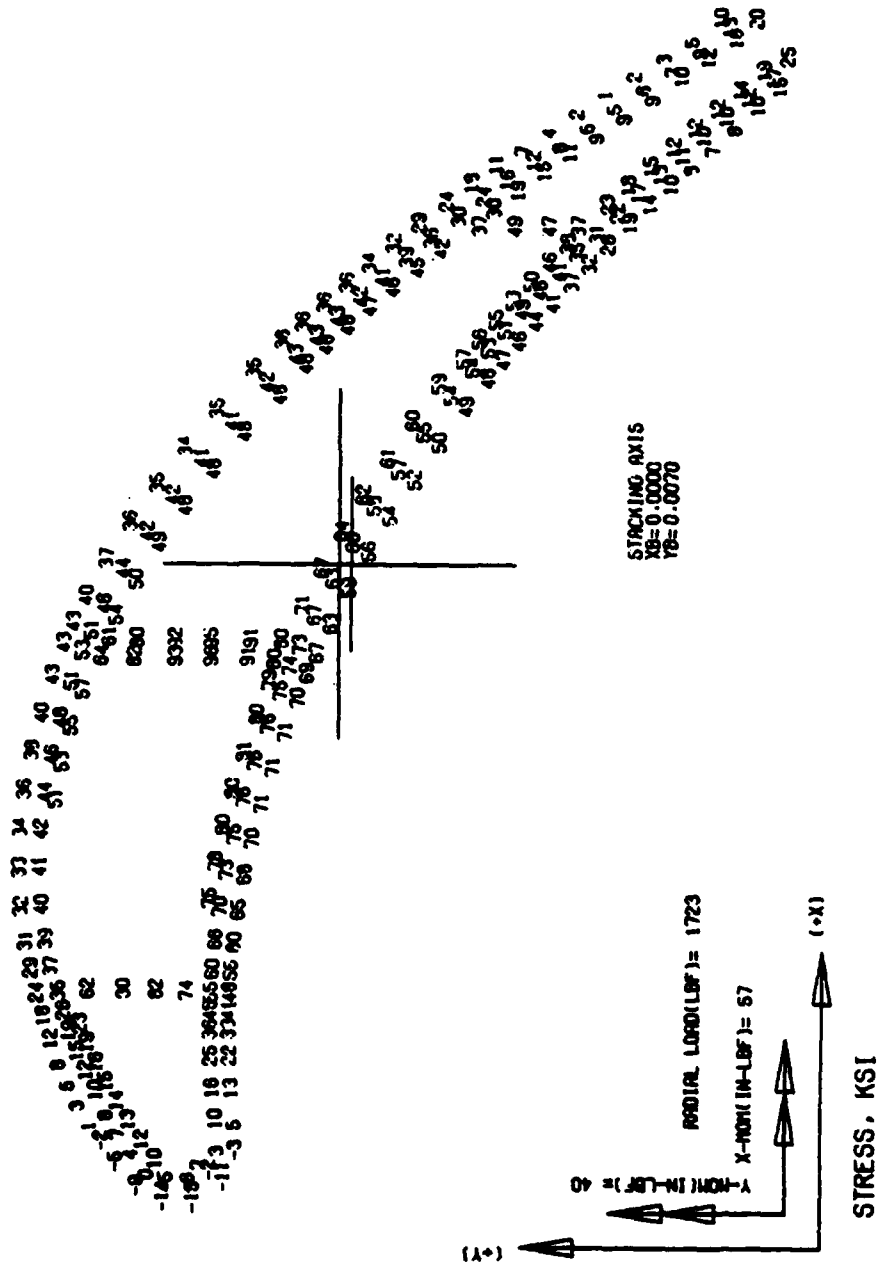
Figure 9. Laminated Turbine Blade Steady-State
Stress Distribution at 2000°F T.I.T.

16

700 hours is shown in Figure 10. The stress distribution at 700 hours is shown in Figure 11. The peak steady-state tensile stress in the center-passage divider fell from 96 ksi to 72 ksi, and the creep strain at this location was 1.6 percent. The leading-edge compressive stress became tensile due to strain relief during the initial creep period, and the creep strain at 700 hours is 1.4 percent. The creep strains for compression and tension were added algebraically to determine a final value. In general, the high tensile stresses along the pressure wall at mid-chord decreased substantially at 700 hours; and on the suction wall, the outer-fiber stresses increased slightly, as shown in Figures 9 and 11.

3) **Disk Stress Analysis** - Previously conducted stress analysis of the fully bladed rotor as reported in AFAPL-TR-77-2 indicated the adequacy and margin for use of this design in room-temperature whirlpit testing. Installation of the rotor in a demonstrator engine and operation at the design speed of 29,692 rpm resulted in increased stresses at the bore and rim, due to thermal gradients in the disk. The anticipated thermal gradients for a 2000°F TIT and normal secondary cooling of the turbine were not severe, and although the resulting increase in stresses reduced the LCF life of the component, its integrity for a short-term demonstration test should not be affected. If long-term cyclic testing in an engine environment is to be considered in the future, a more detailed examination of fatigue life would be required.
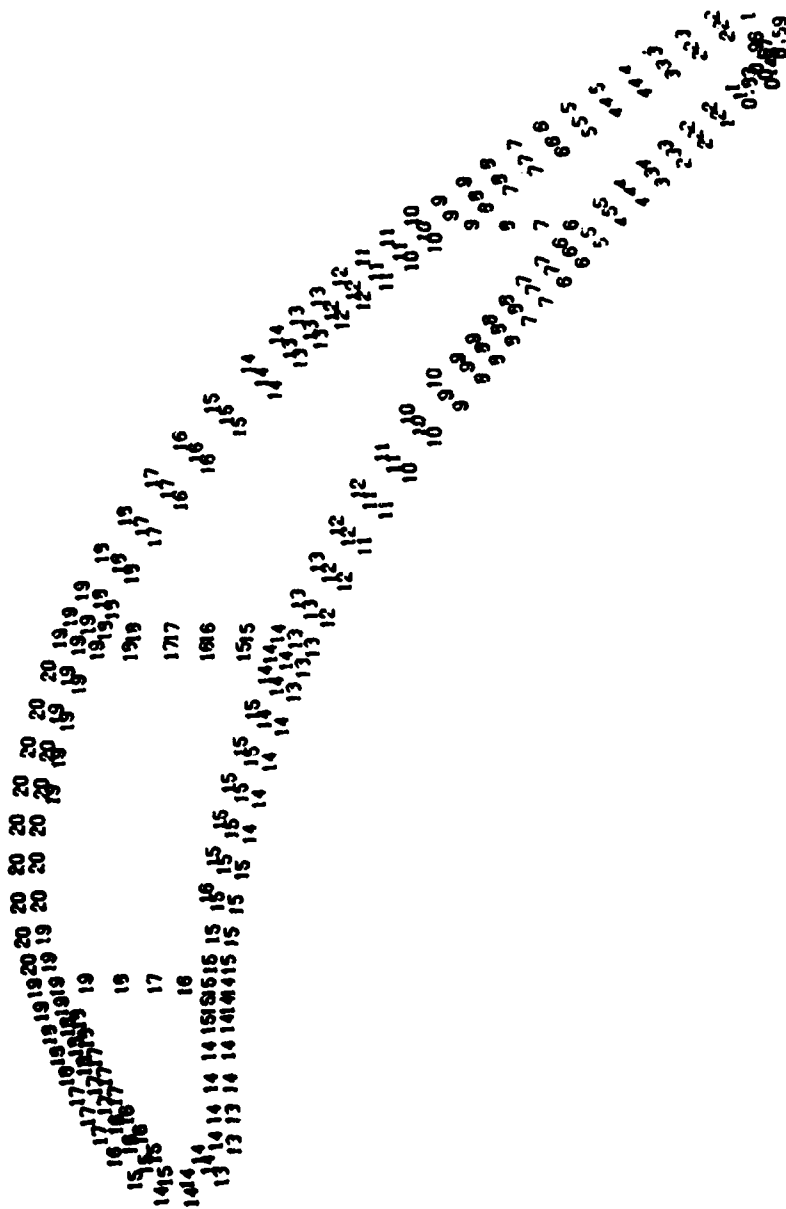
CREEP DISTRIBUTION AFTER TIME = 699.2656
CREEP = INCHES/INCH*.001

Figure 10. Laminated Turbine Blade (T.I.T. = 2000°F).

18
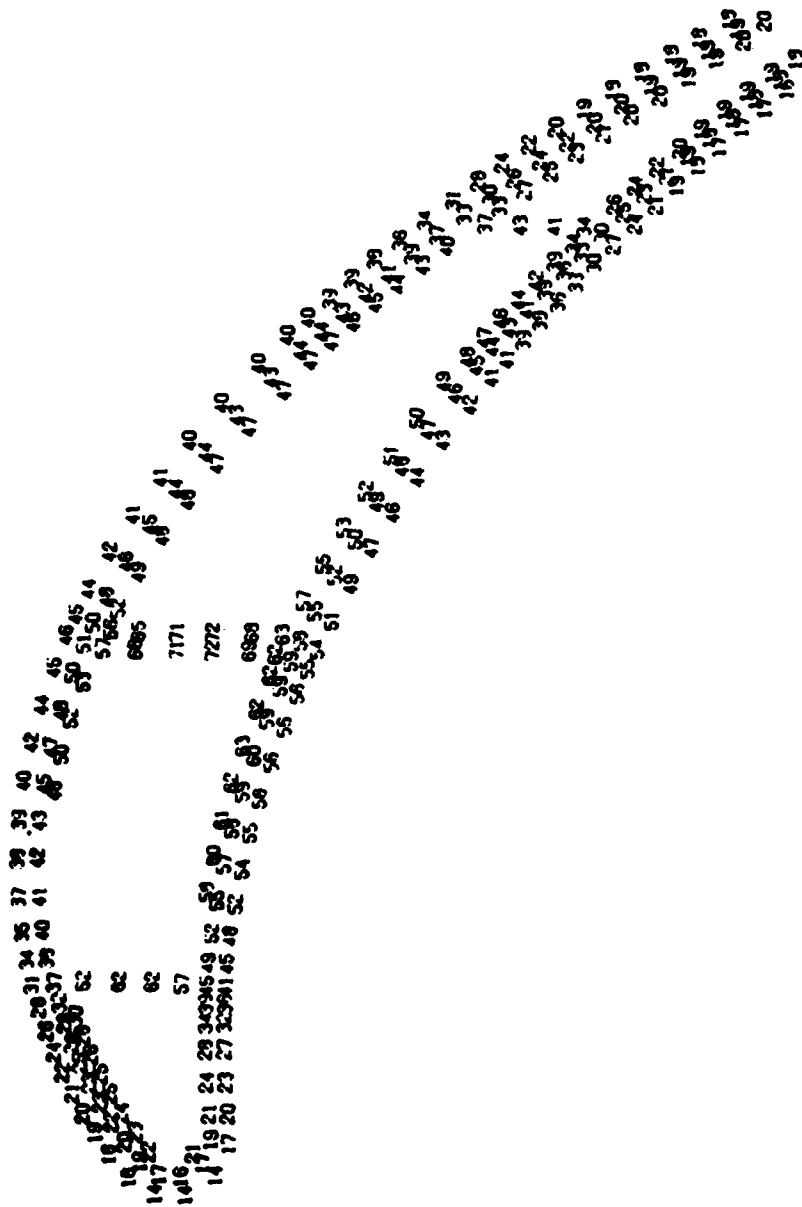
STRESS DISTRIBUTION AFTER CREEP, KSI
MAXIMUM CREEP = 0.020
TIME TO REACH MAX CREEP = 699.2656

Figure 11. Laminated Turbine Blade (T.I.T. = 2000°F)

19

ADVANCED INSTRUMENTATION

The instrumentation of the high-temperature turbine rotating test rig was undertaken to allow measurement of all cooling airflows, pressures, and temperatures, inlet and exhaust hot gas pressures and temperatures, turbine tip clearances, and critical static component metal temperatures.

To measure the laminated turbine blade metal temperatures, two methods were utilized:

1) Thermocouples were placed in grooves in the blade surface and flame sprayed in place to obtain a smooth aerodynamic surface.

2) A radiation pyrometer was installed in the rig to allow measurement of blade-to-blade metal temperature variations, to determine uniformity of cooling.

A review of the laminated turbine blade thermocouple installation was accomplished using the first APL rotor as shown in Figure 12. The following conclusions were reached:

1) The plasma-spray method of installation is limited to the leading-edge and the trailing-edge regions (1/3 chord) of the blade.

2) The center section of the blade cannot be plasma sprayed because the spray angle is too great to obtain an effective bond joint. However, it is believed possible to install calibration thermocouples using furnace brazing techniques. This would provide a reference temperature to compare to the radiation pyrometer measurement.
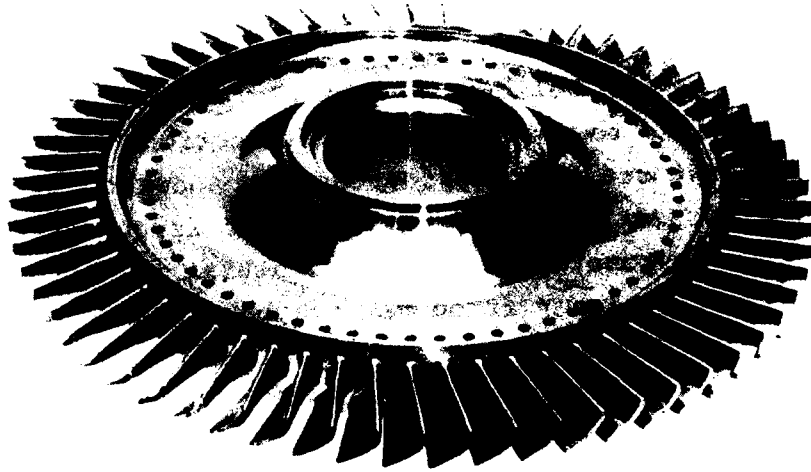
Figure 12. APL Turbine Rotor.

The radiation pyrometer installation was modified to correct for a bellows distortion problem noted on the previous TFE731-3 hot rig testing. The new pyrometer installation is shown in Figure 13. This new approach utilized a double spherical seat for locating and air sealing the probe in the two housings, thereby eliminating the bellows assembly. Two probes of the new design were installed to measure the blade suction- and pressure-side metal temperatures. The pyrometer, as shown in Figure 14, manufactured by Vanzetti Corp., has a higher frequency response than the previous pyrometer used in the initial testing (150 KHz versus 40 KHz). The higher frequency response ensured recording of the highest blade metal temperature during the short time period of viewing each blade. The Vanzetti pyrometer and the associated electronic signal conditioning equipment was tested successfully at AiResearch during the STAGG Gas Generator Test Program.

FABRICATION

The turbine wheels required for the hot-rig testing were bailed from the AFML Laminated Wheel Fabrication Program (Contract F33615-75-C-5211). The rig modifications were completed and were primarily associated with the modification of the radiation pyrometer installation. Also, various expendable instrumentation hardware and test cell air cooling controls were modified for the three major tests. With the redirection, the Waspaloy wheel was used in the AiResearch 1131-1 Advanced Gas Generator Test.

Figure 13. Pyrometer Installation, Optical Temperature Sensor.
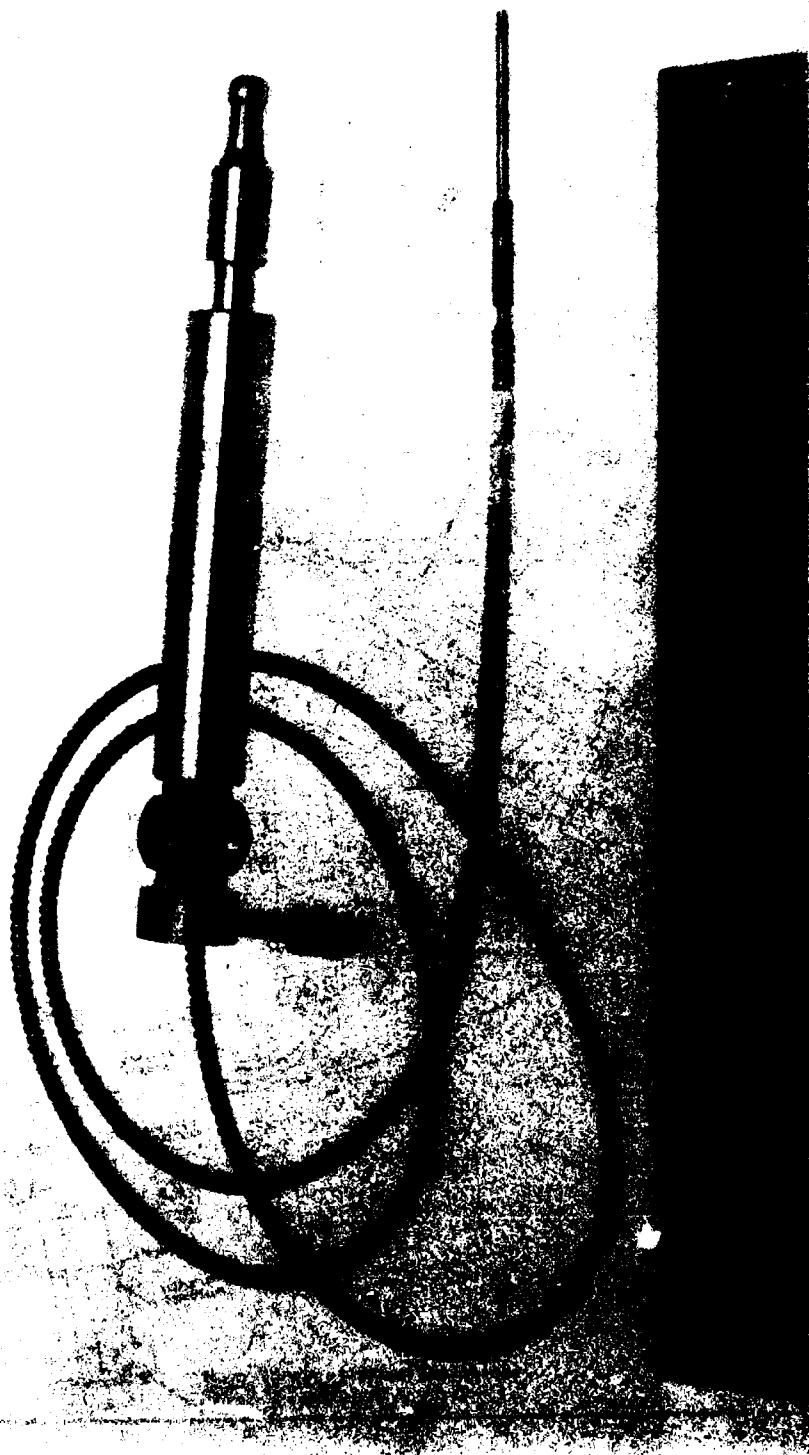
Figure 14. Pyrometer Manufactured by Vanzetti Corporation.

24

AIRFLOW TESTING

An in-process airflow check was performed on the four Waspaloy laminated wheel blanks that were fabricated in the AFML Laminate Wheel Fabrication Program. At this point in the process, the only cooling-flow circuits open were the blade tip discharge holes. Each of these 62 circuits was checked individually by applying 30 in. Hg pressure to their respective inlets on the face of the disk. It should be noted, however, that the flow through these circuits was metered at the tip holes. Therefore, the flow check was significant in only three respects:

1) Verified the cooling passages were open.

2) Measured the flow characteristics and repeatability of the tip discharge holes.

3) Checked for leakage from each cooling circuit or cross flow between cooling circuits.

The results of the airflow testing are shown in Figures 15 and 16. Figure 15 presents the flow distribution of each hole. It also shows the deviation from the mean value for Serial Nos. 001 and 002 wheel blanks of 0.00259 pps. Figure 16 presents the median rank plot on normal probability distribution paper. Note that for the Serial Nos. 001 and 002 wheel blanks, 72 percent of the passages were within 5 percent of the mean, and 98 percent were within 10 percent of the mean. However, Serial No. 003 exhibited a substantial improvement in flow distribution, having 100 percent of the holes within 3 percent of the mean. This improvement was attributed to a modification of the bonding tooling, which provided a more uniform unit load distribution across the wheel blank. This airflow distribution compared favorably to a cast inserted blade configuration, which is allowed ±10 percent variation from the mean.
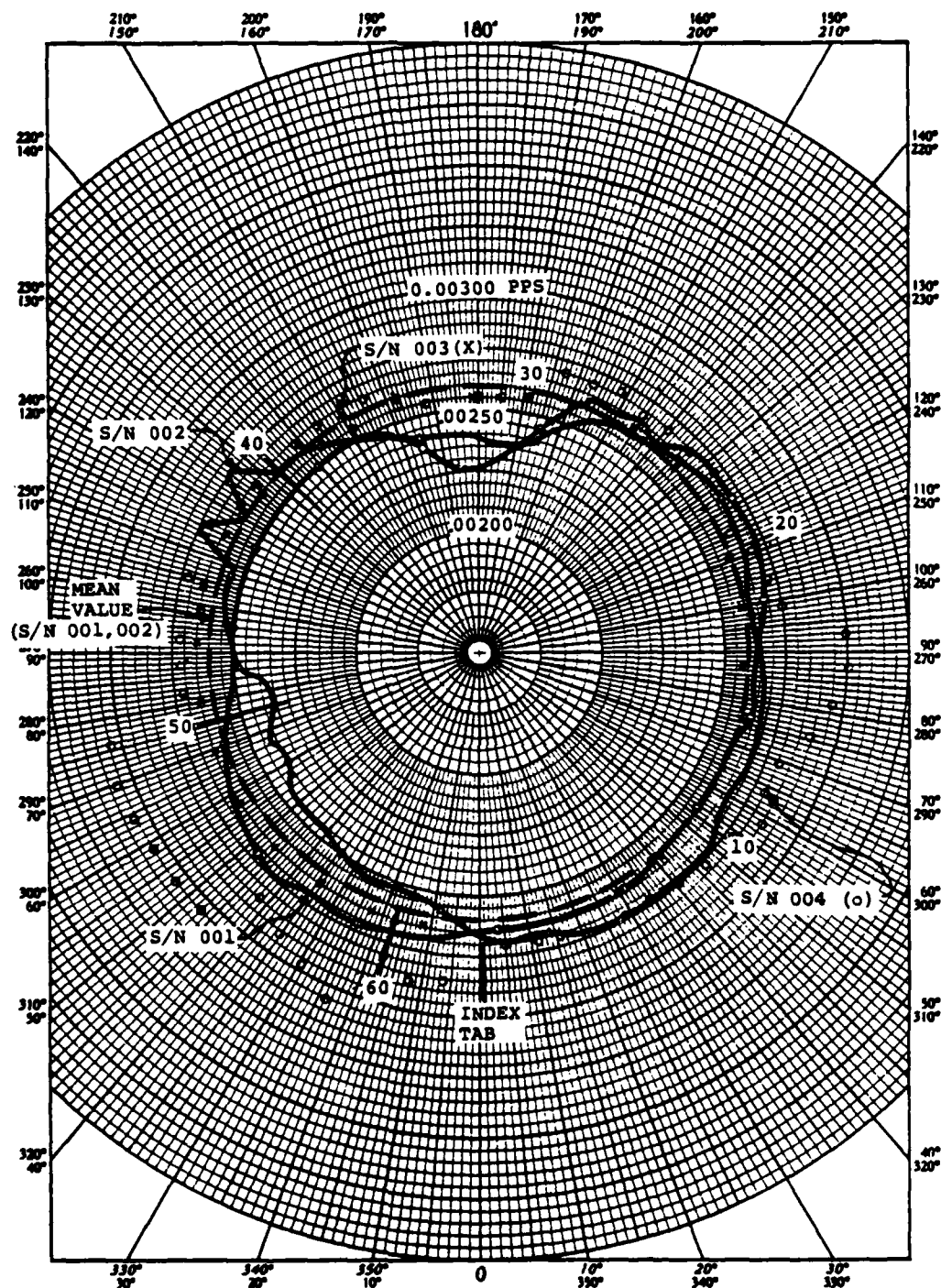
Figure 15. In-Process Flow Check of Laminated Rotor for the Small Axial Laminated Turbine Program (Before Machining).
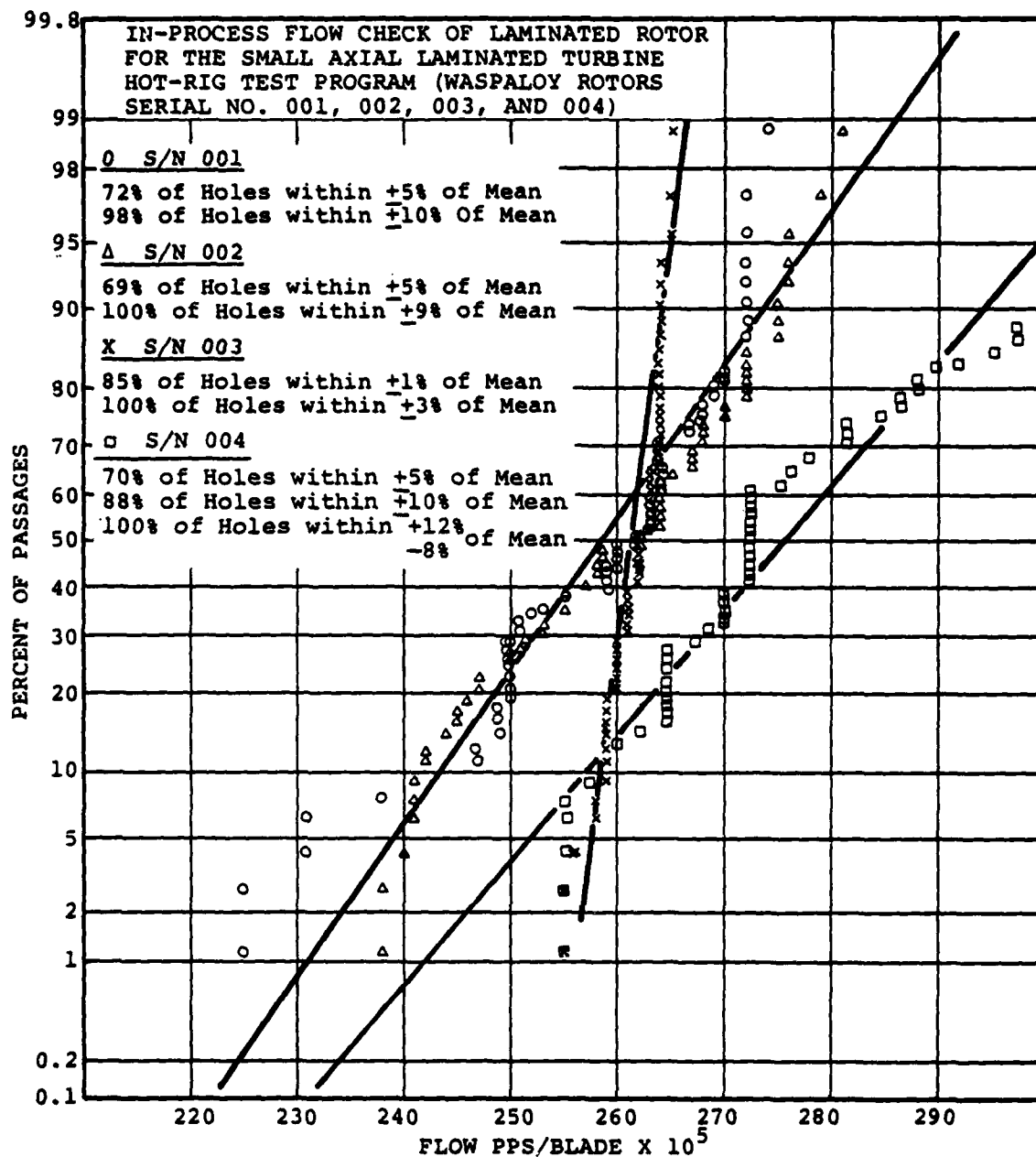
Figure 16. Flow Variation of Cooling Passages, Median Rank Plot.

IN-PROCESS FLOW CHECK OF LAMINATED ROTOR
FOR THE SMALL AXIAL LAMINATED TURBINE
HOT-RIG TEST PROGRAM (WASPALOY ROTORS
SERIAL NO. 001, 002, 003, AND 004)

_0 S/N 001_

72% of Holes within ±5% of Mean
98% of Holes within ±10% Of Mean

_Δ S/N 002_

69% of Holes within ±5% of Mean
100% of Holes within ±9% of Mean

_X S/N 003_

85% of Holes within ±1% of Mean
100% of Holes within ±3% of Mean

_□ S/N 004_

70% of Holes within ±5% of Mean
88% of Holes within ±10% of Mean
100% of Holes within $^{+12\%}_{-8\%}$ of Mean

PERCENT OF PASSAGES

FLOW PPS/BLADE X 10^5

27

The airflow check of Serial No. 004 wheel blank uncovered a secondary leakage problem in this particular part. Since the Serial No. 004 wheel blank was bonded with the same bonding method as Serial No. 003, and the expected airflow variation was not the same, further airflow testing was conducted to isolate the problem. Note in Figure 16 the variation from the mean is +12 percent to -8 percent, and the total flow per blade is about 10 percent higher than previous wheel blanks.

A test was set up with the wheel blank submerged in a clear glass water tank as shown in Figure 17. The cooling passages were sealed with epoxy and black tape, and each blade passage was pressurized with air. The arrow indicates air escaping from a particular laminate (No. +19), which is between each blade and downstream of the trailing-edge of the blade. This accounted for the overall increase in flow per blade. Micrographic examination of a radially oriented slug in this area revealed the separation of Laminate No. +19 was limited to an area at the rim outer diameter and inward about 0.320 inch. This defect was judged acceptable because the separation in the wheel blank was outside the blade section.

The flow characteristics of the internal cooling passages could not be determined until the machining of the blade profile was completed. This machining opened the leading-edge impingement cavity gill discharge holes and the trailing-edge discharge holes. However, this preliminary series of tests did provide an early indication that the geometry of the cooling passages was reasonably fixed by the process, the bond joints were repeatable, and there was no clogging in the passages.
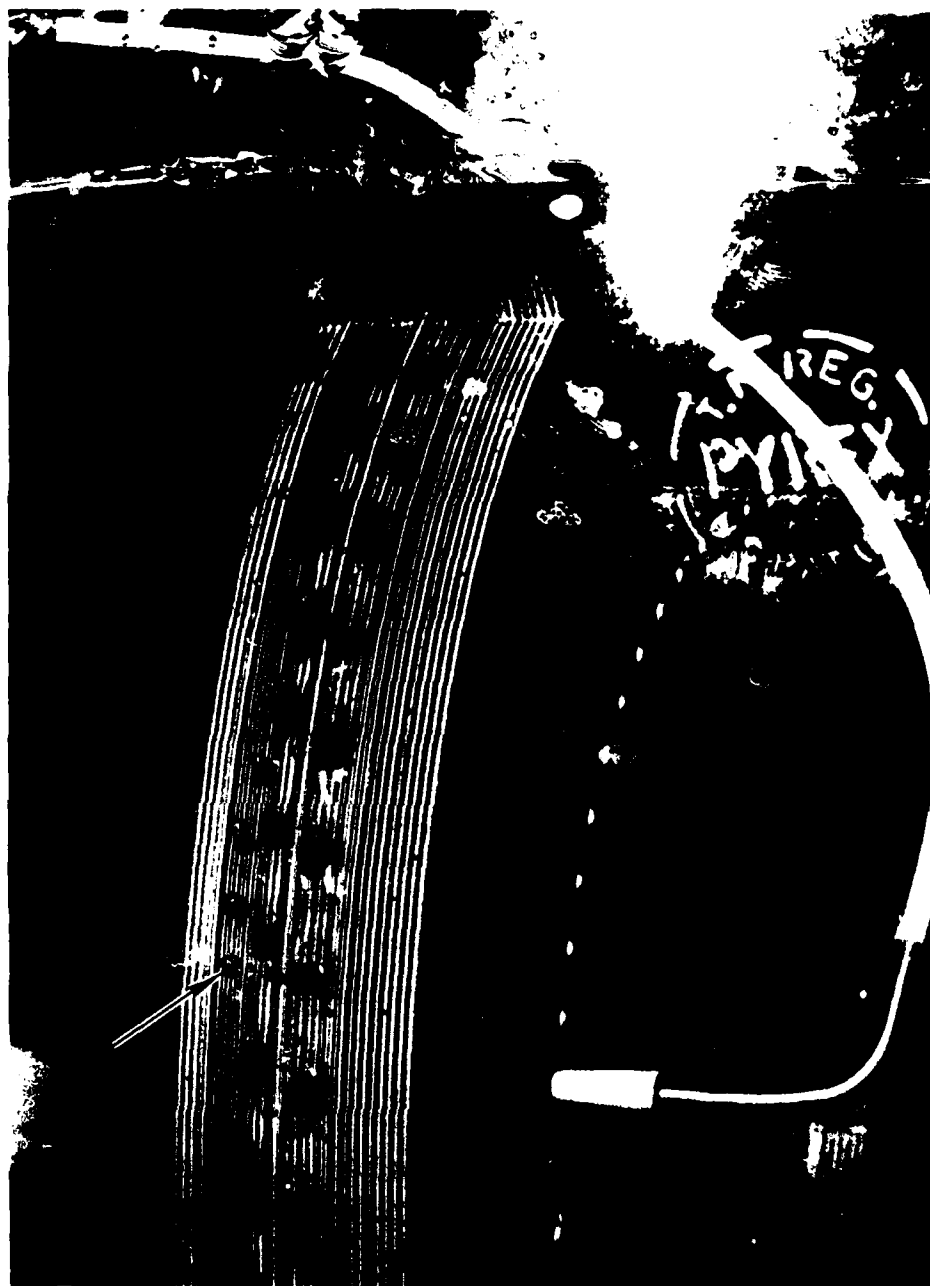
Figure 17. In-Process Air Leakage Check of Laminated
Wheel Blank, Serial No. 4. (Arrow
Indicates Leakage at Laminate No. +19
Between Blades.)

Laminated Turbine Rotor Airflow Test Results (Serial No. 1 Rotor)

The flow check of the laminated rotor (Part 3551198-1, Serial No. 1) and associated data reduction were successfully completed. The objectives of the flow check were to verify:

1)   The cooling design and its flow characteristics

2)   An even discharge distribution

3)   That all cooling passages were open and free from obstruction

Figure 18 shows the laboratory setup. There were 2 parts in the flow check:

1)   Part One - All 62 blades were flow checked at 10 and 30 inches HgG. The objective of this test was to verify that all cooling passages and discharge outlets were open and to determine the flow variation of the blades with respect to the average. The results are presented in Figures 19, 20, and 21. As indicated in these figures, the maximum flow variation was ±5 percent.

2)   Part Two - The objective of this test was to generate the flow curves used to verify the predicted flow distribution on each blade. To simplify the testing, only 15 blades (5 low, 5 medium, and 5 high flows) were selected for flow check. During this testing, the air inlet conditions and the amount of coolant were measured at inlet pressures of 10, 20, 30, and 40 inches HgG.
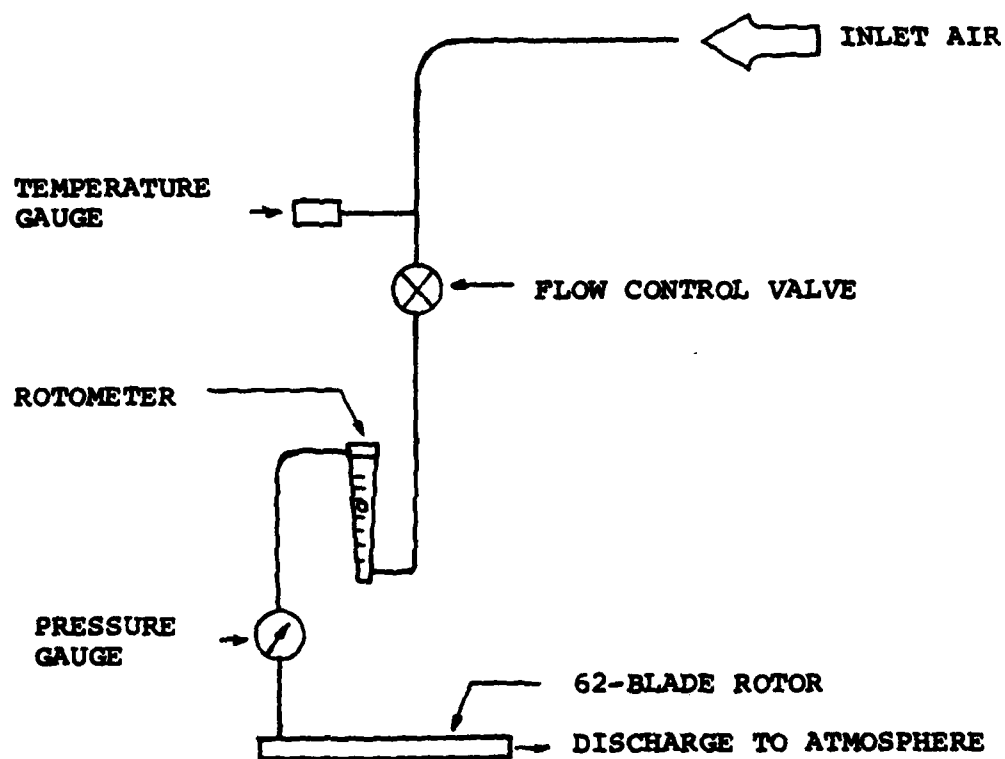
Figure 18. Laminated Rotor: Flow Check Setup.
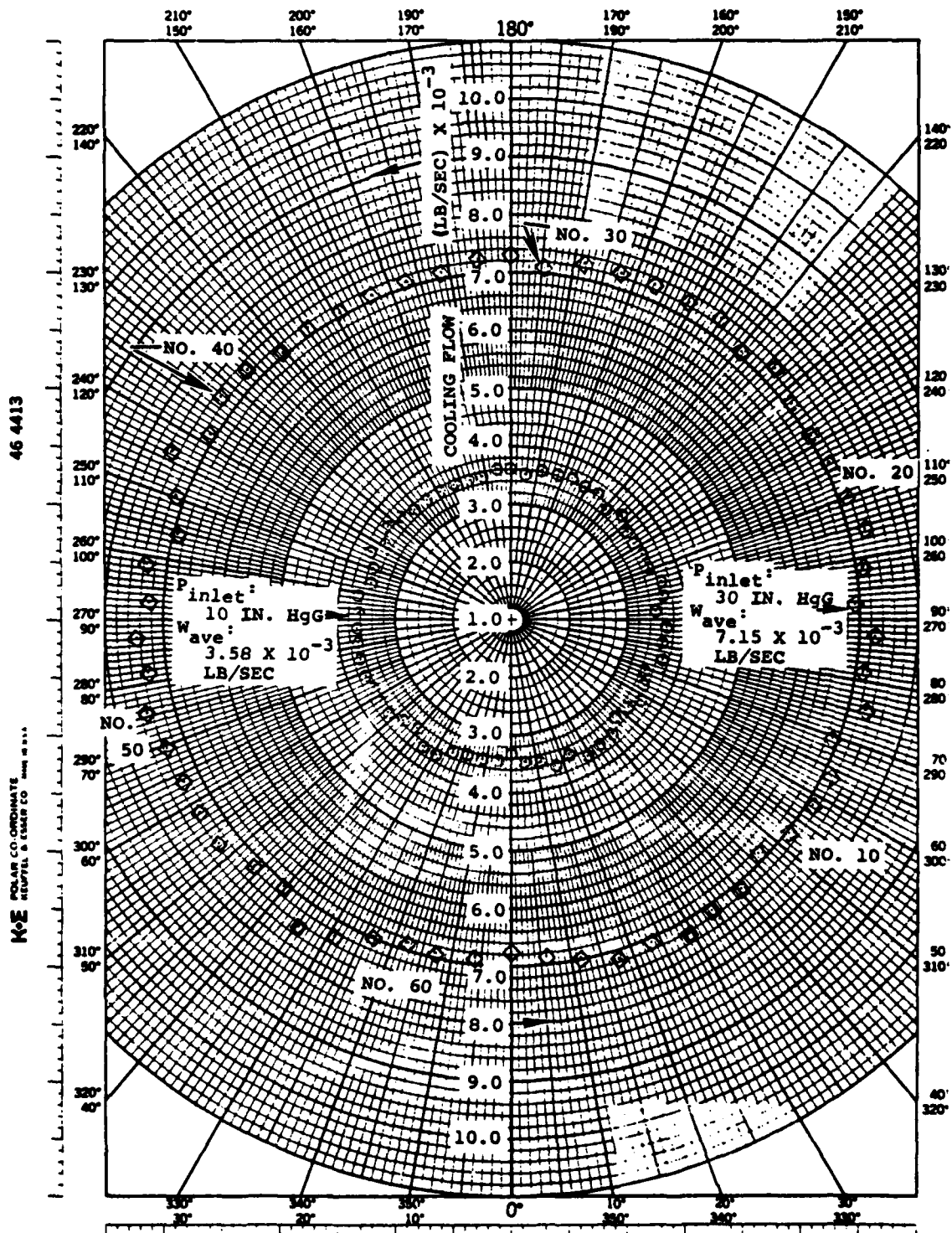
Figure 19. Laminated Rotor: Flow Distribution.
(Part No. 3551198-1 Serial No. 1)

Figure 21. Flow Variation of Cooling
Passages: Median Rank Plot
for $P_{IN.} = 30"$ HgG.

Figure 20. Flow Variation of Cooling
Passages: Median Rank Plot
for $P_{IN.} = 10"$ HgG.

33

The testing was accomplished in three steps as follows:

1) All discharge outlets open to determine the total air-flow through all of the blades

2) Gill and tip outlets closed to determine the amount of trailing-edge air discharge

3) Tip outlet closed to calibrate the amount of tip and gill discharge air.

Figures 22 and 23 show the result of this testing. Figure 24 shows the flow distribution on each blade. Note that the flow split for all circuits agrees very well with design predictions.

Engine Demonstration Testing

Various mechanical component tests were performed on the wheel prior to committing the high-temperature rotor to an engine demonstration test, which verified the mechanical integrity and durability of the laminated turbine. The following sections describe the design and development testing that led to the first successful engine test of the laminated turbine rotor.

Design and Development

The axial turbine rotor selected by the Air Force for engine development testing was the high-pressure turbine rotor in the AiResearch Model TFE731 Turbofan Engine (Ref. 2), as shown in Figure 25. The engine utilized for the demonstration test was a two-spool, advanced-gas-generator derivative of the fan engine that included a variable-geometry, low-pressure tubine with variable load capability. This permitted adjustment of the high-pressure rotor speed and inlet temperature conditions, and allowed testing of the laminated rotor in an actual engine environment.

---

2. Furst, D.G., R.W. Vershure, J.A. Pyne, and J.J. Clark, "Integral, Low-Cost, High-Temperature Turbine Feasibility Demonstrator (Small Laminated Axial Turbine Program)" AFAPL-TR-77-2, February 1977.
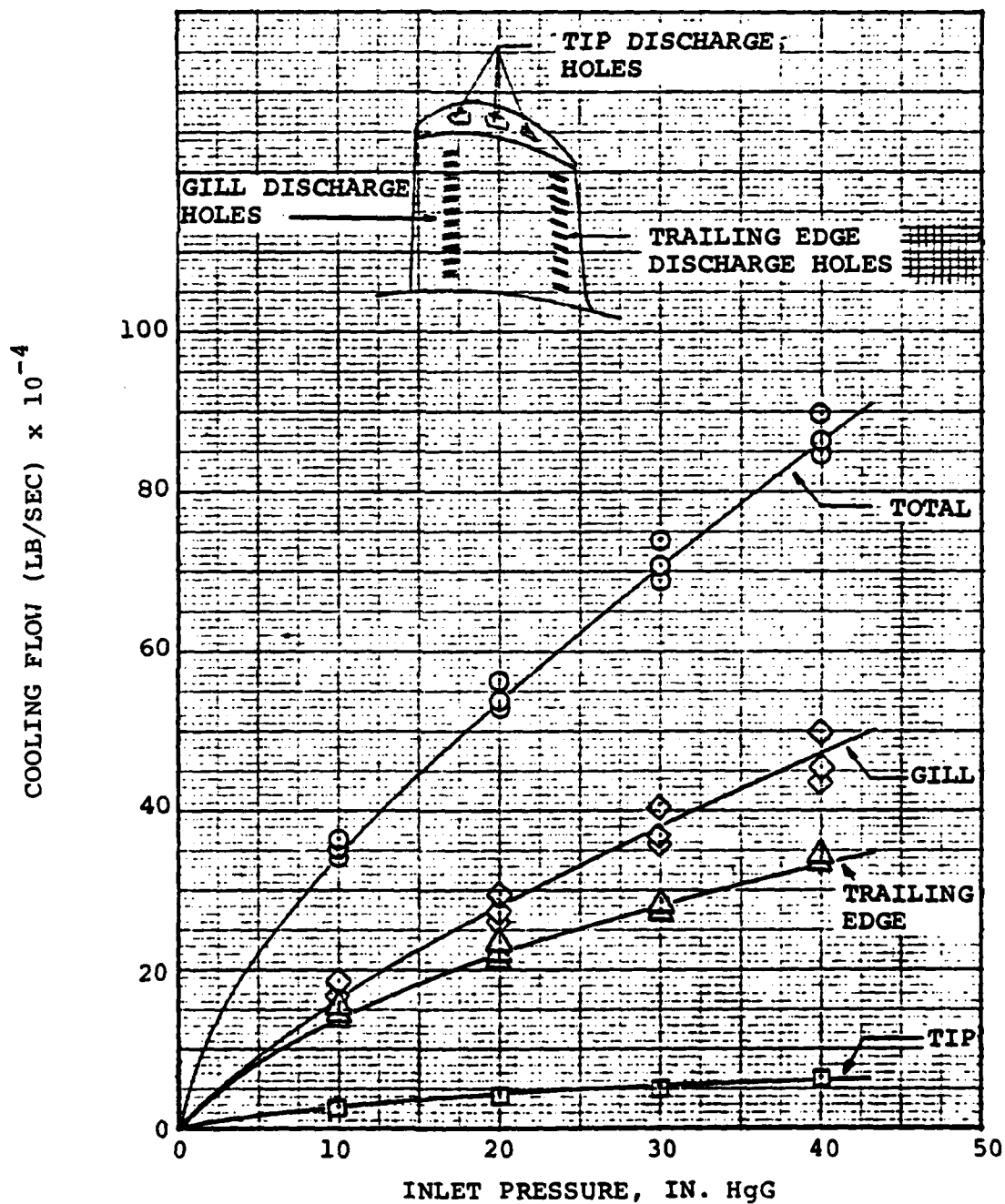
Figure 22. Laminated Rotor: Flow Check Result,
Cooling Flow Versus Pressure.
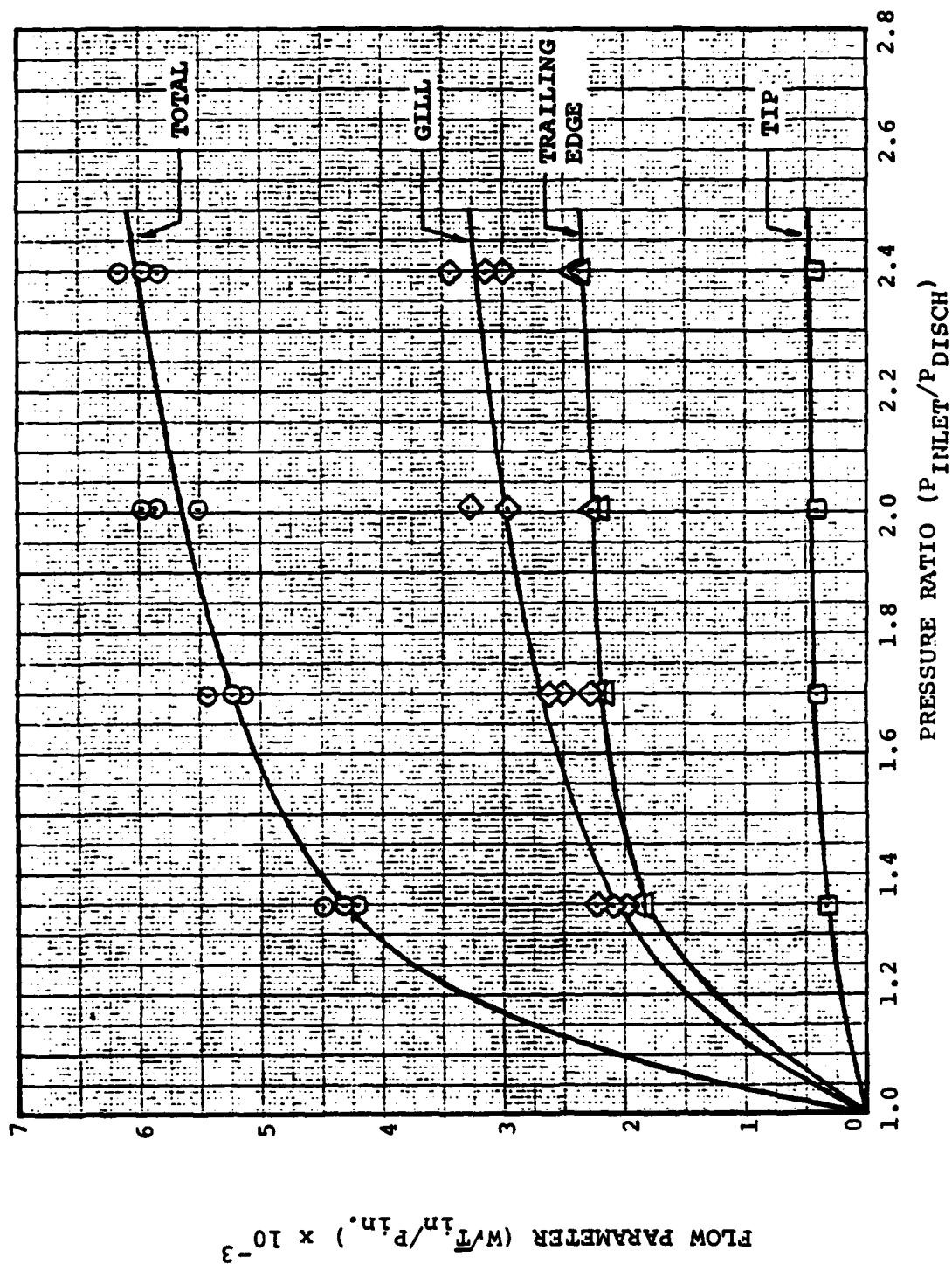
Figure 23. Laminated Rotor: Flow Check Result, Flow Parameter Versus Pressure Ratio.

TIP: DESIGN: 6.8% Wc
ACTUAL: 7.16% Wc

GILL:
DESIGN: 54.08% Wc
ACTUAL: 53.93% Wc

TRAILING EDGE:
DESIGN: 39.12% Wc
ACTUAL: 38.91% Wc

TOTAL COOLING: Wc
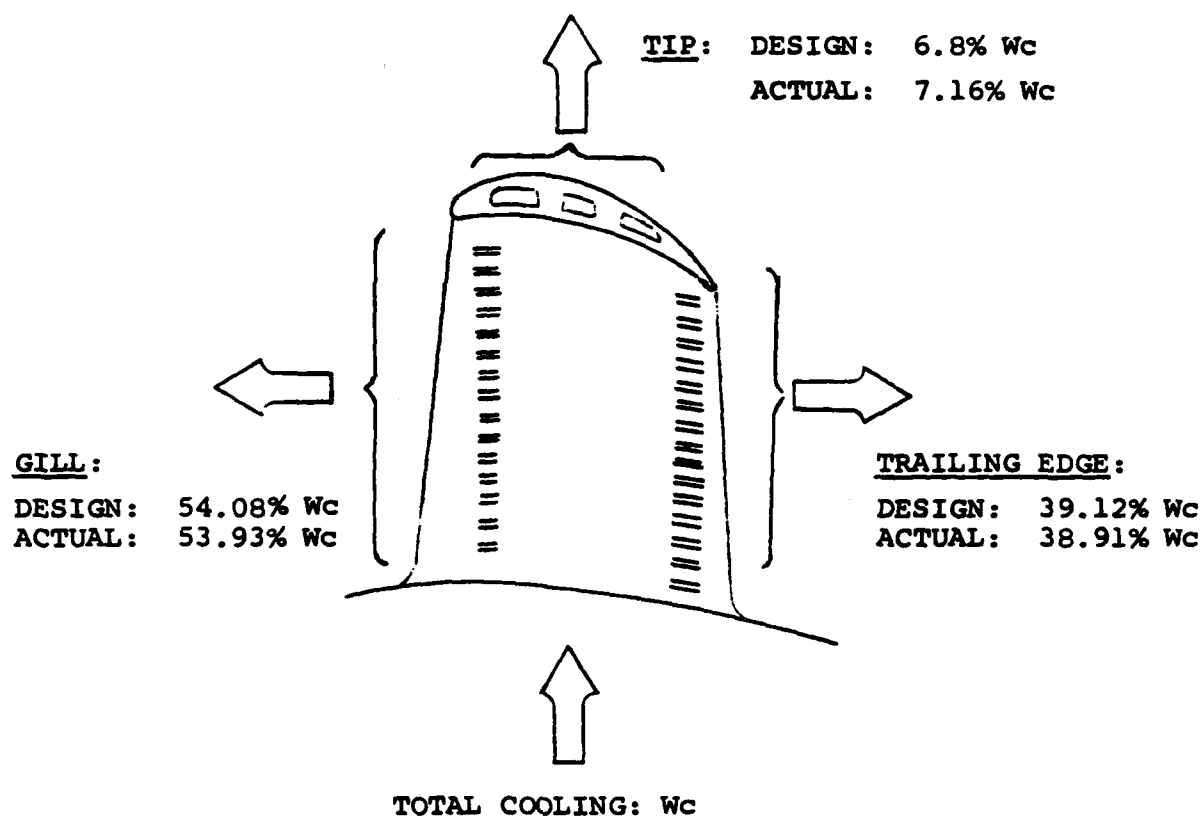
FLOW DISTRIBUTION					
		ACTUAL FLOW AT INLET PRESSURES:			
LOCATION	DESIGN	40" HgG	30" HgG	20" HgG	10" HgG
TIP	6.8%	7.05%	7.04%	7.41%	7.14%
T.E.	39.12	38.73	39.44	38.89	38.57
GILL	54.08	54.22	53.52	53.70	54.29

Figure 24. Blade Flow Distribution.

TFE 731 TURBOFAN ENGINE
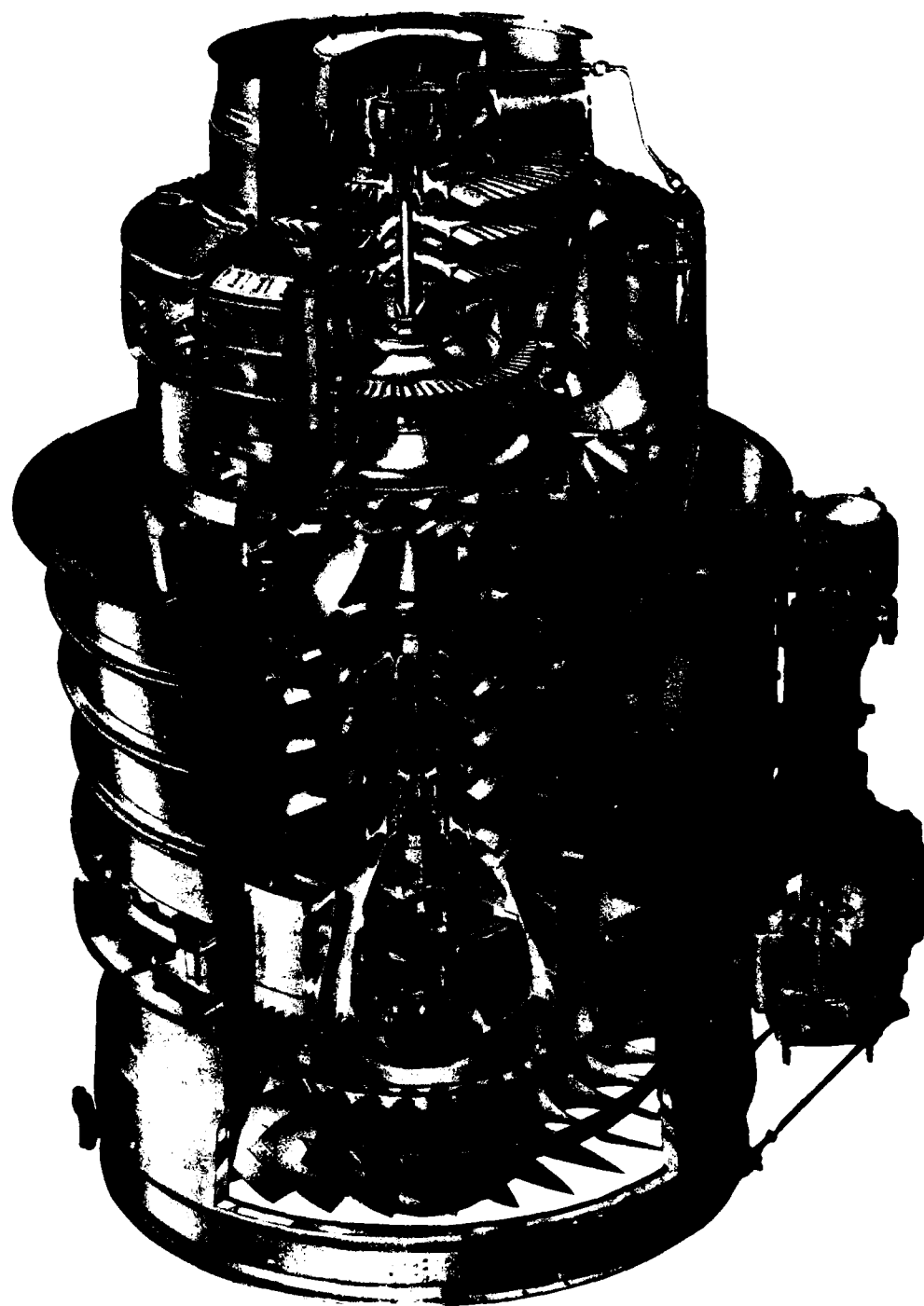
Figure 25. TFE731 Turbofan Engine.

MS 4636-10

Laminated Turbine Rotor - The high-pressure turbine rotor tested was the AiResearch integral, laminated, turbine rotor shown in Figure 26. This turbine rotor is 11 inches in diameter and has a design speed of 29,692 rpm. There are 62 blades integral to the disk. The blades are quite small with a 1.3-inch span and 0.8-inch chord. The laminated turbine was produced from thin sheet laminates of Waspaloy sheet material that are bonded together. Complex internal passages were formed from a combination of laminate configurations that were initially photoetched from sheet material. When properly stacked and bonded, the resulting component was finish-machined to the final aerodynamic contour.

The selected blade cooling concept utilizes impingement cooling of the leading edge with suction-side film discharge slots, convection cooling of a two-passage center section, and convection cooling with center discharge in the trailing-edge section. The temperature and life predictions achieved for three candidate materials--Waspaloy, Astroloy, and AF2-1DA--are shown in Table 2. Waspaloy was selected for the initial wheels, primarily because of sheet material availability, even though Astroloy and AF2-1DA have higher temperature capabilities.

Mechanical Integrity Component Tests

The mechanical integrity component tests and evaluations of the laminated rotor prior to the engine test consisted of mechanical property test data from the bonded wheel blank, airflow testing, a holography vibration test, a growth and overspeed test, and final nondestructive inspections.

Mechanical Property Data - The mechanical property testing of the turbine wheel was completed using test specimens removed from laminate material in the wheel blank outside of the finished wheel and prior to final machining. In Table 3, mechanical

39
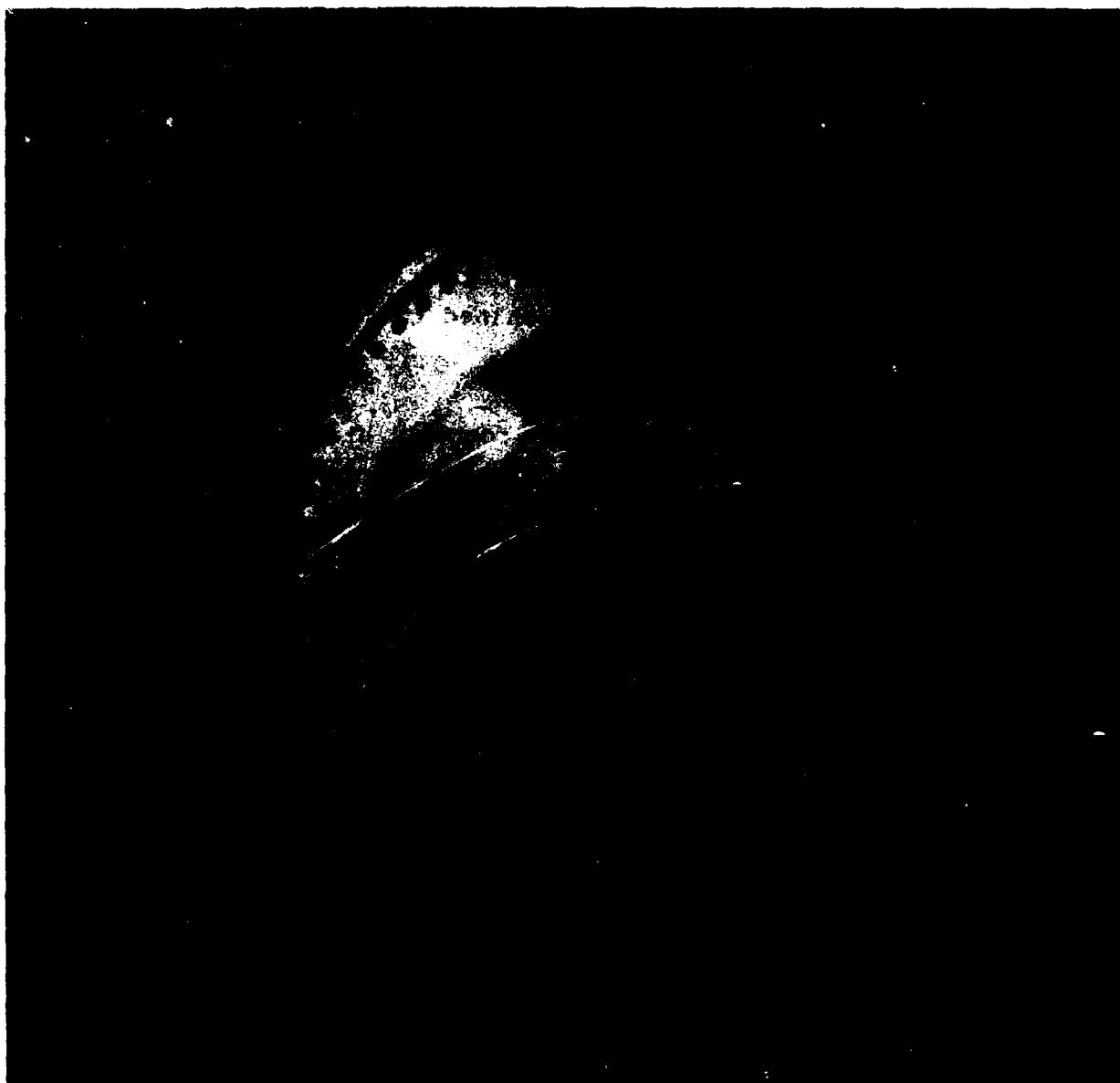
Figure 26.   Laminated Turbine Wheel.

TABLE 2.   TWO-PERCENT CREEP LIFE VERSUS AVERAGE
TURBINE INLET TEMPERATURE.

Turbine Material	Turbine Inlet Temperature °F	Life At Temperature hrs.
Waspaloy	2320	20
Astroloy	2530	20
AF2-1DA	2600	29

TABLE 3. WASPALOY LAMINATED WHEEL MECHANICAL PROPERTY TEST RESULTS.

Specimen Direction	Test Temperature (°F)	UTS (ksi)	YS (ksi)	Elong (%)	RA (%)	Stress Rupture
Target Goals						
Transverse	R.T. & 1400	100	--	3	--	--
Longitudinal	R.T. & 1400	125	--	5	--	--
Longitudinal	1700	--	--	--	--	20 ksi/25 Hr.
Transverse - Bore	1400	105.5	96.5	2.6	4.2	---
	1400	101.6	97.9	2.9	6.1	---
	1400	119.6	94.5	3.8	5.6	---
Average	1400	108.9	96.3	3.1	5.3	--
Longitudinal - Blade	1400	133.3	102.7	17.4	22.1	---
	1400	134.9	102.4	20.0	25.3	---
	1400	133.6	102.4	21.6	27.7	--
Average	1400	133.9	102.5	19.7	25.0	--
Longitudinal - Blade	1700	--	--	52.9	52.2	20 ksi/25.4 Hrs.
	1700	--	--	32.0	51.8	20 ksi/22.1 Hrs.
	1700	--	--	44.1	56.3	20 ksi/25.3 Hrs.
Average	1700	--	--	43.0	53.4	20 ksi/24.3 Hrs.

42

property data for the wheel displays strength and ductility in both the longitudinal and transverse directions with respect to the laminates. These properties exceeded the target design requirements. The stress-rupture properties and high ductility at temperature also confirmed that a satisfactory wheel had been produced.

Airflow Test - An airflow bench test was conducted on the laminated turbine wheel. The results are shown in Figure 27. The actual percentage flows from the leading and trailing edges compare very favorably to the design values. Also, the repeatability of flow blade-to-blade was verified with a maximum variation in flow of ±4 percent. This compares favorably to cast inserted blades, which have an allowable variation of ±10 percent. It was concluded from this test that the laminate process appears to produce precision cooling passages that are consistent and have a minimum variation in geometry.

Growth and Overspeed Test - The laminated wheel was growth tested in a whirlpit facility to determine the response of the wheel structure to overspeed conditions, and to verify its mechanical integrity. The results of the growth and overspeed test are presented in Figure 28, where the total diametral growth has been plotted as a function of speed. A maximum total growth of less than 0.002 inch occurred in the center of the bore, with a smaller amount of growth at the rotor tip. The maximum speed was 36,500 rpm—or 123 percent of the design speed.

Holography Vibration Test - A holography vibration test of the laminated wheel was conducted with the mating front seal plate and curvic coupling rotor as shown in Figure 29. This test setup and assembly is identical to the engine installation. The seal plate functions as an inlet plenum for the blade cooling air and provides some damping at the wheel-rim/seal-plate interface.

LAMINATED TURBINE ROTOR, 3551198-1, S/N 1

TIP DESIGN: 6.8% W_C

ACTUAL: 7.16% W_C

LEADING EDGE

DESIGN: 54.03% W_C

ACTUAL: 53.93% W_C

TRAILING EDGE

DESIGN: 39.12% W_C

ACTUAL: 38.91% W_C

TOTAL COOLING: W_C
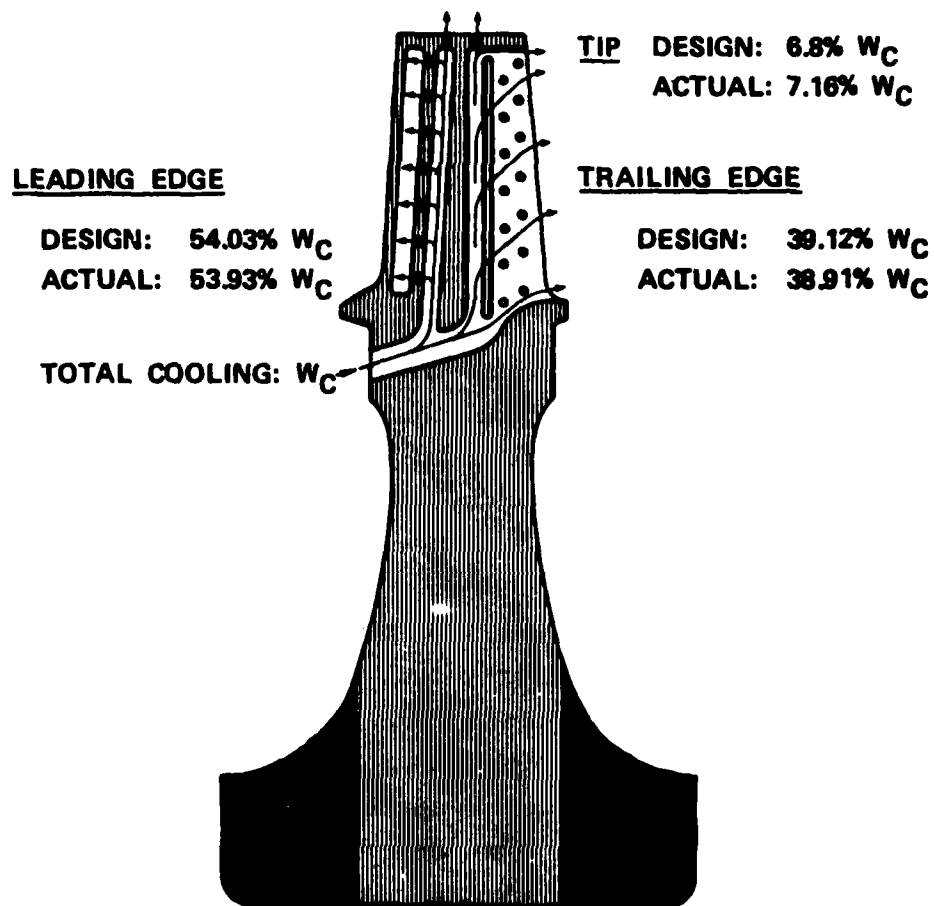
Figure 27. Selected Blade Cooling Concept.

LAMINATED TURBINE ROTOR, 3551198-1, S/N 1
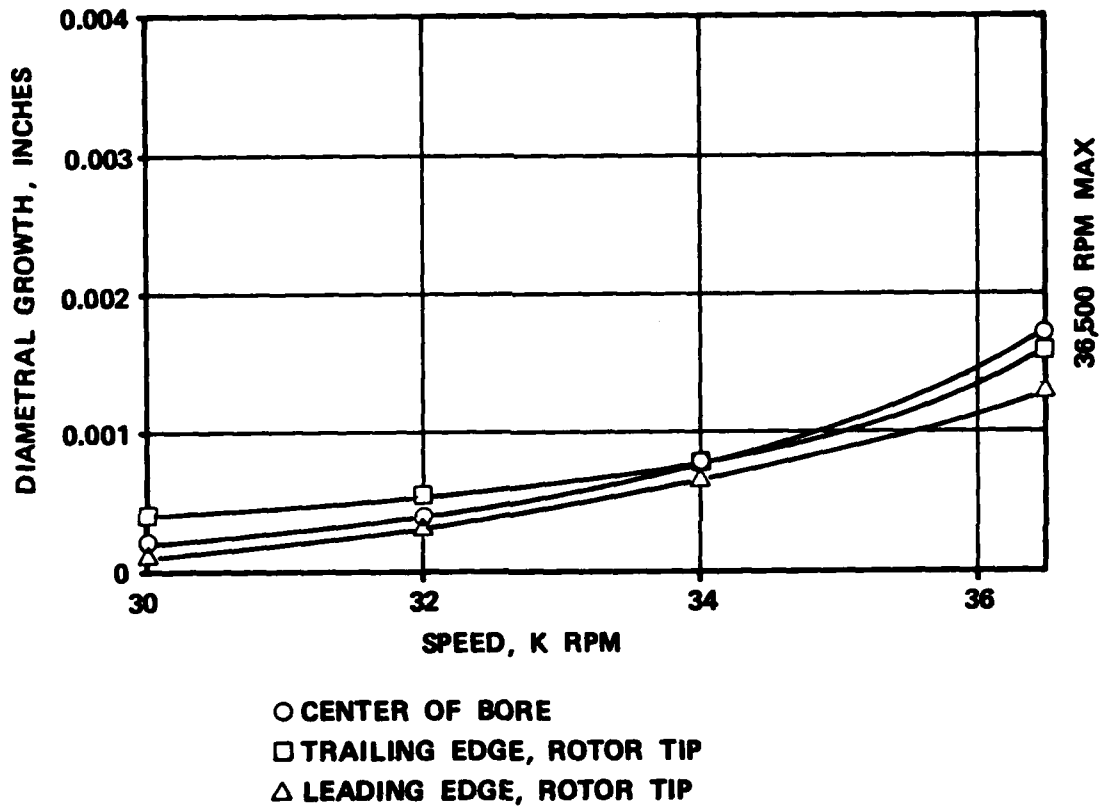
Figure 28.   Overspeed Test Results.

COOLING-AIR
DISCHARGE

FRONT
SEAL
PLATE

COOLING-AIR
SOURCE
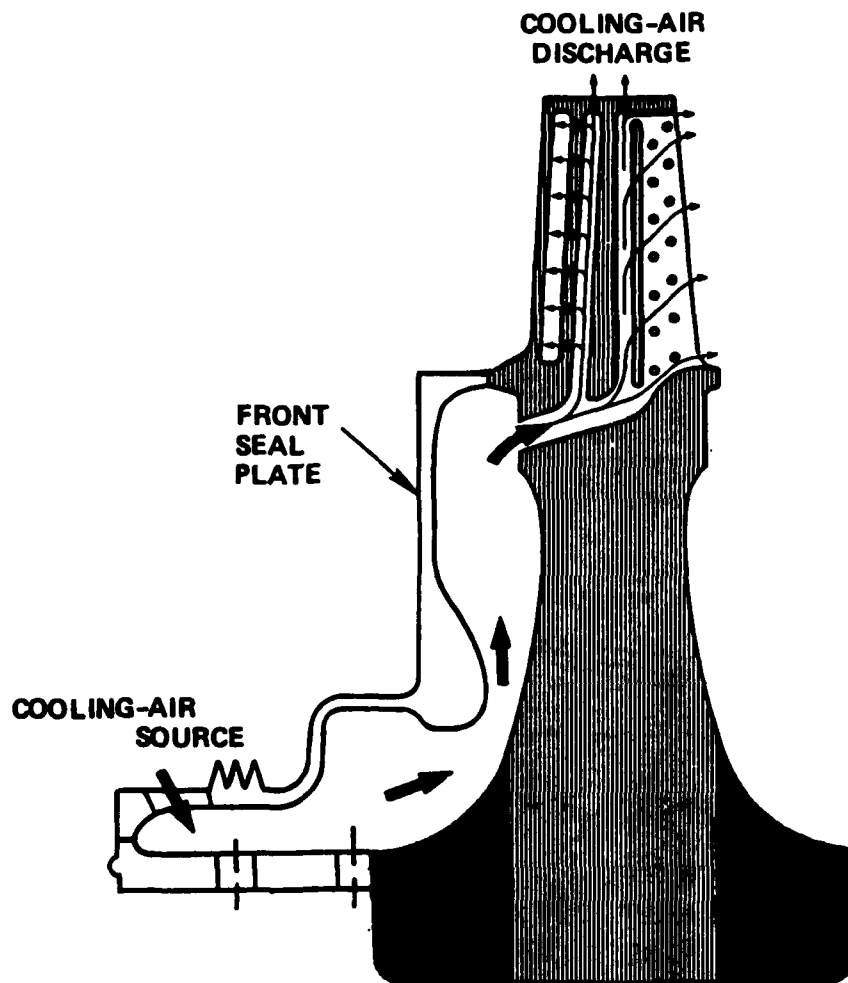
Figure 29.   Holography Test Setup.

46

The objective of the test was to determine the resonant vibration frequencies and mode shapes of the integral laminated wheel, to ensure safe operation in the engine demonstration test. The driver was a crystal gauge located on the upstream face of the disk web. The sensors were also crystal gauges with two located on the disk and three on a blade. A constant 200-volt input was maintained on the crystal driver, and the relative amplitude was recorded in millivolts on the sensor gauges.

The holograms in Figures 30(a) through 30(f) are for six resonant modes of operation at 4,034 Hz, 10,214 Hz, 15,326 Hz, 16,048 Hz, 17,106 Hz, and 24,297 Hz. A Campbell diagram was constructed, as shown in Figure 31, with a temperature correction applied based on a metal temperature of 1400°F. The blade/disk system is highly coupled as indicated by the holograms and the multiplicity of resonant frequencies for essentially the same blade mode. The spread in frequencies for each mode depicted in the Campbell diagram is a result of studying the total number of holograms and grouping them into six blade modes. Also, for comparison, the TFE731 cast inserted blade holography results are shown for two production wheels. The two production wheels tested appear to have less spread in frequency for a given mode than the laminated wheel. This is primarily due to variations in blade-to-disk coupling as the nodal pattern in the disk changes, and secondarily due to blade-to-blade geometry variations. Modes 3 and 5 should be damped by the seal plate since there is no tendency for a nodal circle to develop where the disk and seal plate join. The Modes 1, 2, 4 and 6 will not be damped since a nodal circle is present at this juncture. By avoiding the resonant modes established from this holography test, safe operation of the laminated wheel was possible in the engine at idle speed and 100-percent speed.

47

Figure 30(a). Vibration Hologram, Mode 1, 4034 Hz.
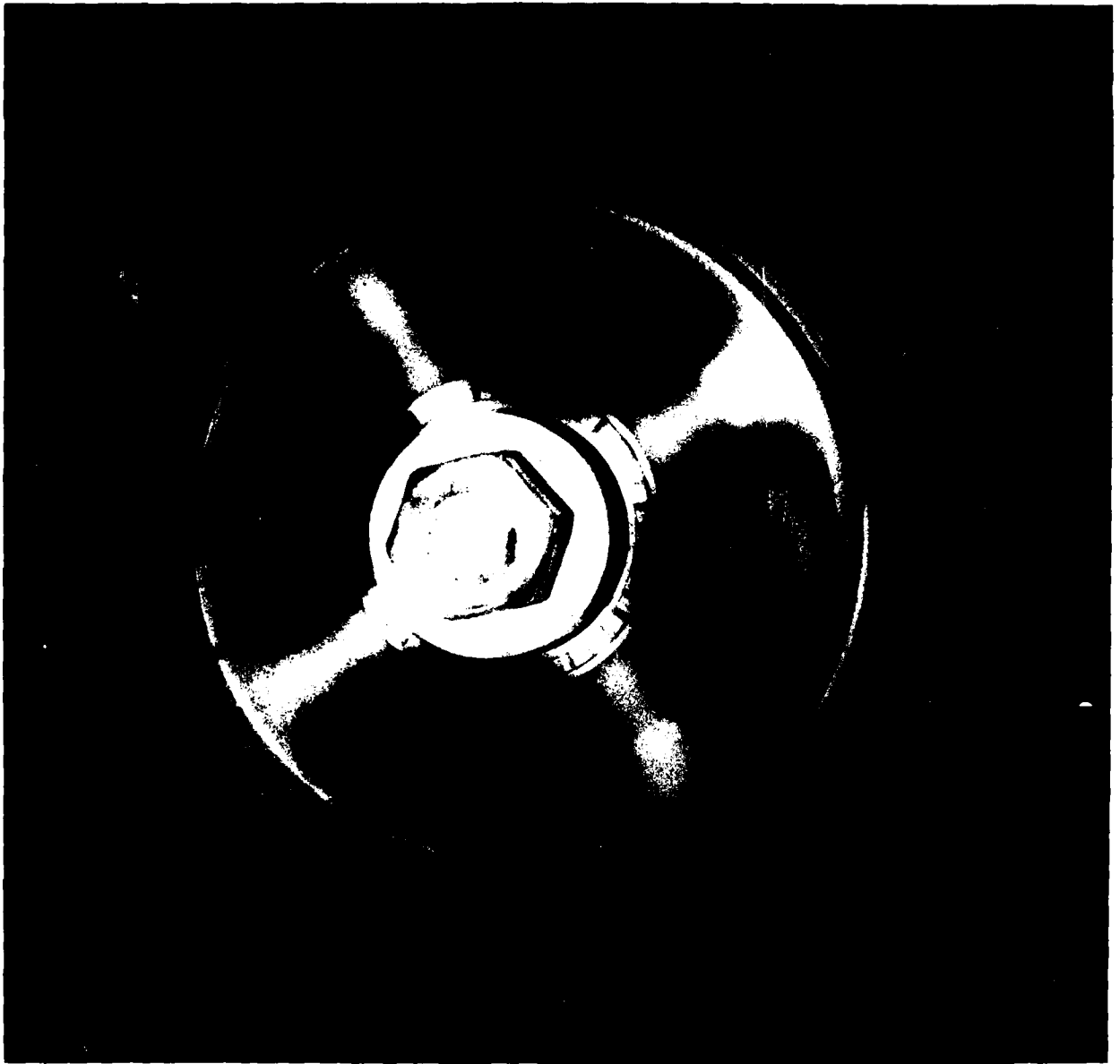
Figure 30(b). Vibration Hologram, Mode 2, 10,214 Hz.

49

Figure 30(c).   Vibration Hologram, Mode 3, 15,326 Hz.

50
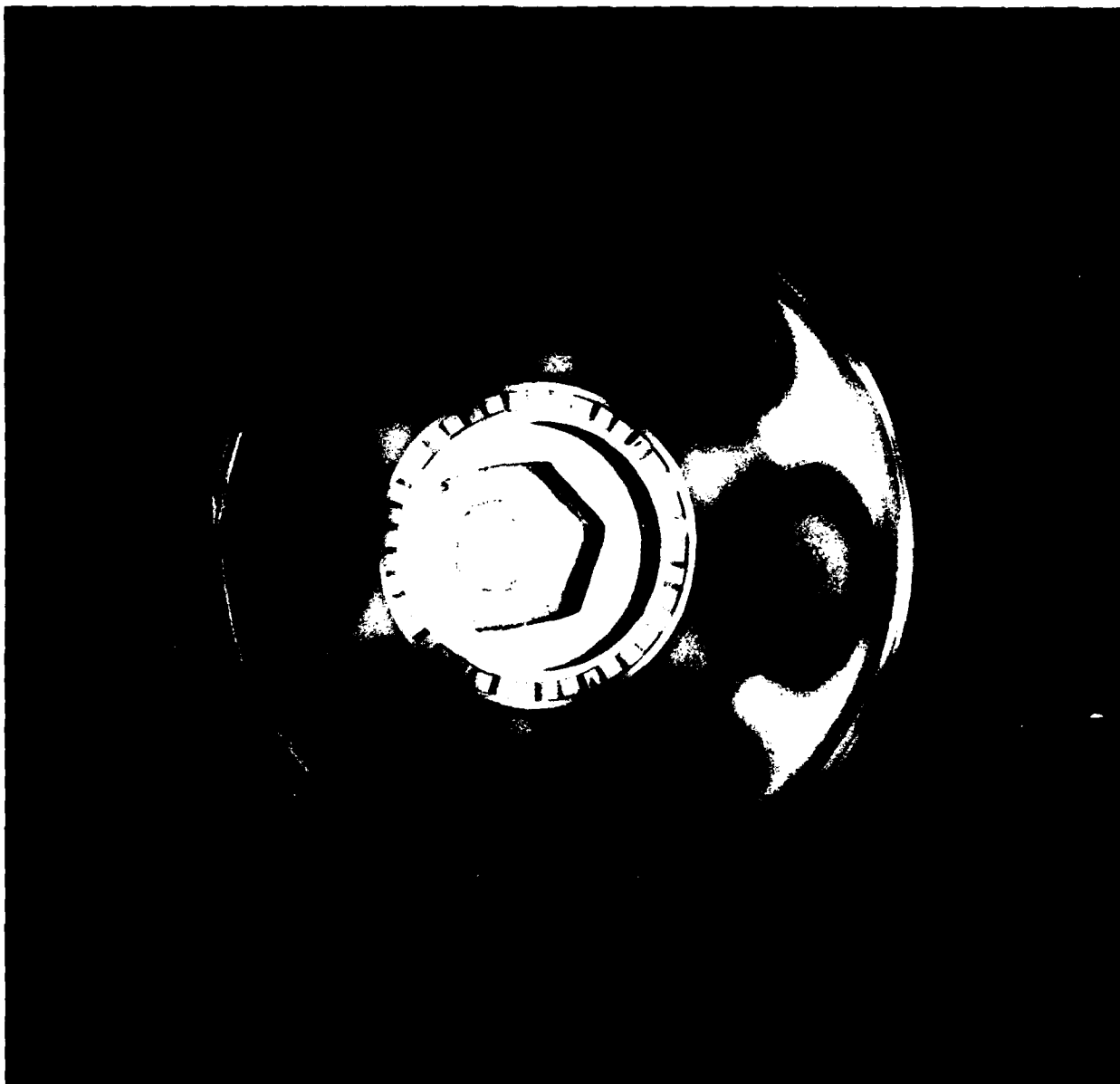
Figure 30(d).   Vibration Hologram, Mode 4, 16,048 Hz.
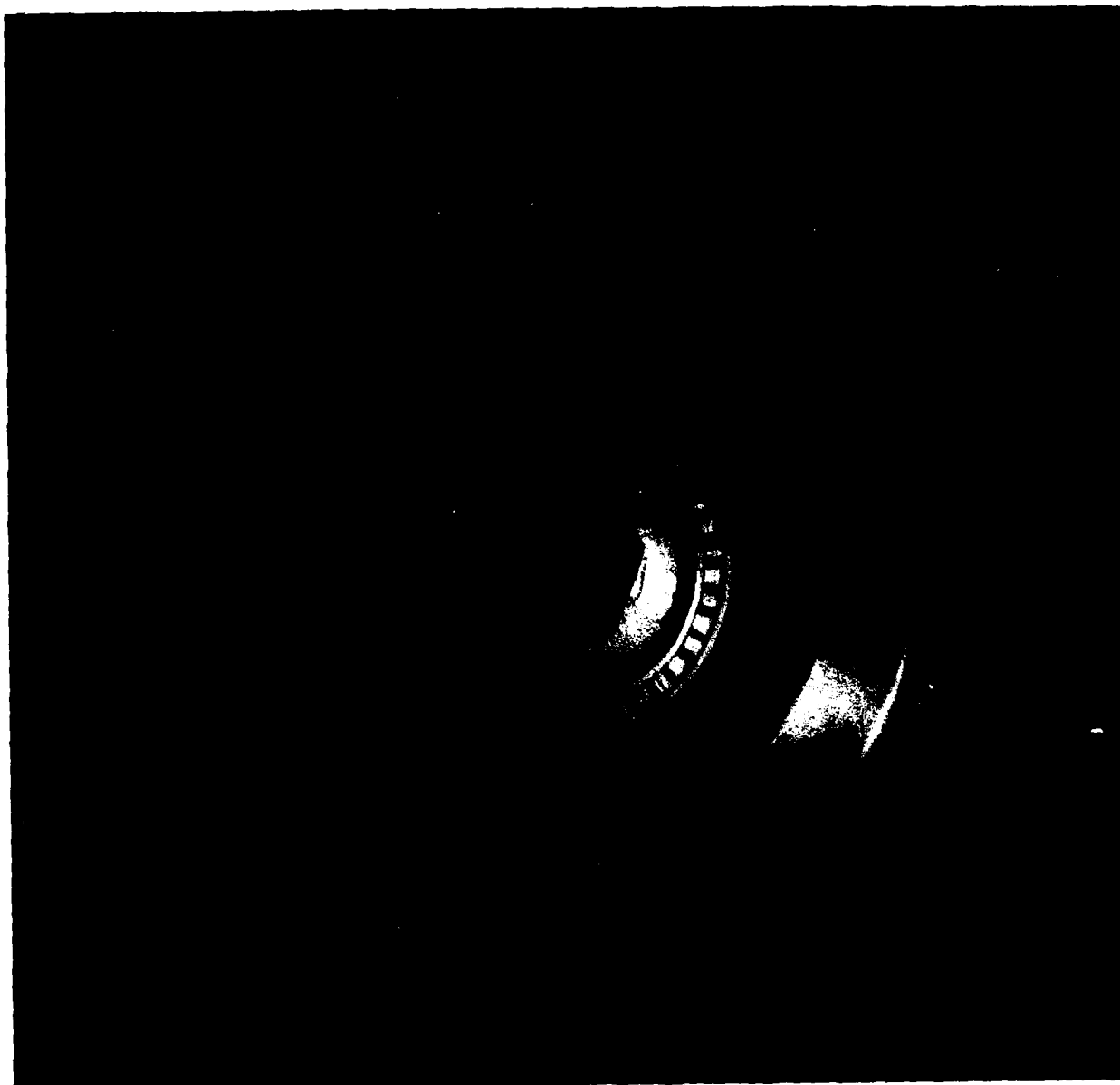
Figure 30(e). Vibration Hologram, Mode 5, 17,106 Hz.

52
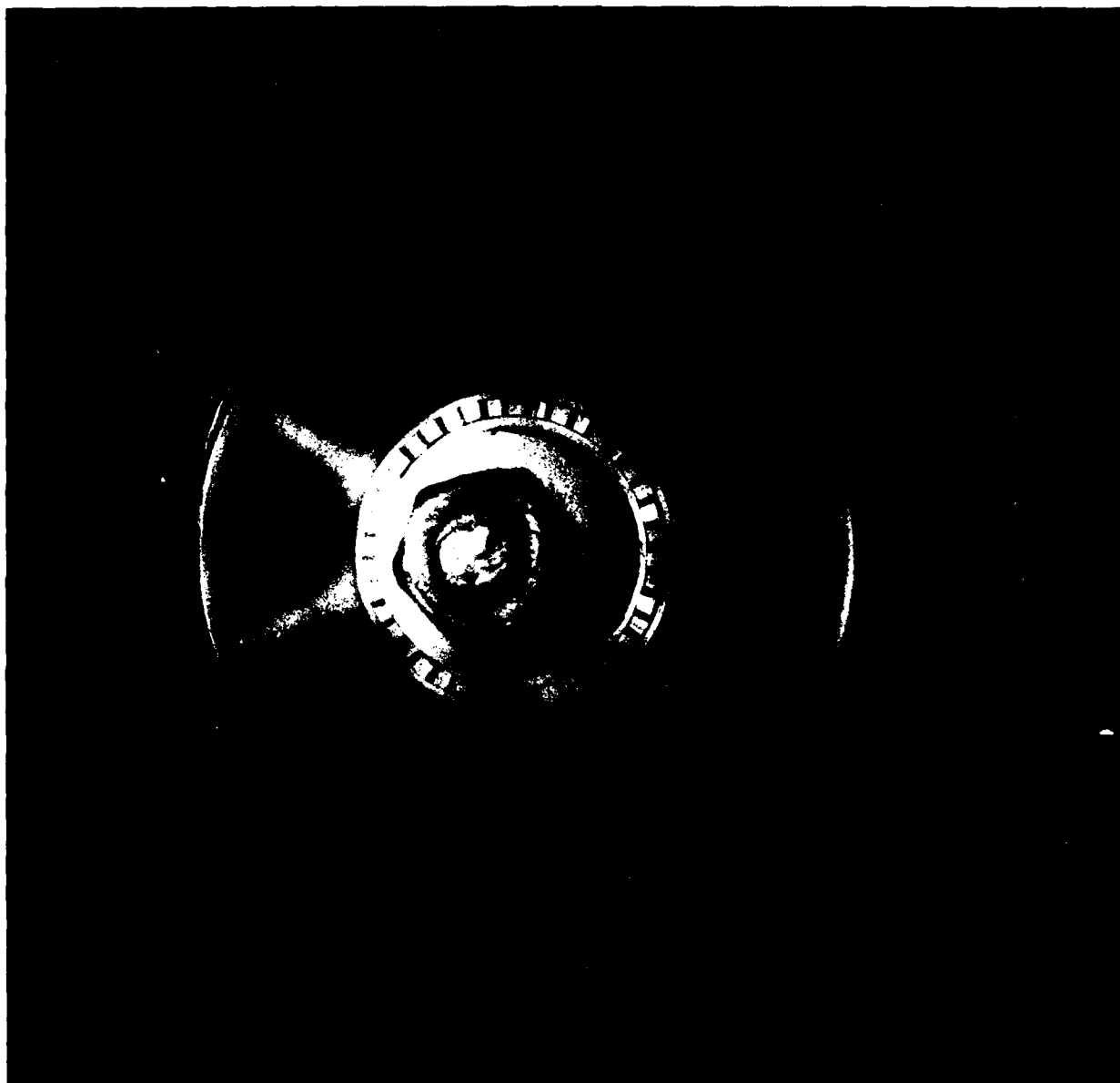
Figure 30(f). Vibration Hologram, Mode 6, 24,297 Hz.

53
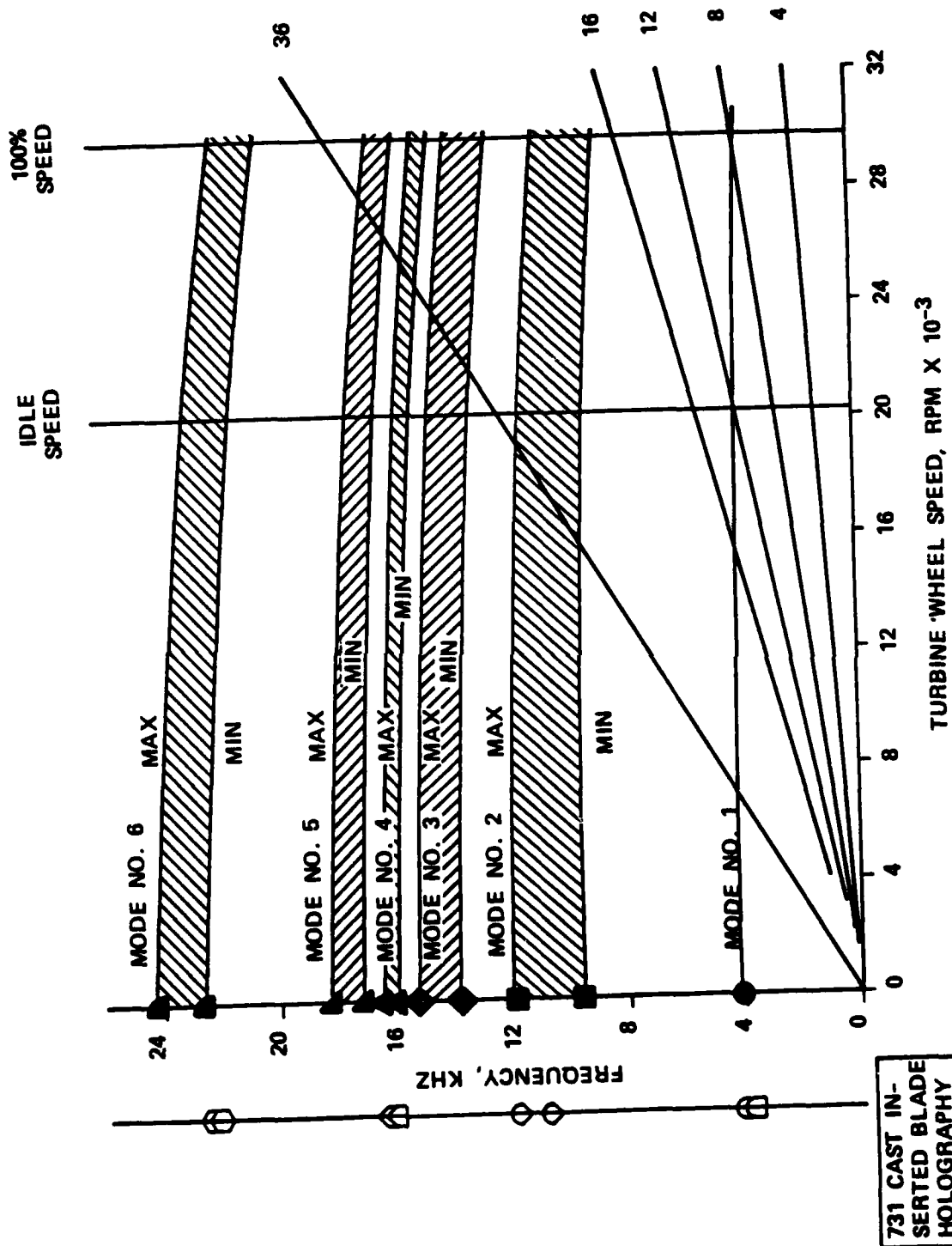
Figure 31. Campbell Diagram for Laminated Turbine Wheel.

54

Nondestructive Inspection - An ultrasonic inspection of the disk area of the wheel and a Zyglo inspection were performed before and after the growth and overspeed test. No delaminations or cracks were noted either in the blades or in the bore area. Therefore, it was concluded that the laminated turbine rotor was ready for engine demonstration testing.

Engine Test

The objectives of the demonstration test were to determine the heat-transfer performance of the laminated turbine wheel, and to establish its mechanical integrity and durability in an actual engine environment. The high-pressure rotor assembly with the cooled laminated turbine wheel is shown in Figure 32.

Instrumentation - The primary instrumentation used to determine the heat-transfer performance was a *Vanzetti radiation pyrometer system. The pyrometer was installed, as shown in Figure 33, to directly measure the blade trailing-edge metal temperature during engine operation. Three of the blades (Numbers 34, 35, and 38) were plasma sprayed with an aluminum oxide coating in the pyrometer target area. The coating raises the apparent temperature reading above adjacent blades. The coated blades serve as a blade number reference that correlates back to the airflow test on the individual blades. The basic Vanzetti system components, shown in Figure 34, are the cooled optical probe with a quartz lens and fiber optics bundle, which transmits the light to a germanium detector, and a temperature control unit which has either digital display or oscilloscope and tape recording capability. The probe was air cooled with the air constantly scrubbing and cleaning the lens during operation. The temperature calibration with the use of a black-body radiation source

---

*Vanzetti Infrared and Computer Systems, Inc., Canton, Mass.

55

AIR FORCE COOLED LAMINATED AXIAL TURBINE ASSEMBLY

MODEL 1131-1, BUILD 3

BLADE TIP & TRAILING EDGE COOLING AIR DISCHARGE

HIGH PRESSURE ROTOR ASSEMBLY

GILL HOLES FOR COOLING AIR DISCHARGE

Figure 32.

MS 5003-3

56
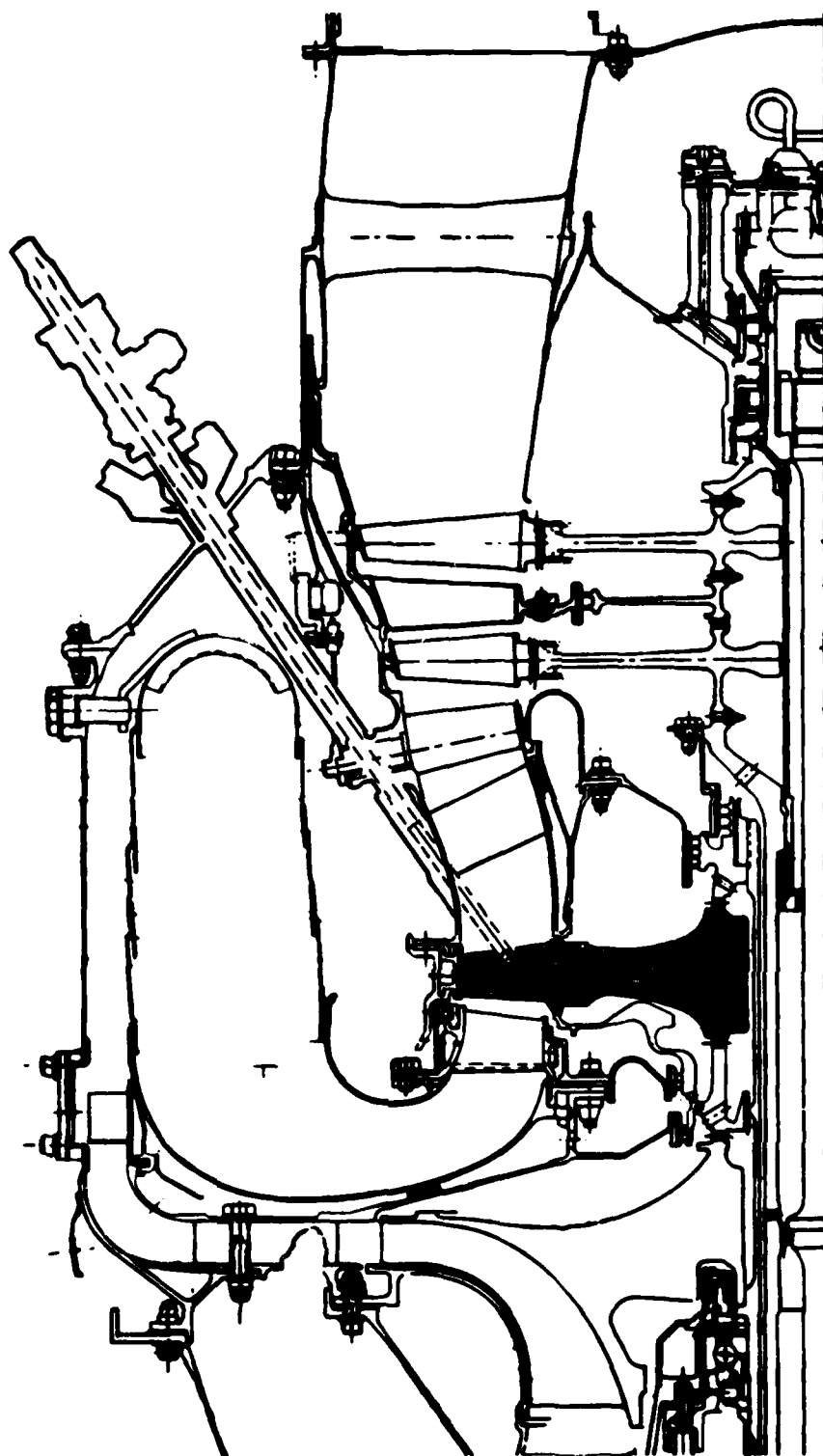
Figure 33. Vanzetti Pyrometer Installation.
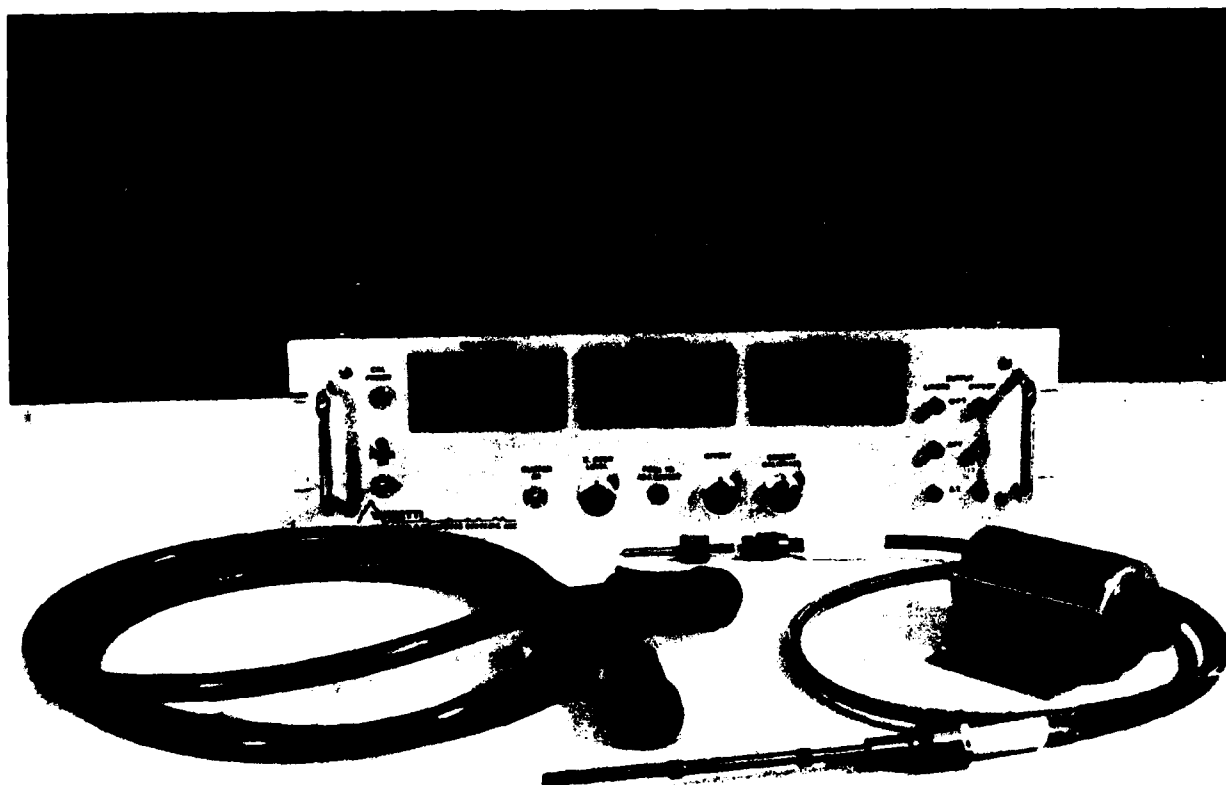
Figure 34. Basic Vanzetti System Components.

MP-67554

achieved an accuracy of ±0.6 percent at the 1400°F operating temperature level. This method of blade temperature measurement was very reliable, accurate, and easily adapted to the engine.

Test Cycle - The engine test cycle, shown in Figure 35, was about one hour in duration with operation at an idle speed of 20,300 rpm, and rapid acceleration and deceleration to the maximum speed of 29,600 rpm on the high-pressure rotor.

Test Results - The engine demonstration test results were:

1) Twenty cycles were successfully completed with a total operating time of 20 hours and 45 minutes. Two hours were at a maximum turbine inlet temperature of 2030°F and at the maximum power setting.

2) A hot-end visual inspection of the laminated rotor was performed on the test stand after the third cycle of operation and the rotor appeared to be in excellent condition.

3) At each maximum power setting, an oscilloscope trace of the blade trailing-edge temperatures was recorded. Figures 36(a) and (b) show the pyrometer temperature distribution after 10 hours of operation. Figure 36(b) is enlarged to show the coated reference blades starting with Number 34. The average temperature recorded was 1334°F, with a peak blade temperature of 1375°F. The airflow test results correlated very well with the peak blade temperature. This particular blade (No. 59) exhibited a lower than average airflow through the trailing-edge passage with a correspondingly high metal temperature. Also, the blade-to-blade temperature variation was within ±1.5 percent of the average.
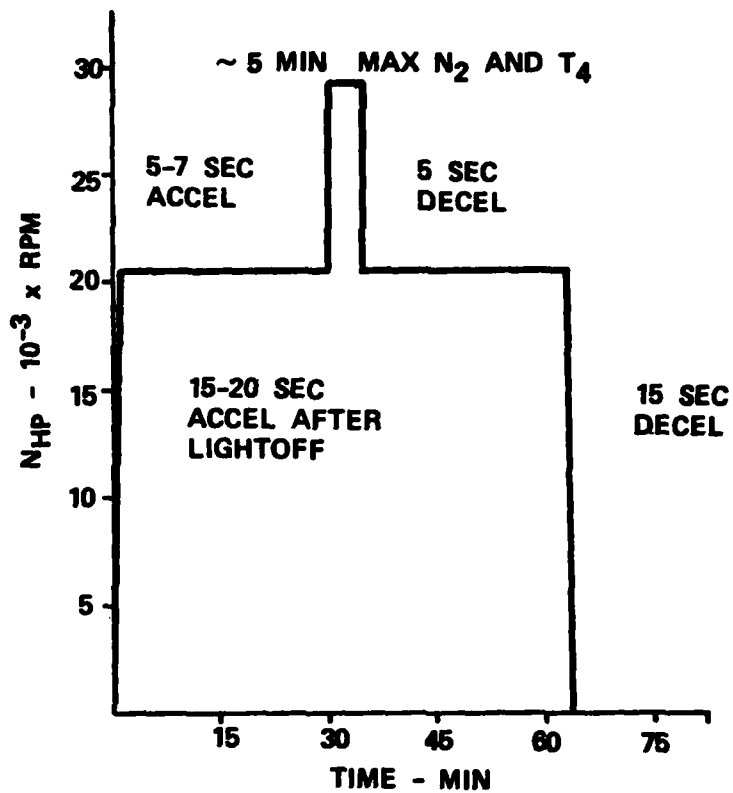
Figure 35. Typical Engine Test Cycle on the Laminated
HP Turbine Rotor.

START
BLADE NO. 34 (REF)

1 SET

MAX. TEMP.
1375°F

AVE. TEMP.
1334°F

(A)

COATED BLADES (REF)
NO. 34
NO. 35
NO. 36
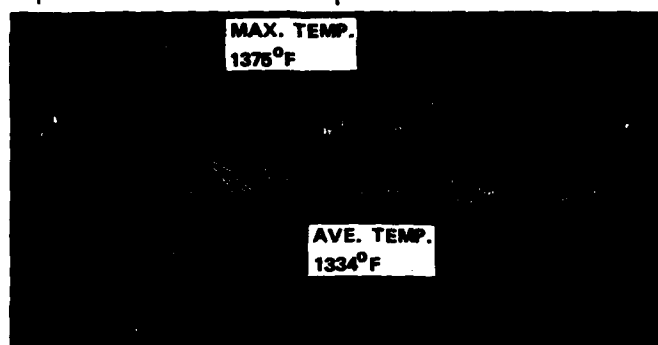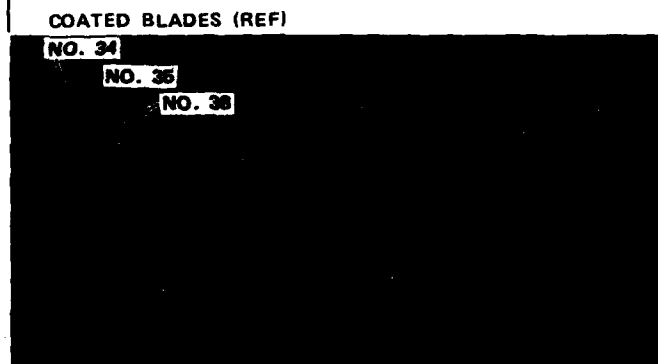
(B)

Figure 36. Pyrometer Temperature Distribution After
10 Hours of Operation.

4) The resulting inferred bulk airfoil cooling effectiveness, which is a measure of the heat-transfer performance, was 0.52 measured versus 0.53 predicted.

5) A comparison of the pyrometer temperature recordings indicated no shift or deterioration of the cooling scheme throughout the demonstration.

6) Post-test inspection of the laminated wheel, which is shown in Figures 37, 38, and 39 indicated the laminated turbine was in excellent condition after the engine test.
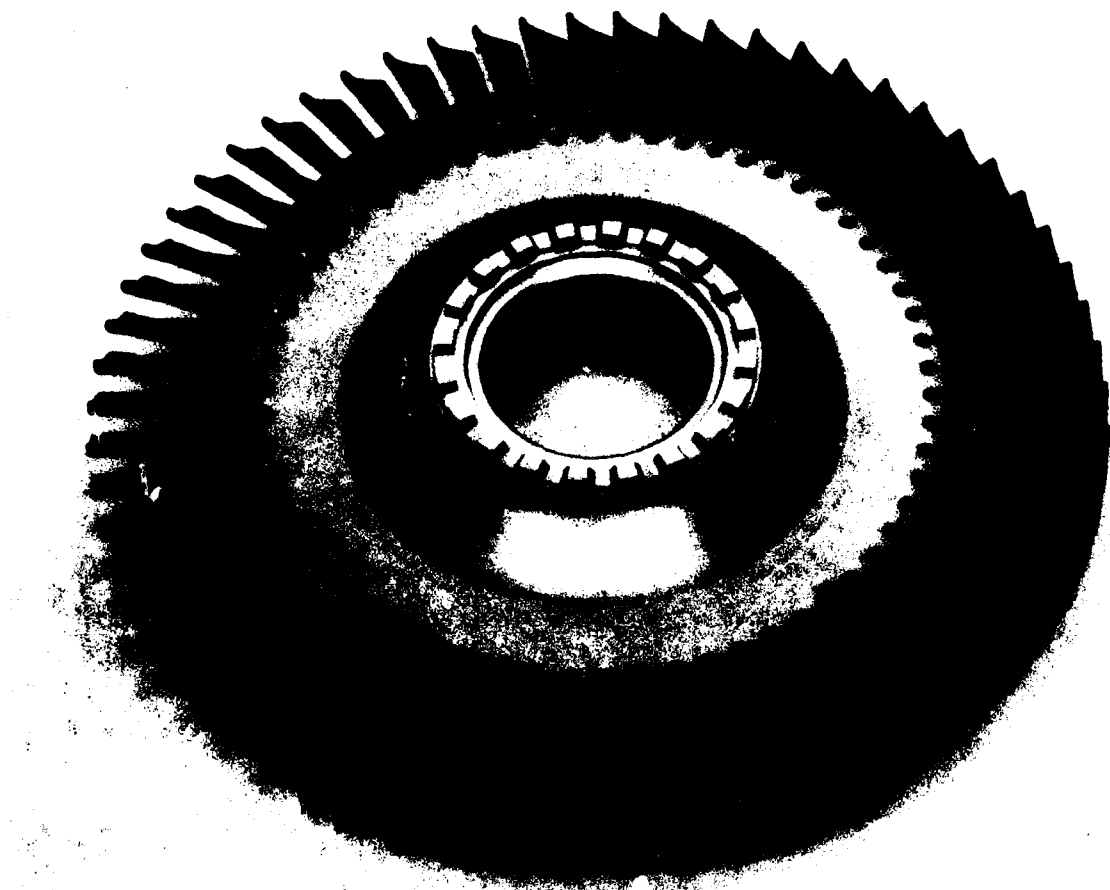
Figure 37.   Axial Laminated Turbine Rotor 3551198-1,
            Serial No. 1 Post-Test Condition After 20
            Cycles and 20 Hours and 45 Minutes of
            Operation in the 1131-1 Advanced Gas Generator
            Engine Demonstration.

Figure 38. Axial Laminated Turbine Rotor 3551198-1, Serial No. 1 Post-Test Condition After 20 Cycles and 20 Hours and 45 Minutes of Operation in the 1131-1 Advanced Gas Generator Engine Demonstration.

Figure 39. Axial Laminated Turbine Rotor 3551198-1, Serial
No. 1 Post-Test Condition After 20 Cycles and
20 Hours and 45 Minutes of Operation in the 1131-1
Advanced Gas Generator Engine Demonstration.

SECTION II - SMALL LAMINATED AXIAL TURBINE DESIGN
INTRODUCTION

A small cruise-missile engine high-pressure, cooled, axial, turbine rotor was designed and the tooling manufactured using the AiResearch laminated manufacturing process. The turbine design was based on combining the technology gained from several Air Force programs - the "Low Aspect Ratio Turbine" (LART) Program (Contract No. F66315-74-C-2017), for the aerodynamic design, the "Integral, Low-Cost, High-Temperature Turbine Feasibility Demonstrator" Program (Contract No. F33615-74-C-2034) for the feasibility demonstration, and the "Manufacturing Methods For The Fabrication of Cooled Laminated Axial Turbine Wheels" Program (Contract No. F33615-75-C-5211) for the manufacturing process development.

Laminated Turbine Rotor Design Summary

The thermal and mechanical design of the high-pressure turbine rotor was conducted with the objective of meeting expendable engine life goals at the maximum rated power condition conforming to the cycle parameters listed below.

Turbine Inlet Temperature	= 2300°F
Rotor Speed	= 63,000 RPM
Blade Relative Total Temperature	= 1982°F
Compressor Discharge Pressure	= 327.6 psia
Core Flow	= 10.0 lbm/sec
Compressor Discharge Temperature	= 910°F
Turbine Inlet Pressure	= 316.1 psia

With a rotor tip diameter of 6.65 inches, the airfoil tip speed is 1830 ft/sec and represents a challenging design parameter for this turbine. The design mission for the turbine rotor is 7 hours, 6 minutes in duration and includes 36 minutes at maximum power operation. A life goal of 50 mission hours was established at the outset of this effort and was deemed to be sufficiently conservative to ensure adequate design margin.

The laminated turbine rotor was designed within configurational constraints that would apply to a typical two-spool expendable engine of this size class, such as the AiResearch TFE Model 1050-12. These constraints include a bore diameter of 1.35 inches to accommodate the passage of a gas generator tie-shaft and a low-pressure spool shaft, and an axial length of realistic proportions. Curvic couplings, both fore and aft, have been included in the design and analysis. A twin-knife stepped labyrinth seal has been included on the forward side of the rotor as a critical element of the airfoil cooling flow supply scheme. A secondary flow analysis of the gas generator portion of the TFE Model 1050-12 was conducted to quantify flow and thermal boundary conditions surrounding the rotor for incorporation into a thermal analysis at the design condition.

The disk employs a side-entry cooling scheme, as shown in Figure 40, which offers the best compromise of possible coolant supply methods. This approach yields adequate rotor burst margin, provides for efficient usage and distribution of cooling air, and presents the opportunity for post-bonding ultrasonic inspections of the critical bore region to verify bond integrity. The use of a tangential cooling flow inducer to accelerate the fluid to wheel speed at the supply orifice is planned and will result in a 100°F reduction in coolant relative temperature with respect to the rotor blades.

The rotor is fabricated using Astroloy laminates of both 0.015-inch and 0.020-inch thicknesses, which are diffusion bonded together following photochemical machining (PCM) of internal passages. This process allows for a complex blade cooling geometry and a novel approach to supplying coolant to each blade at the disk rim. The thinner laminates are used sparingly in the turbine near the aft portion of the airfoil, where they allow increased internal flow area and improved cooling. The forward and aft portions of the disk, outboard of the airfoil chord region, are solid end plates of Astroloy separately bonded to the central laminated structure (see Figure 40). The end plates
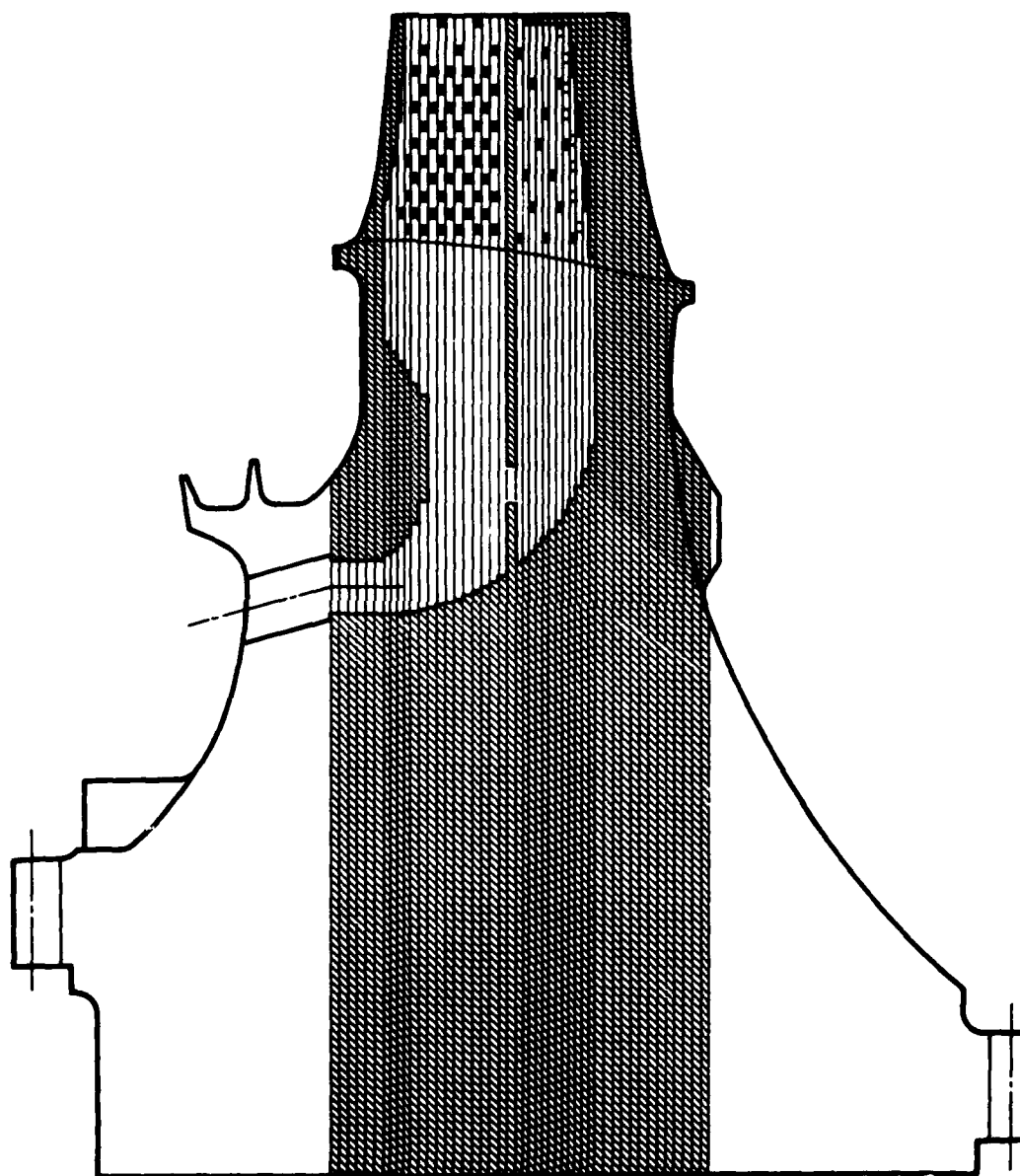
Figure 40.   Small Laminated Axial Turbine Design.

reduce the number of laminates required in the rotor with benefits in processing time, dimensional tolerances, and design simplicity.

Aerodynamic Design

The laminated-rotor turbine is a scaled version of the Low Aspect Ratio Turbine (LART), which has been designed and developed under Air Force Contract F33615-74-C-2017.

The laminated rotor scale factor was determined by the required flow function of the TFE Model 1050-12 cycle. The linear scale factor is 0.4 of the LART size. The flow path is shown in Figure 41. Since the laminated turbine operates at a condition different from the LART design point, the predicted aerodynamic performance of the laminated turbine has been modified accordingly. The TFE 1050-12 high-pressure (HP) turbine design point is shown below:

Corrected Flow	1.025 lbm/sec.
Pressure Ratio	2.694
Inlet Temperature	2760°R
Inlet Pressure	316.1 PSIA
Speed	63000 RPM
Work	164 BTU/lbm

Based on the LART cold rig test results, at the HP turbine operating pressure ratio and speed, the tested efficiency is 91 percent at 1-percent clearance over blade height. However, since 1-percent clearance is not practical for the laminated rotor size, increasing the operating clearance to a practical range of 1.5 percent results in a 90-percent efficiency of the HP turbine. The performance penalty due to rotor-cooling is accounted for in the cycle model. The amount of cooling flow is considered a total loss to the cycle. This assumption has been substantiated through rig testing of similar cooled turbines.

Figure 41. HPT Hot Flowpath

70

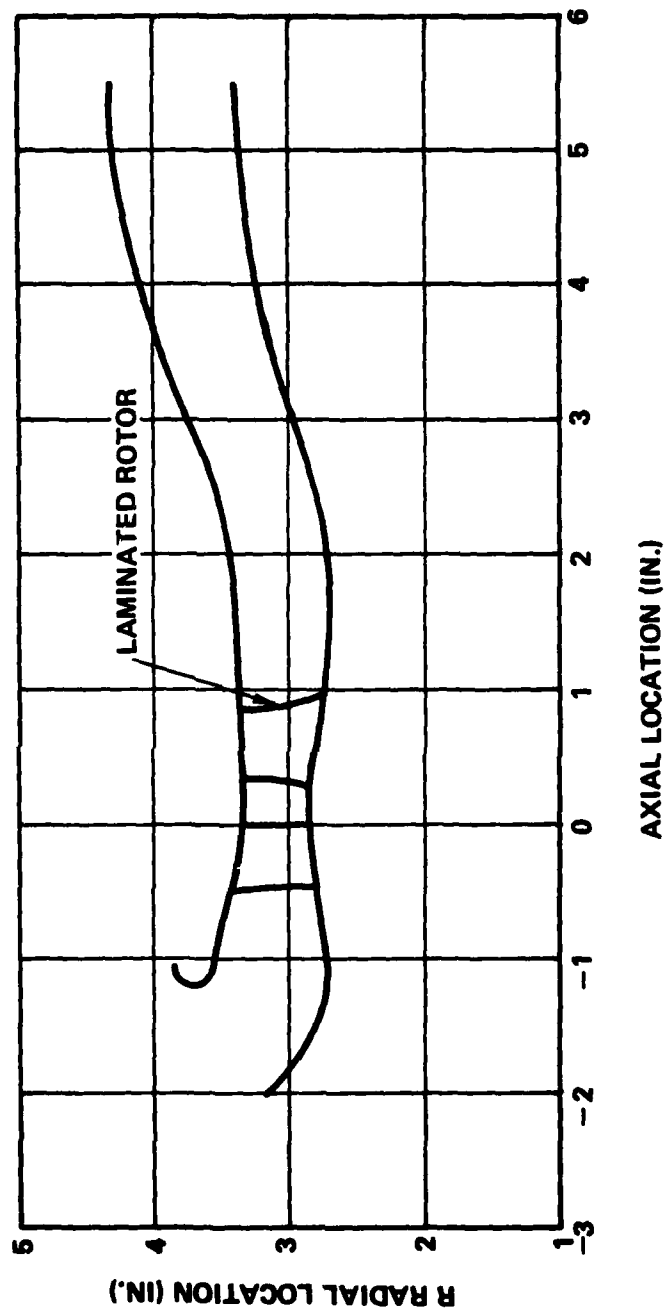A direct scale of the rotor blade would produce a trailing-edge thickness of 0.016 inch, which is below the minimum value of 0.018 inch considered acceptable for the laminated design. Therefore, to maintain the same trailing-edge blockage, the number of blades has been reduced from 50 to 46. The rotor solidity is maintained by scaling the airfoil up accordingly. The slight reduction in aspect ratio has no significant effect on turbine performance.

In support of the rotor heat-transfer and stress analyses, aerodynamic loading analyses have been performed for five airfoil sections. A typical loading at midspan is shown in Figure 42.

Airfoil Design and Analysis

Cooling Design Synthesis and Thermal Analysis - The small physical size of the turbine airfoil relative to laminate sheet thickness, laminate fabrication dimensional limitations, and profile machinery tolerances, makes it very difficult to achieve a cooling circuit design commensurate with the turbine operating conditions and available material properties. In particular, the trailing-edge region of the airfoil cannot be internally cooled due to its small thickness and the desire to avoid the expensive and necessarily delicate machining procedures which might be required. Several typical airfoil cooling circuits were examined for feasibility, and it became apparent that film cooling the trailing-edge region offered temperature reductions which would greatly enhance rupture life of the component. The final airfoil design selected is a one-pass, two-cavity cooling scheme as shown in Figure 43.

Cooling air is supplied to the leading-edge cavity at a pressure of 217 psia, passing through a dense array of pin fins and exiting at the tip. The trailing-edge cavity supplies the pressure-side film cooling holes and also uses pin fins for heat-transfer enhancement. Film cooling holes are etched with a
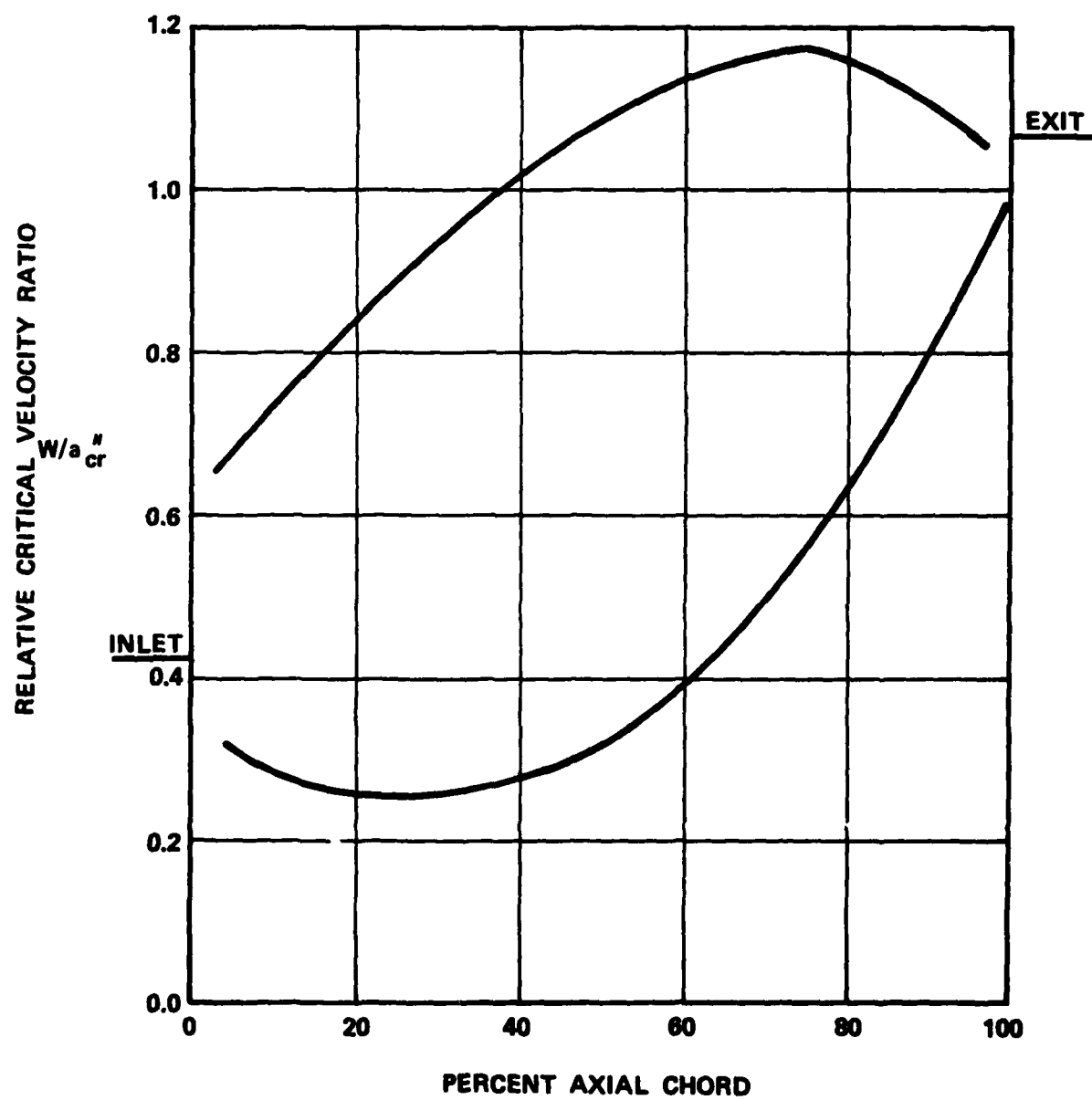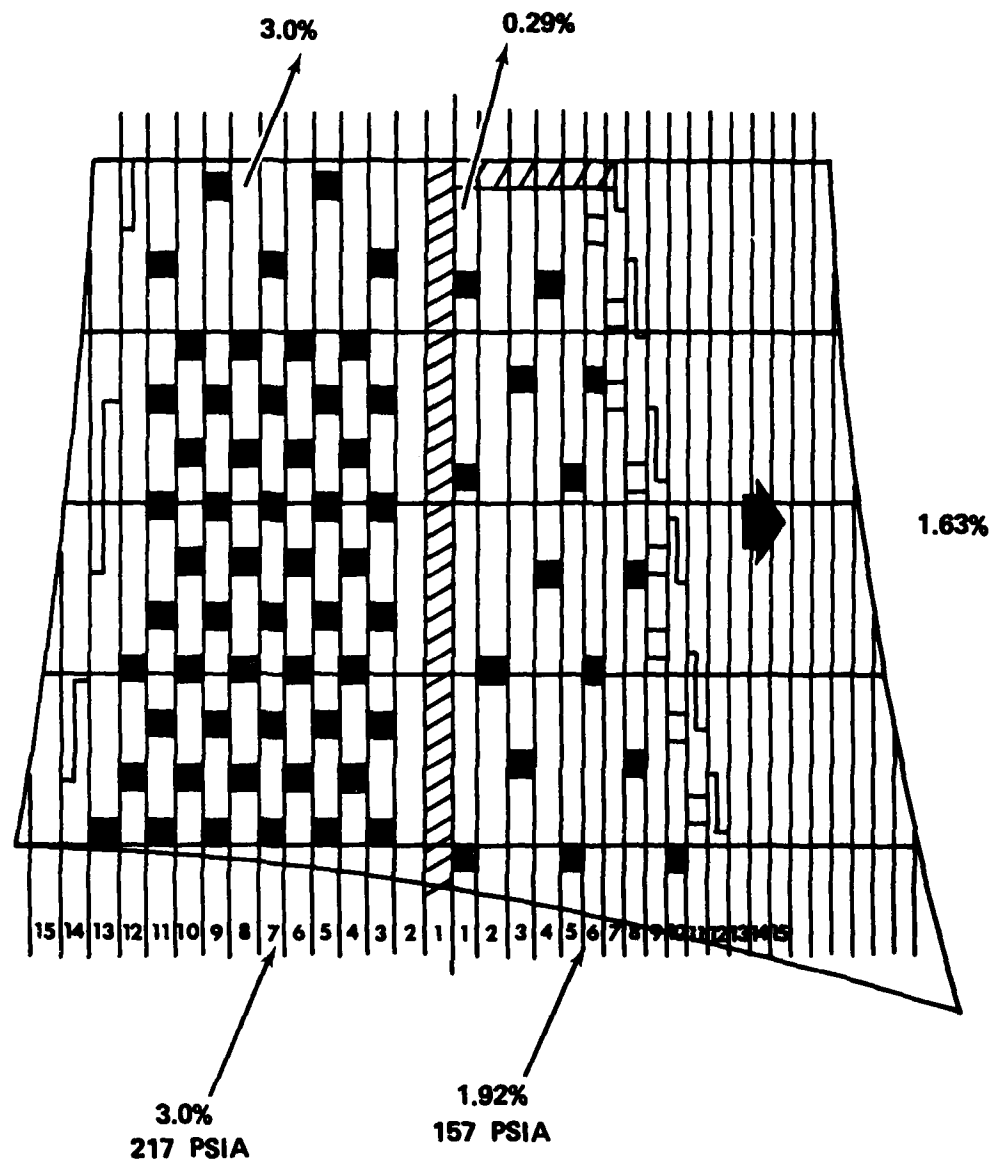
71

Figure 42.   Mid-Span Blade Loading.

Figure 43. CME Laminated Turbine Blade Cooling Scheme
4.9-Percent Core Flow

73

radial angle of 30°, taking full advantage of the etching capability to improve film effectiveness. The cooling air is throttled down to 157 psia for the trailing-edge cavity in order to optimize the cooling air velocity through the film cooling holes. A blade tip dust hole in the trailing-edge cavity provides cooling for the tip.

The design of the airfoil cooling air passage depends on the allowable minimum etch width. The Astroloy sheets must be etched with passages perpendicular to the sheet surface. A staggered half-etch technique is used in the airfoil to maximize the flow area by etching halfway through one side of the laminate sheet then half etching through the other side of the laminate after indexing. Thinner 0.015-inch laminate sheets are used in the trailing edge to further maximize the cooling airflow area by allowing the passage to more closely follow the external contour of the airfoil. Airfoil wall thicknesses represent a compromise between the optimum taper ratio and maximizing the cooling flow area to increase cooling effectiveness. Table 4 sumarizes the airfoil wall thicknesses.

The cooling flow characteristics of the airfoil were determined using the AiResearch CHANFLO computer program. CHANFLO con siders the impact of heat transfer between the coolant and passages for known external boundary conditions, fluid frictional effects, solid body rotation effects, passage area changes, expansions and contractions, and variations in fluid transport properties. Figure 43 summarizes the airfoil cooling flows. A total of 4.90-percent W_{core} is used.

Preswirl nozzles are used to reduce the effective cooling air temperature seen by the rotor by accelerating the flow through the nozzles in the direction of wheel rotation. It was decided that a bore-entry cooling scheme was not practical for the cruise-missile engine, since bore-entry cooling schemes are normally used in conjunction with a mid-stage compressor bleed

74

**TABLE 4. CME LAMINATED TURBINE
WALL THICKNESSES**

Radius in.	Span %	Nominal in.	Minimum in.
2.822	0	0.023	0.018
2.946	25	0.023	0.018
3.070	50	0.020	0.015
3.194	75	0.018	0.013
3.319	100	0.017	0.012

cooling air supply system to offset the solid body temperature rise going from the bore of the disk to the airfoil.

External heat-transfer boundary conditions were calculated at the design point using aerodynamic data and airfoil geometry. Film coefficients were calculated using AiResearch computer program 700 which uses cylinder in cross flow for the leading-edge and turbulent flat plate for the suction and pressure sides. The film coefficients were then corrected for free-stream turbulence effects based on information from literature and component testing experience.

The heat-transfer and pressure-drop characteristics of the airfoil cooling air cavities were assumed to be similar to smooth wall passages with pin fins, since the flow is parallel to the laminate direction. The general approach to solving flow distribution problems for cooled turbine blades at AiResearch is a computerized compressible-flow network analysis. This computer program assumes the pin fins to be circular in shape. The radial spacing of the pins in the analysis, therefore, was reduced so that the flow area between two round pins of two different rows would have the same flow area as the two corresponding square pins in the actual airfoil. The pin-fin locations are·shown in Figure 43.

The rotor blade critical life section occurs at a radial station where temperatures and stresses combine in a fashion that produces a minimum life. Since creep-rupture life is very sensitive to temperature level, the critical section can usually be identified by examination of the turbine inlet temperature radial profile. The inlet temperature profile used in this analysis is shown in Figure 44 and was assumed to be similar to other AiResearch axial turbines with reverse-flow burners.

With the critical section at 25 percent of the radial span (measured from the hub) a two-dimensional, steady-state, thermal
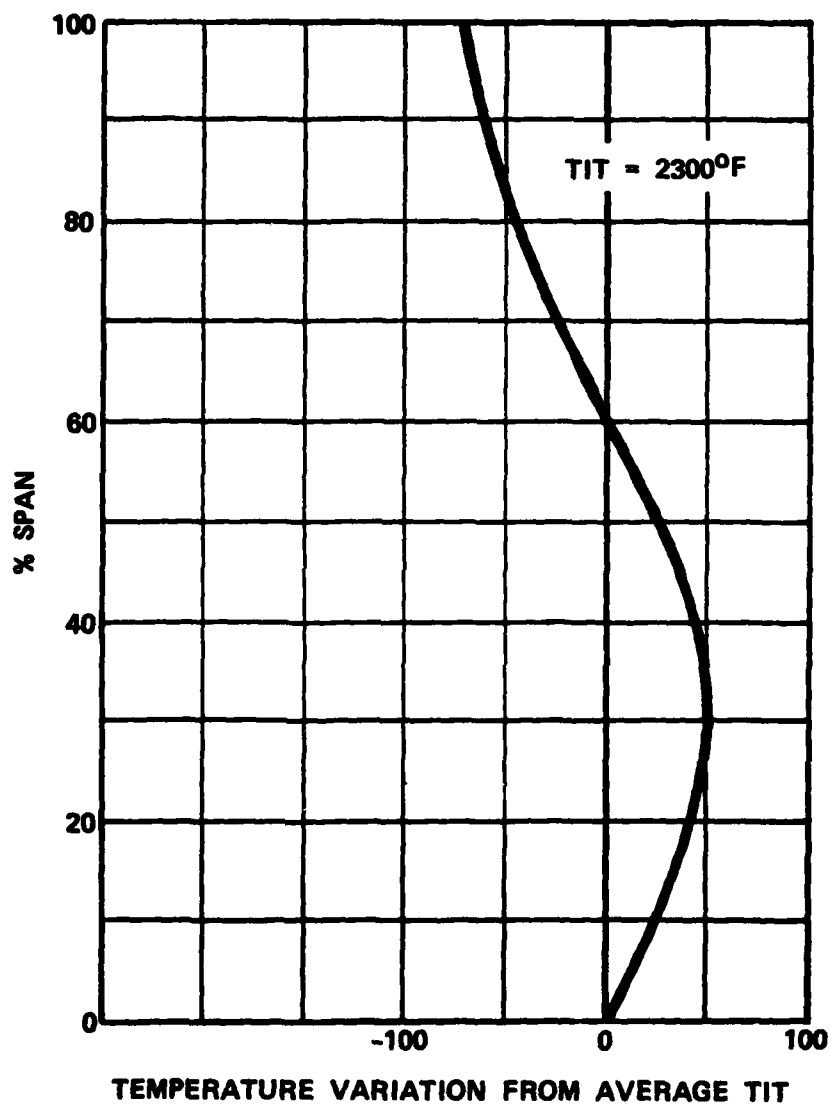
Figure 44. Cruise Missile Engine Turbine Inlet Profile

analysis was completed to assess the effectiveness of the cooling design in maintaining acceptable local temperatures. Temperature and heat-transfer coefficient boundary conditions utilized in the analysis are shown in Figures 45 and 46. Isotherms predicted at the critical span section are presented in Figure 47 and indicate a range in temperature from 1300°F in the centerbody region to 1850°F at the extreme trailing edge. The section mass-average temperature of 1500°F results in a cooling effectiveness of 0.50 for the design.

The acceptability of these predicted temperatures can be judged based on the design philosophy employed, which recognizes a limited ability to cool the trailing edge because of the small physical size of the airfoil. The blade orientation has, therefore, been adjusted to induce compressive loading in the trailing edge at the expense of higher tensile stresses at the centerbody on the suction side. These centerbody stresses are tolerable because of the lower metal temperatures and, therefore, a balanced life design is achieved.

Airfoil Stress Analysis and Life Predictions - The stress analysis of the airfoil is directed toward achieving a design solution that avoids excessively high local stresses which might lead to short-term tensile or fatigue failure, and toward making a quantitative prediction of airfoil creep-rupture life. The analysis takes two forms which complement one another in satisfying design criteria. The first of these is a three-dimensional finite-element analysis, and the second is a one-dimensional, finite-difference, creep-rupture analysis.

In this design effort, the three-dimensional finite-element stress analysis was conducted using the AiResearch computer program ISO3DQ and was directed at several specific objectives.
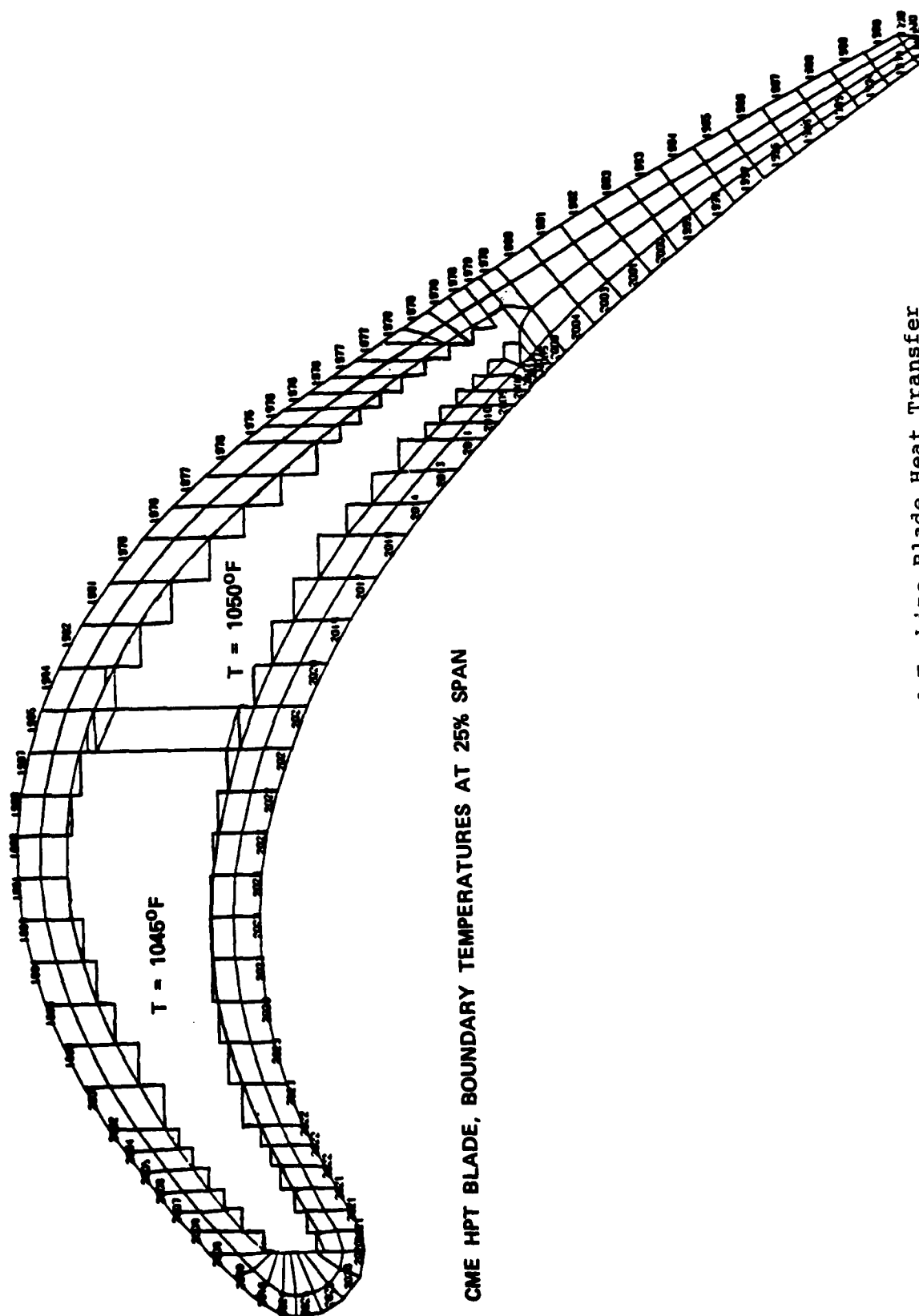
CME HPT BLADE, BOUNDARY TEMPERATURES AT 25% SPAN

T = 1045°F

T = 1050°F

Figure 45. CME Laminated Turbine Blade Heat Transfer
Boundary Temperature (°F)

79

h = 1920

h = 750

CME HPT BLADE HTC's AT 25% SPAN
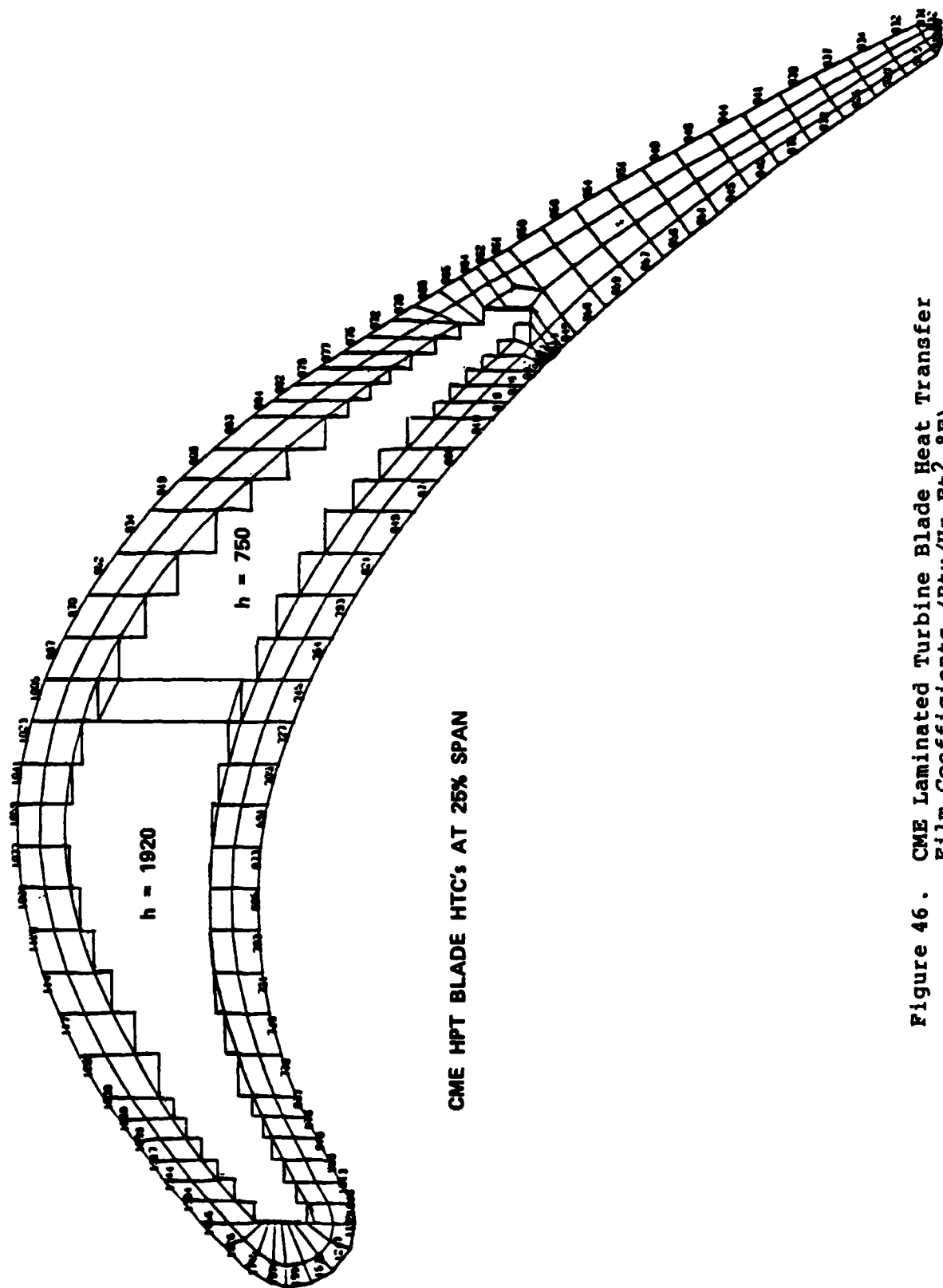
Figure 46. CME Laminated Turbine Blade Heat Transfer
Film Coefficients (Btu/Hr-Ft2-°F)

CME HPT BLADE ISOTHERMS
AT 25% SPAN
BULK TEMPERATURE = 1500°F
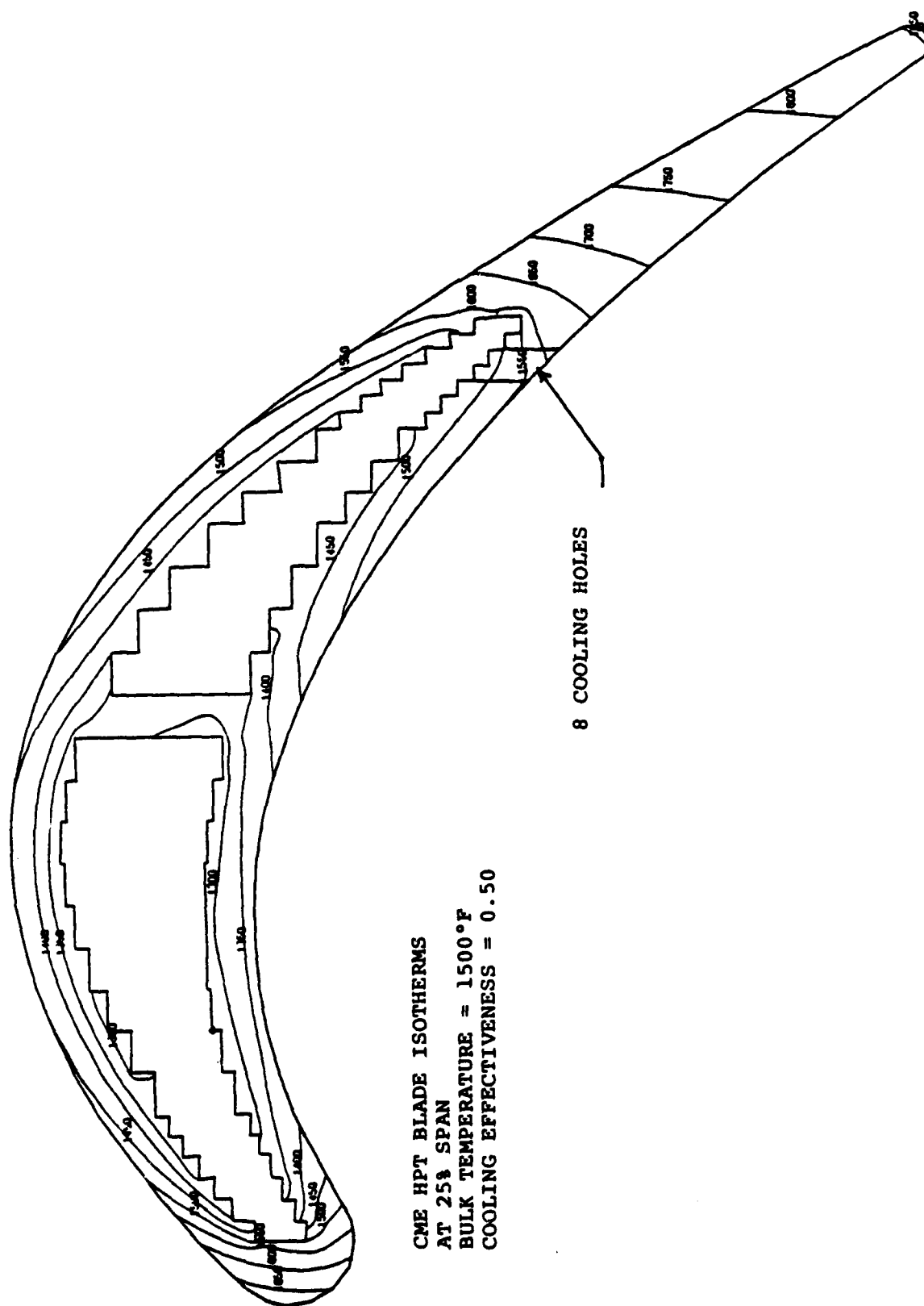COOLING EFFECTIVENESS = 0.50

8 COOLING HOLES

Figure 47.   CME Laminated Turbine Blade Isotherm Plot.

81

1) Limit the maximum peak stress of any point on the blade to less than the minimum yield strength, which is 97 ksi at 1550°F.

2) Minimize the background stresses for the film cooling holes in order to avoid any crack initiation at the holes.

3) Select blade lean and tilt values which provide optimum trade-off between blade peak stress and blade creep life objectives.

4) Provide quantitative substantiation, and hence increased confidence in the simpler one-dimensional stress calculations used for blade life estimation.

A 1000-node finite-element model was prepared, suitable for ISO3DQ type analysis (see Figure 48). The pins between the two walls were modeled as linear springs. The root was constrained for displacements in the radial direction. In-plane thermal expansions at the root were precalculated, and used as prescribed boundary conditions in subsequent runs. Root boundary conditions are, however, not very critical, since the region of interest lies between 25 percent and 50 percent of the blade span. A two-dimensional airfoil temperature distribution, calculated separately by the blade thermal analysis at the 25-percent span, was also included. Radial variation of the temperature was, however, ignored. Gas loads were also included in the analysis.

After several iterations between the three-dimensional blade stresses and blade life calculations, a lean of six degrees for the blade was adopted. This represented the best compromise between the blade stress and the blade life requirements.

Figures 49 through 51 show the blade stress distribution obtained for a 6-degree lean and zero-degree tilt. Various other
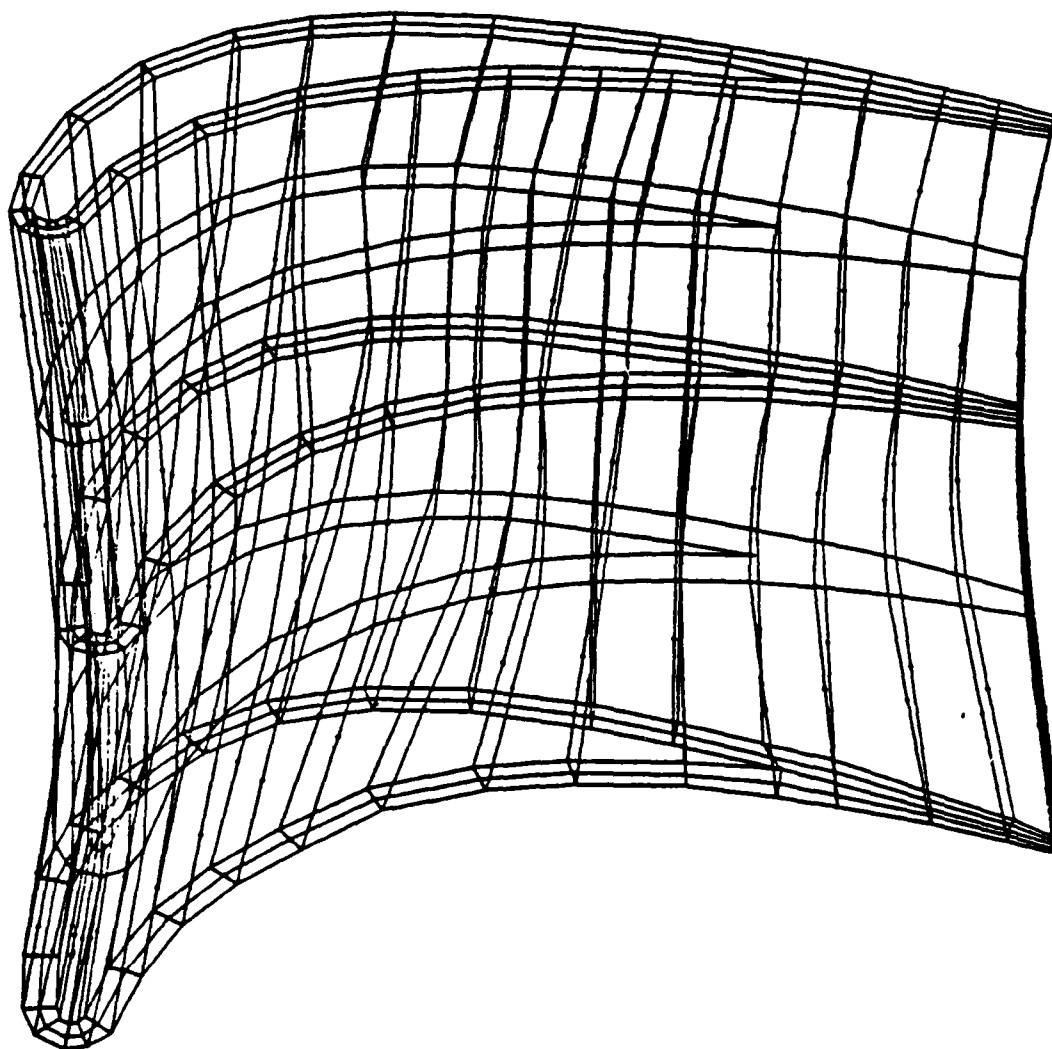
Figure 48. CME Laminated Turbine Blade Three-Dimensional Finite Element Stress Model.

40-PERCENT SPAN

25-PERCENT SPAN
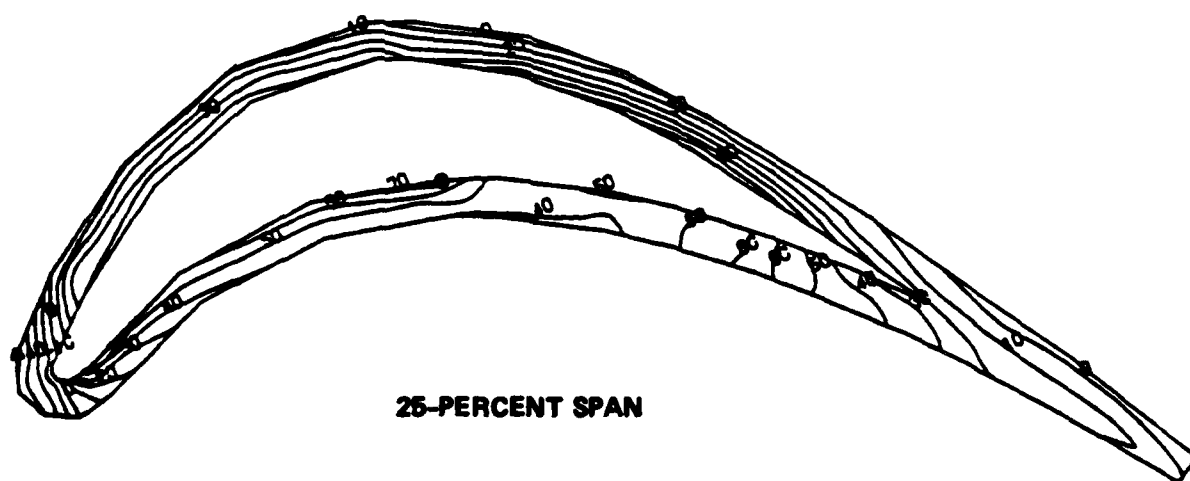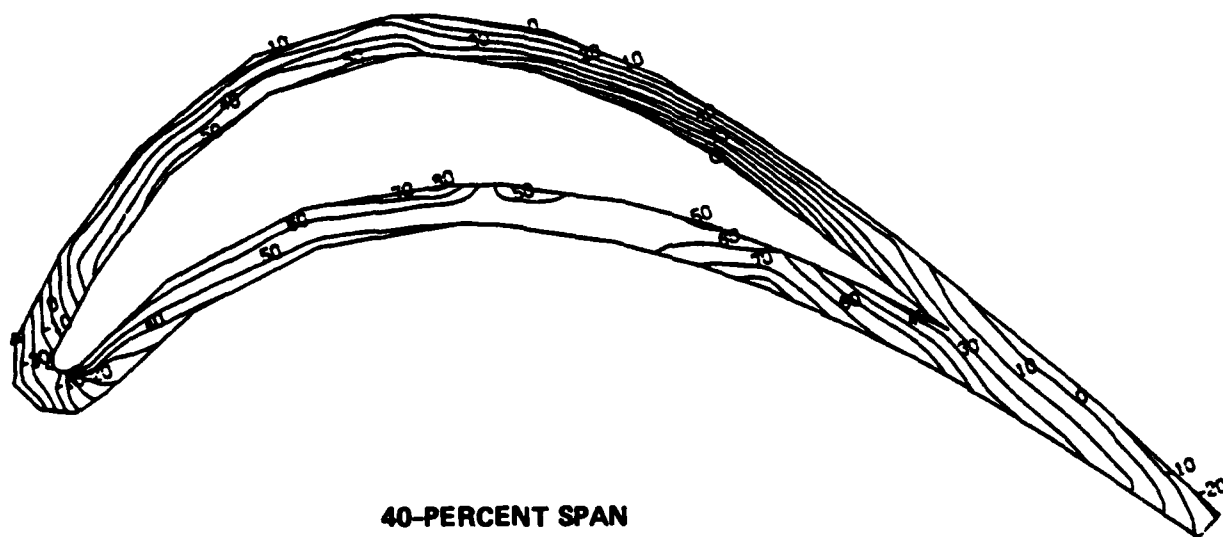
Figure 49.   CME Laminated Turbine Blade Radial Stresses (KSI).

84

CME BLADE   6 DEG LEAN

◄──── EXTERNAL

INTERNAL ──►

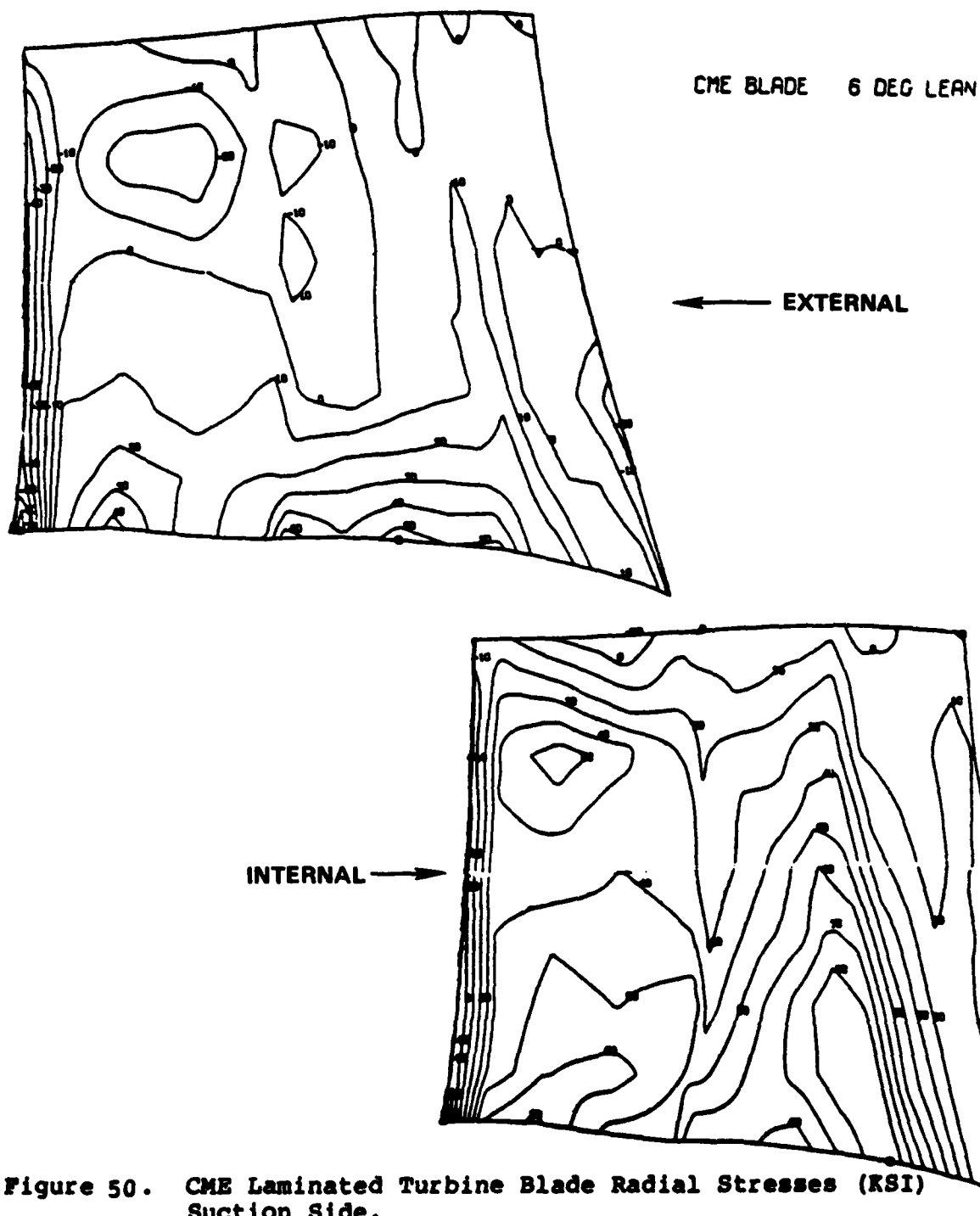**Figure 50.   CME Laminated Turbine Blade Radial Stresses (KSI)
Suction Side.**

CME LAMINATED TURBINE BLADE
RADIAL STRESSES (KSI)
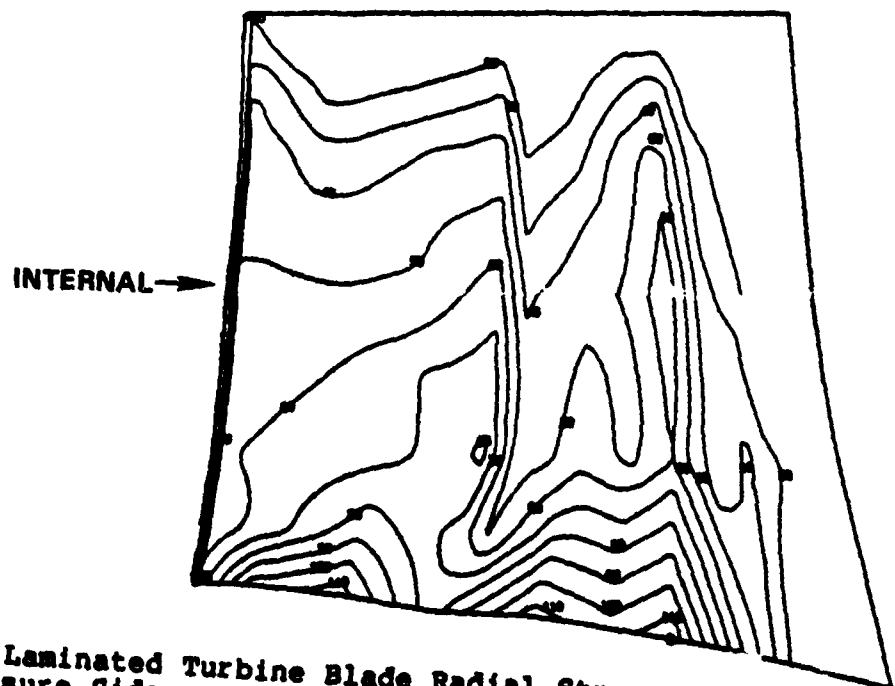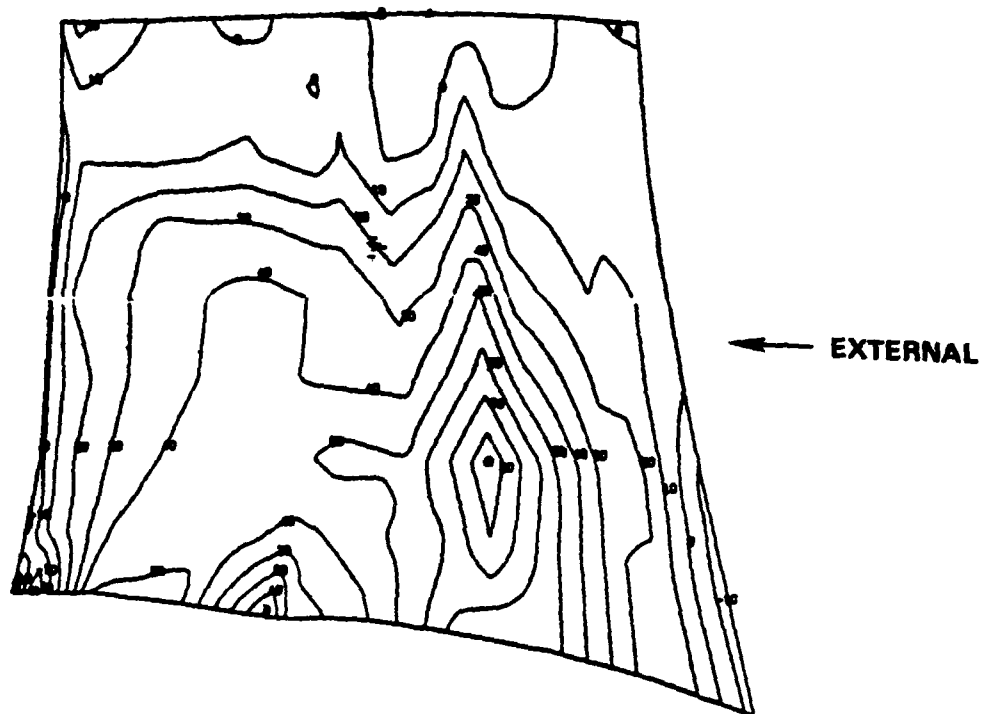PRESSURE SIDE

← EXTERNAL

INTERNAL →

Figure 51 . CME Laminated Turbine Blade Radial Stresses (KSI)
Pressure Side.

86

combinations of lean and tilt were also considered. Other design changes, such as the addition of one more rib near the trailing edge, were also analyzed but not adopted.

On the airfoil, suction surface stresses of 80 ksi magnitude are present locally and compressive stresses can be noted at the trailing edge due to the lean orientation selected. The pressure-surface stress display indicates the peak airfoil stress of 83 ksi occurs at the 25-percent span at about two-thirds of the axial chord position. At the local temperatures where this occurs, Astroloy has a minimum yield strength of about 100 ksi. The position of film holes with their attendant stress concentrating effect is shown to be in the vicinity of 40 ksi background stress levels. This is not anticipated to cause any local problem for this application.

The second form of analysis used to make quantitative life predictions employs techniques used at AiResearch on all cooled turbine blade designs currently in production and as such has substantial empirical verification. A two-dimensional beam-type analysis of the turbine blade is used to predict radial forces, shear forces, and bending moments at the critical section due to rotation and aerodynamic loading. These boundary conditions are placed upon a two-dimensional plane section model at the critical span, and a creep analysis is performed using the strain compatibility approach. Program 872 considers the creep behavior in the form of $d\epsilon = K\sigma^n \, dt$ for the given material using Larson-Miller creep data as input. The program uses a single radial blade section but provides the capability of allowing the section creep behavior to occur over a finite radial length of the blade, thus providing a measure of the loading change effect on a particular section due to the section rotation. The program assumes plane sections to remain plane.

The rotor blade life prediction criteria most appropriate for this application define life exhaustion as a point in time
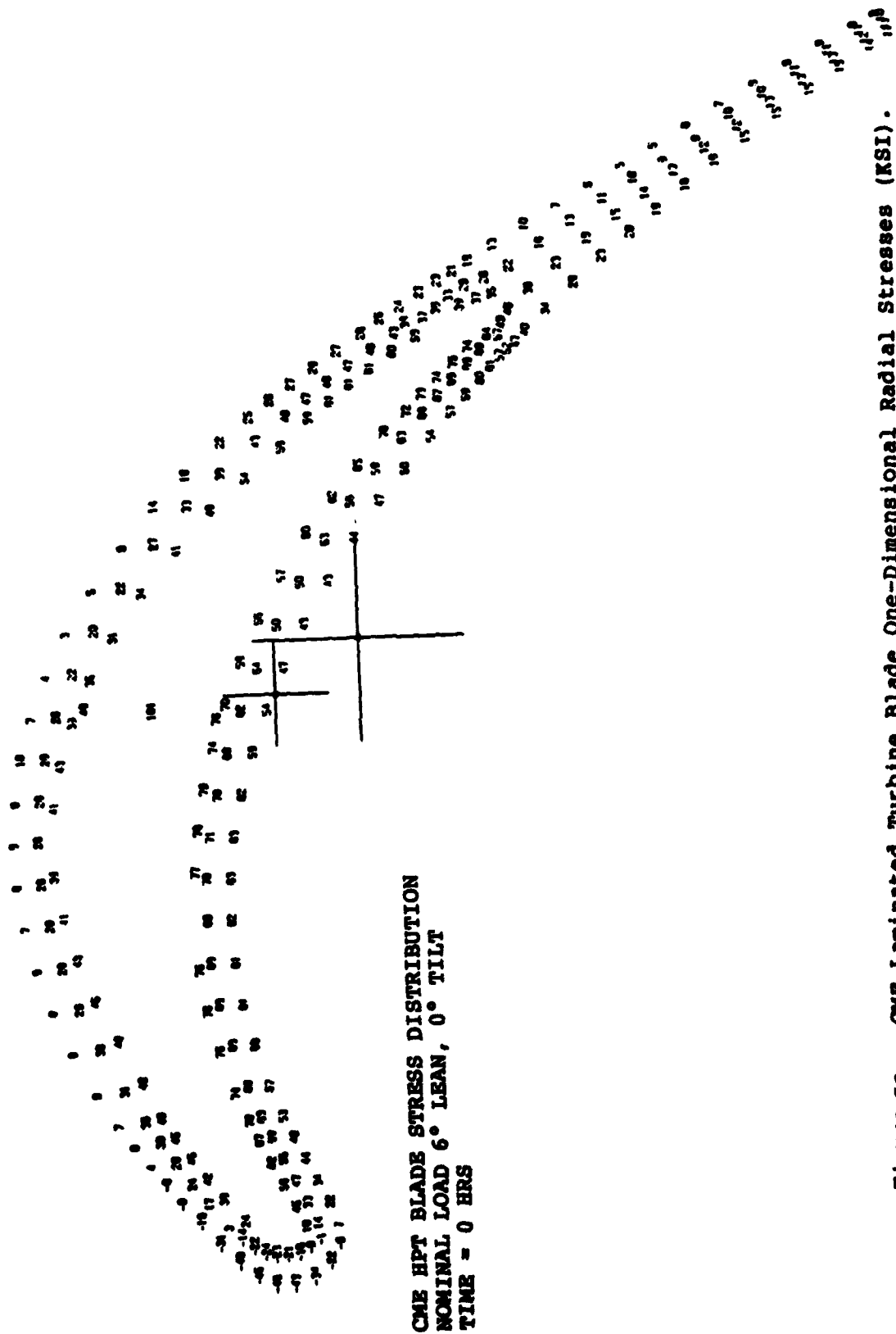
87

when a portion of the available material ductility has been exhausted at any point in the component such that crack initiation is imminent. For cooled turbine blading, a 2-percent creep strain is typically taken as the life-limiting condition. Fatigue damage of either high frequency or low frequency origin is often combined with it.

Figure 52 summarizes the nominal radial elastic stresses at 25-percent span (radius = 2.946). Results include thermal centrifugal and aerodynamic loads. The -3σ and typical 2-percent creep curves used for the life analysis are shown in Figure 53. The 2-percent creep curves are the best available estimated creep characteristics for Astroloy laminate material.

Figures 54 and 55 summarize the stress and strain distribution after 2-percent creep has been reached for a nominal blade. Maximum creep occurs at the trailing edge. Figure 56 presents the results of creep-rupture analysis of the airfoil with lives presented on a Weibull plot to indicate the statistical failure distribution from a nominal blade at 81 hours down to a "minimum characteristic life" of 12 hours. The latter value is obtained by combining nominal life, life with -3σ minimum material properties, life with maximum airfoil contour tolerance, and life with 50°F added to calculated metal temperatures. These independently define the worst-case deviations in life-determining parameters. The expression used to calculate the minimum characteristic life is presented below.

$$\text{Log } L_{min} = \text{Log } L_{NOM} - \sqrt{\sum_{i=1}^{3} (\text{Log } L_{NOM} - \text{Log } L_i)^2}$$

where L_i = Life for each parameter considered independently.

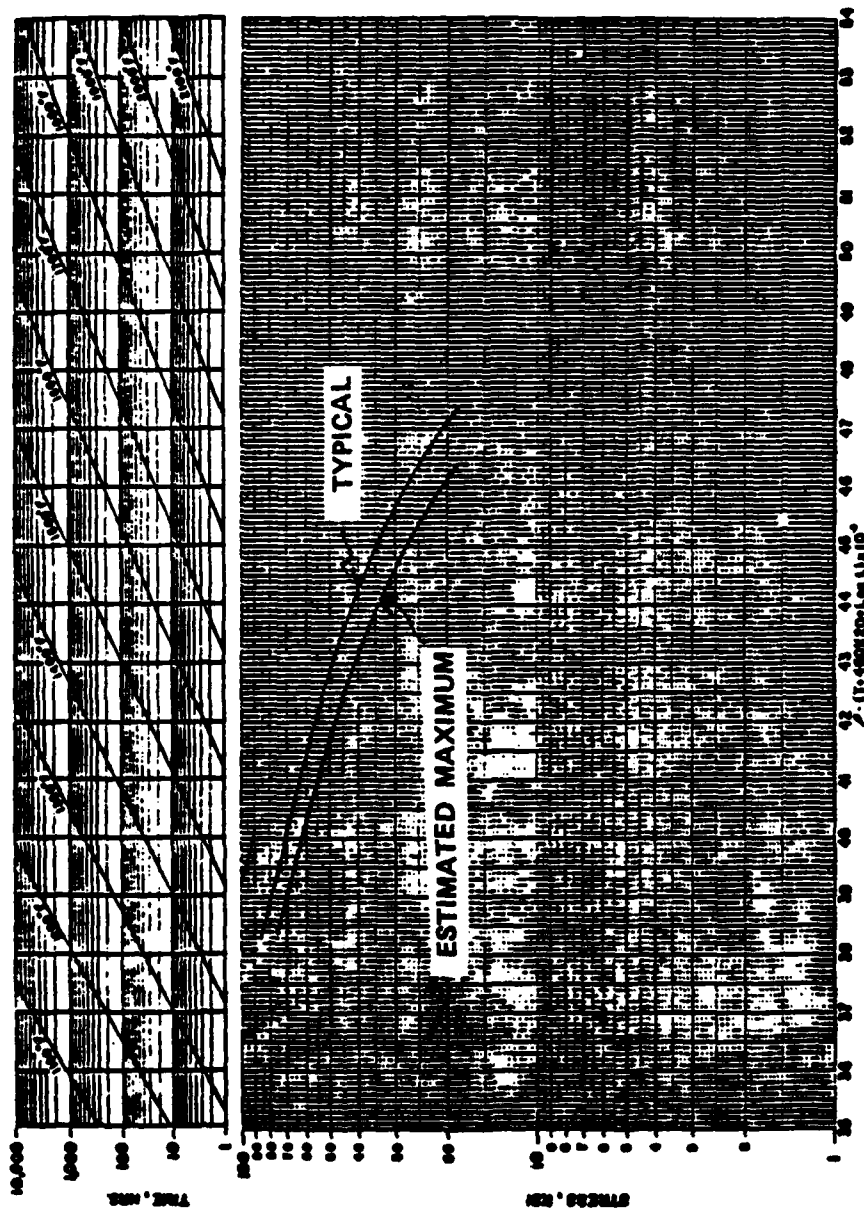CME HPT BLADE STRESS DISTRIBUTION
NOMINAL LOAD 6° LEAN, 0° TILT
TIME = 0 HRS

Figure 52. CME Laminated Turbine Blade One-Dimensional Radial Stresses (KSI).

Figure 53. CME Laminated Turbine Blade Material Curves for Life Analysis.

STRESS DISTRIBUTION
TIME = 80.9 HRS
NOMINAL BLADE

91
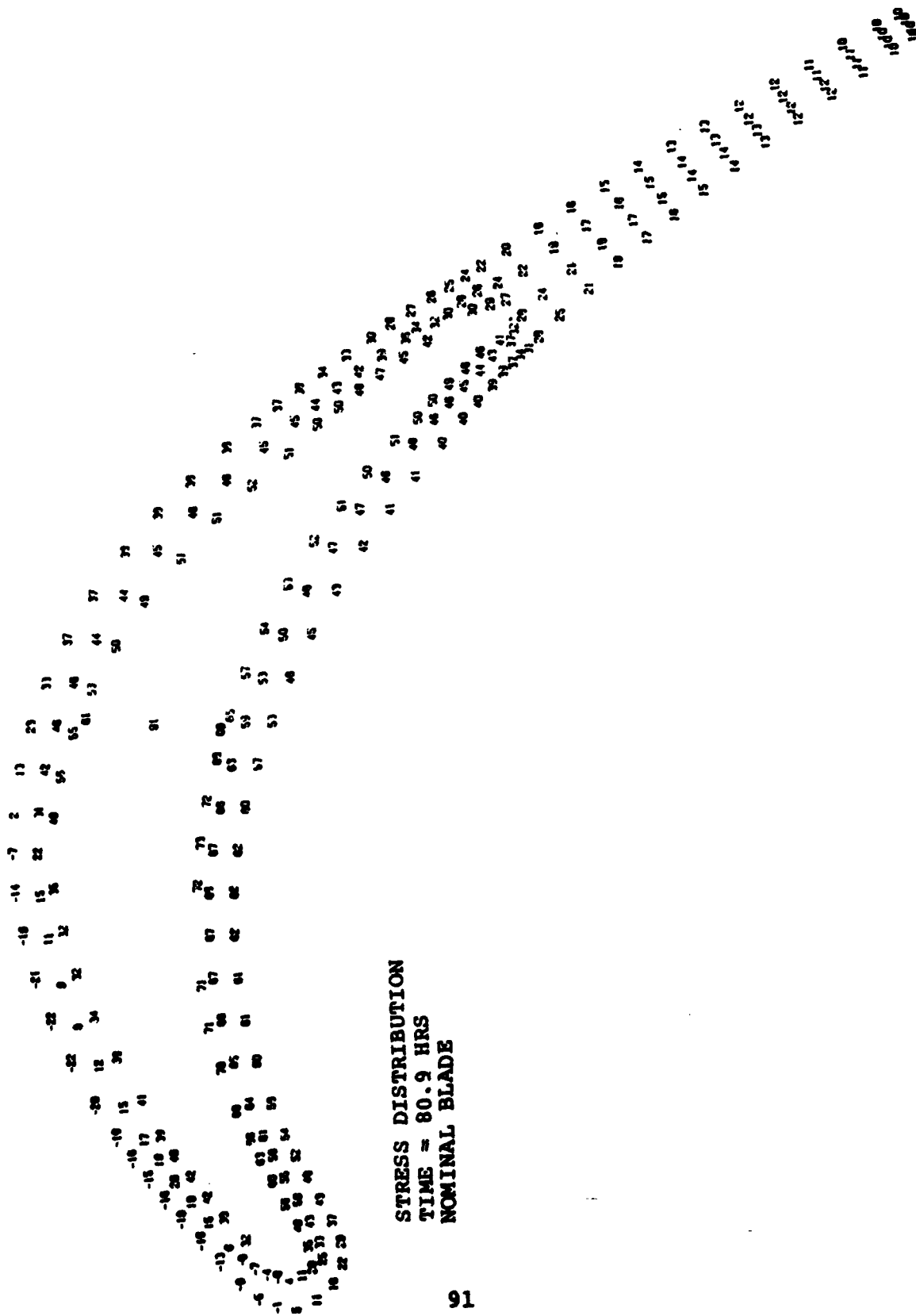
Figure 54. CME Laminated Turbine Blade Radial Stress Distribution After Creep (KSI).

CREEP DISTRIBUTION
TIME = 80.9 HOURS
NOMINAL BLADE
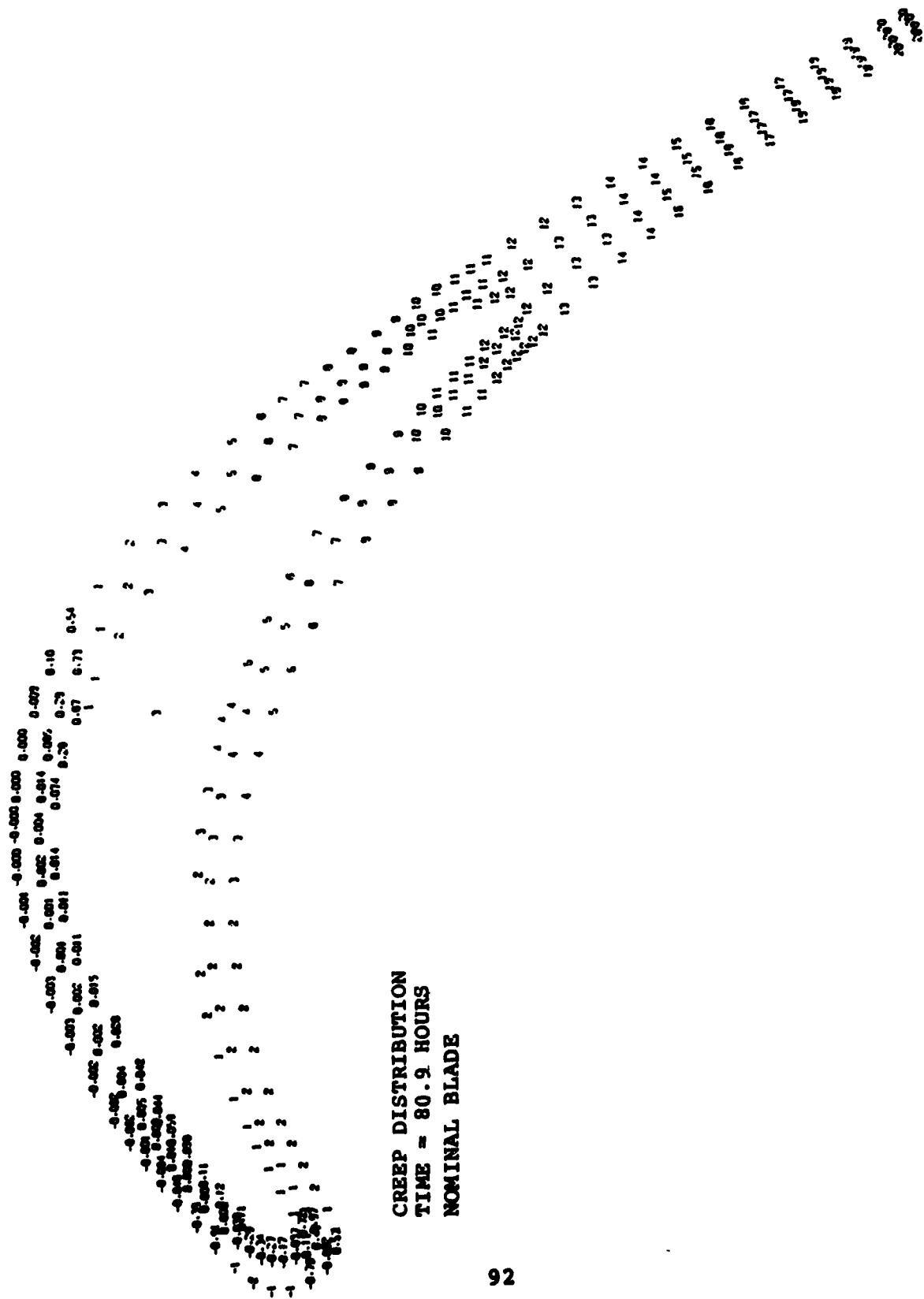
Figure 55. CME Laminated Turbine Blade Creep Distribution Strain - In./In. x 10^3.

LIFE CONDITION	FIRST ELEMENT TO 2% 2% CREEP LIFE
NOMINAL	81 HRS
+50°F ΔTm	24 HRS
MIN MATERIAL PROPERTIES	20 HRS
MAX CONTOUR TOLERANCES	49 HRS
-3σ LIFE	12 HRS
B50 LIFE	81 HRS

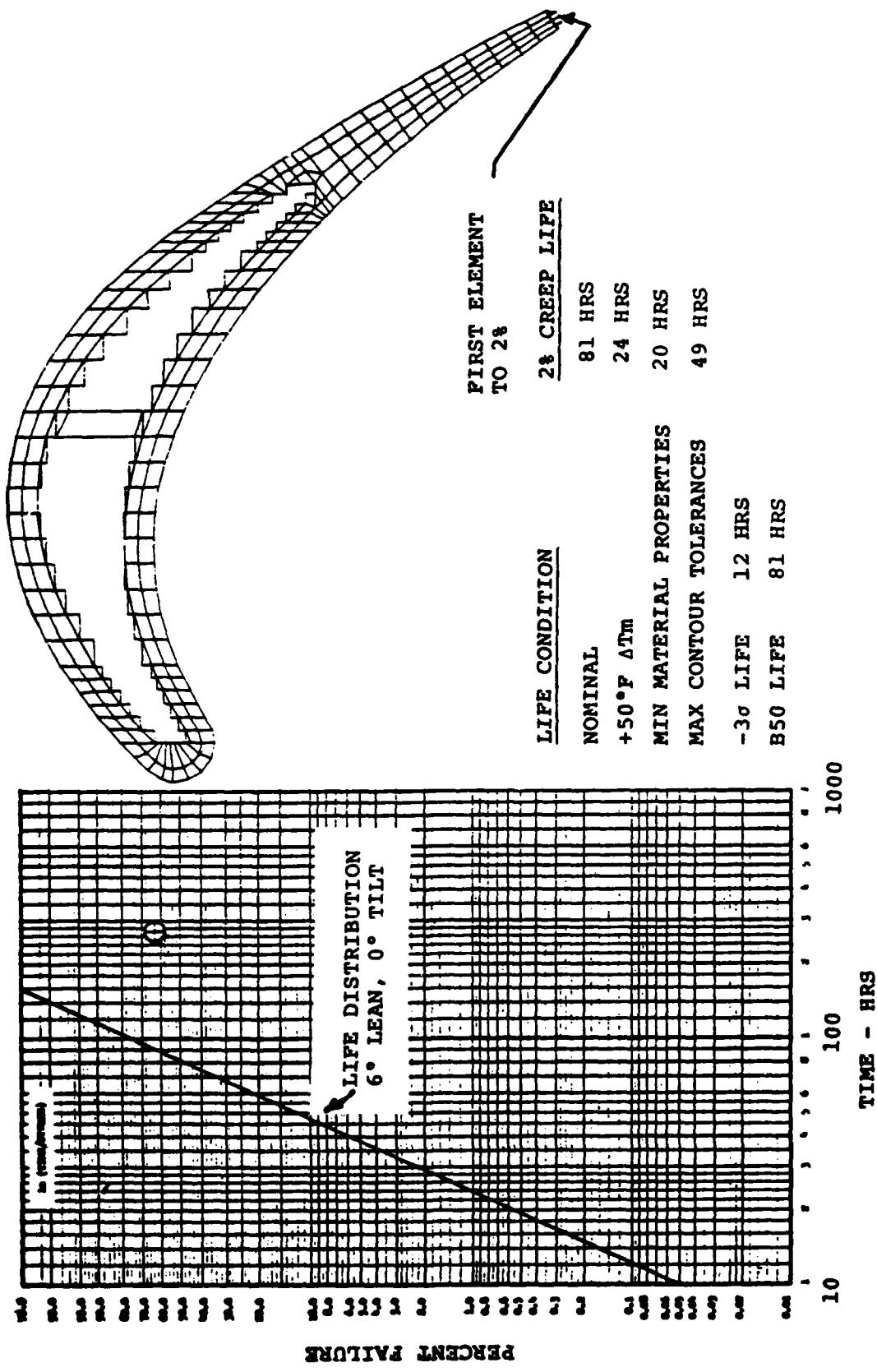LIFE DISTRIBUTION
6° LEAN, 0° TILT

PERCENT FAILURE

TIME - HRS

Figure 56 . CME Laminated Turbine Blade 2-Percent Creep Life Summary.

Vibration Characterization - A three-dimensional finite-element
vibration analysis of the laminated rotor airfoil was conducted
using AiResearch computer program ISOVIBE. The objective was to
characterize the mode shapes and frequencies of free vibration of
the airfoil to isolate potential interference problems with
upstream excitation sources and to determine if mode shapes
result in high vibration stress levels in regions of appreciable
mean stress. A finite-element model was prepared for this
purpose as shown in Figure 57. Pin-fin masses, areas, and stiff-
nesses were correctly simulated by radial ribs. The rotor disk
was not included in the analysis, since this required consider-
able additional complexity in the analysis. Instead, the blade
root was fixed in space with several constraint systems. The
disk was assumed to vary in stiffness from some lower bound to an
infinitely stiff case. The temperature effects at maximum T.I.T.
conditions were included by correcting for the changes in the
material modulus at 100-percent speed condition. A linear
temperature variation from zero to 100-percent speed was
implicitly assumed in drawing the Campbell Diagram in Figure 58.
Aerodynamic loading was also included in the analysis.

The resulting natural frequencies are presented in the
interference diagram of Figure 58 for the rigid blade root con-
dition. A possible stator count of 24 vanes in the TFE
Model 1050-12 has been included as an excitation source. The
potential for lower frequencies as a result of less than per-
fectly rigid root constraints has been assessed and would have to
be considered in a stator vane count selection. If an inter-
ference with the third mode occurred in the upper portion of the
operating range, it would not likely have any impact on the
design integrity due to predicted location of peak vibratory
stress. By the same evaluation, an interference with the second
mode, which is torsional, would produce higher alternating
stresses in the region of the pressure-side film holes and should
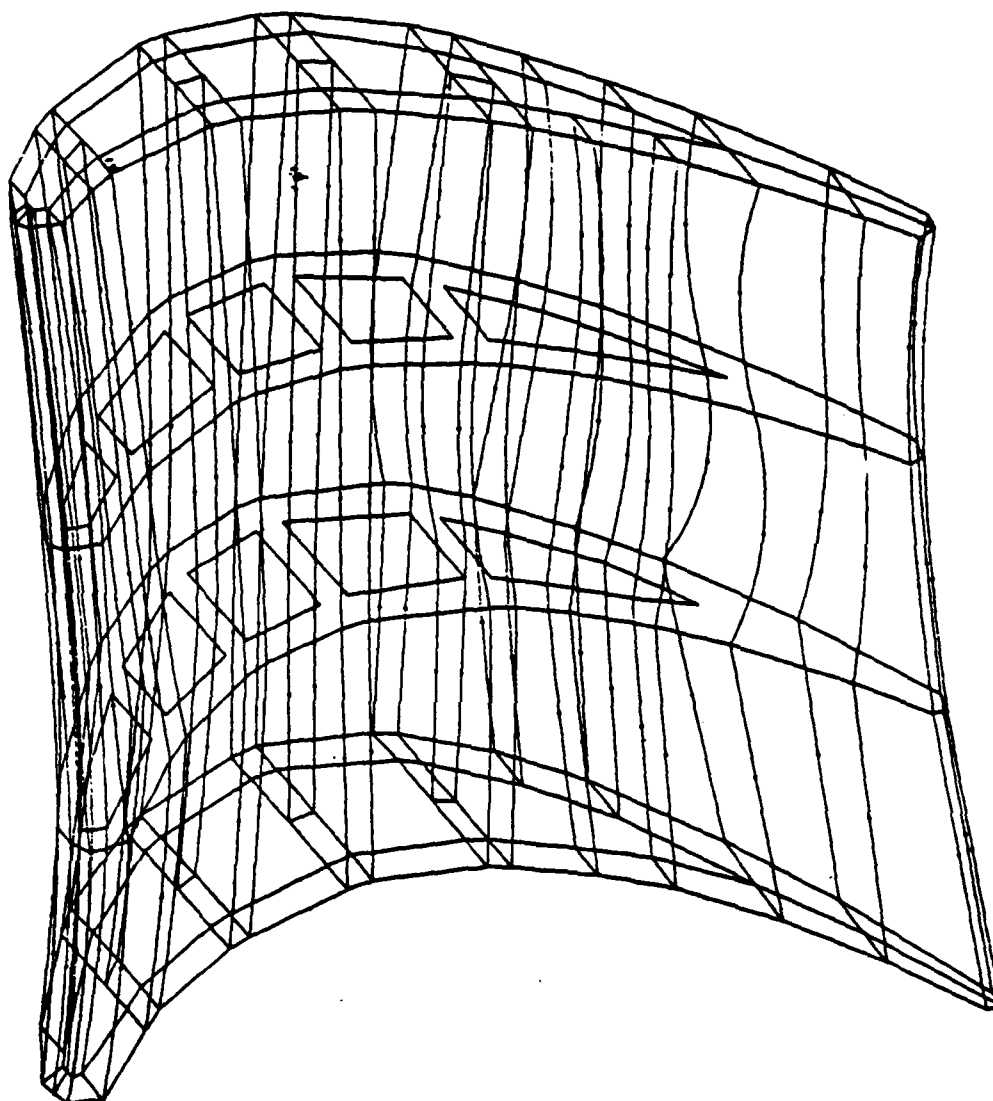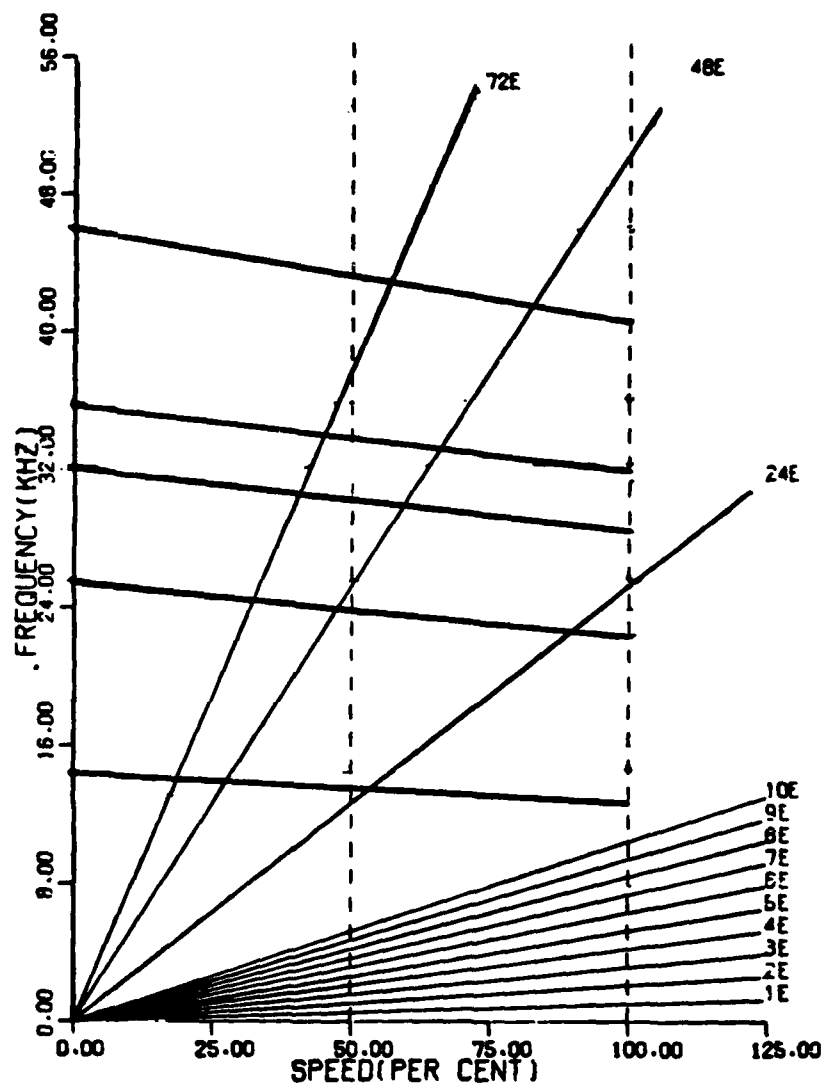be avoided by a judicious stator vane count selection. Mode

Figure 57. CME Blade ISOVIB Model.

95

Figure 58. CME Blade - Campbell Diagram for Rigid Blade Root Case.

shapes are presented for the first five fundamental frequencies in Figures 59 through 63.

A check on high-cycle and low-cycle fatigue damage combination was made by constructing a modified Goodman Diagram, as shown in Figure 64. This diagram was constructed with minimum values of ultimate and endurance strengths. For a maximum calculated blade stress of 84 ksia, the diagram gives an allowable alternating stress of 15 ksia. Since experience with unshrouded cooled blades had indicated vibratory stress levels to be less than 10 ksia, the design should be adequate, even in the unlikely circumstance that the location of the peak vibratory and peak steady-state stresses coincide.

Disk Design and Analysis

Structural Design Features - Since the integral rotor disk and blade design is fabricated from a series of individually etched laminates, it is possible and desirable to achieve complex internal geometry in both the disk and airfoil.

The disk design features a side-entry coolant inlet. The coolant is introduced into the rotor by 23 holes of 0.125-inch diameter. (Figures 65a to 65c illustrate the disk design.) These holes are slightly sloped as shown in Figure 66a in order to avoid creating a stress concentration in an anticipated higher stress region resulting from the step seal overhang to the main body of the disk. Internal cooling passages leading to the blade root inlets have been designed to achieve favorable cooling flow and load distribution characteristics. Each cavity supplies coolant to three blades, but within each laminate it feeds only two blades at a time. This is achieved by using two different feed region laminate etching patterns, alternating with each other (see Figures 65b and 65c). Besides providing additional cooling area for the disk, this design feature also results in a
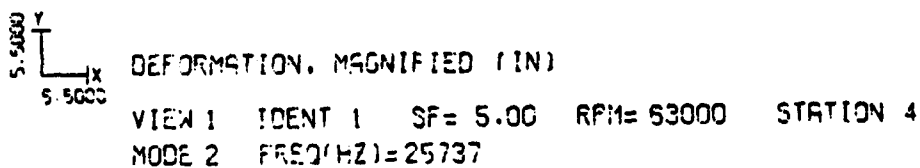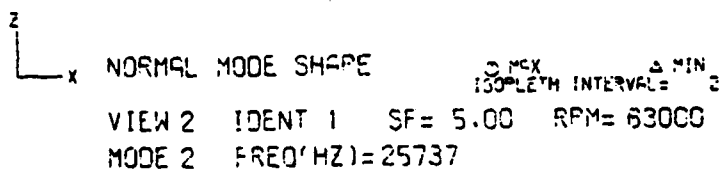
97
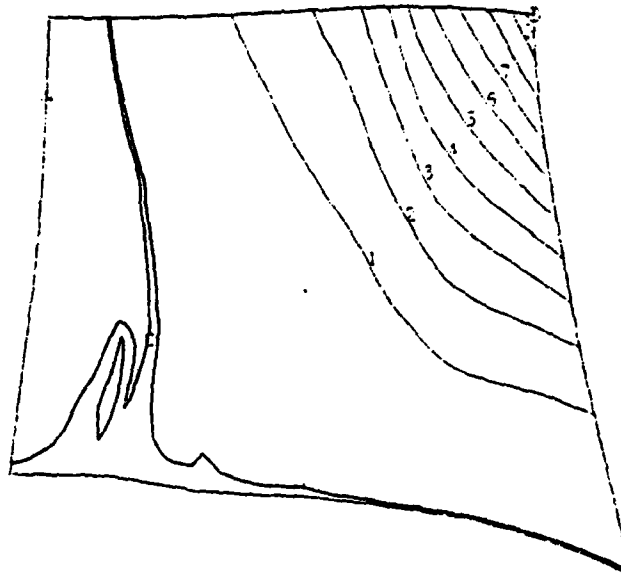
NORMAL MODE SHAPE

VIEW 2   IDENT 1   SF= 5.00   RPM= 63000
MODE 1   FREQ(HZ)=14713

C   CME BLADE - VIBRATION ANALYSIS
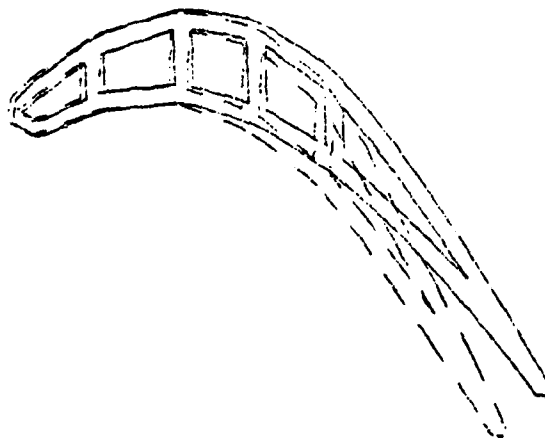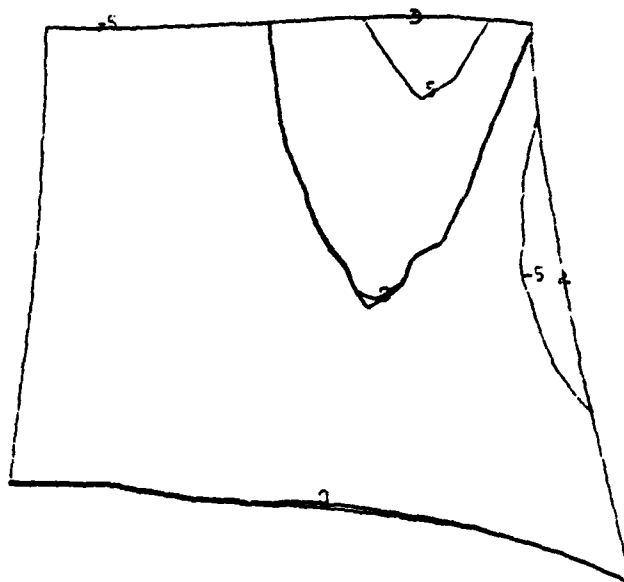
DEFORMATION, MAGNIFIED (IN)

VIEW 1   IDENT 1   SF= 5.00   RPM= 63000   STATION 4
MODE 1   FREQ(HZ)=14713

Figure 59.   CME Blade Mode Shapes - Mode 1.

NORMAL MODE SHAPE

VIEW 2   IDENT 1   SF= 5.00   RPM= 63000
MODE 2   FREQ(HZ)= 25737

CME BLADE – VIBRATION ANALYSIS

DEFORMATION, MAGNIFIED (IN)

VIEW 1   IDENT 1   SF= 5.00   RPM= 63000   STATION 4
MODE 2   FREQ(HZ)= 25737

Figure 60.   CME Blade Mode Shapes – Mode 2.
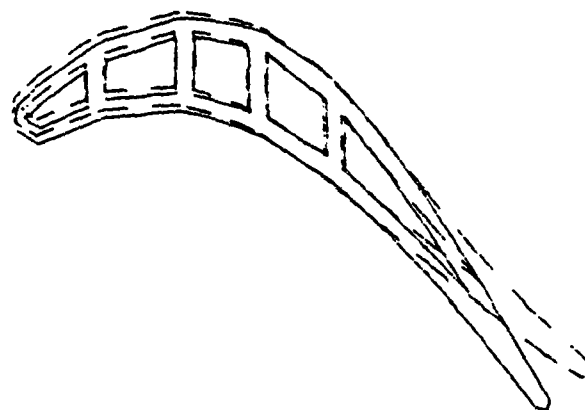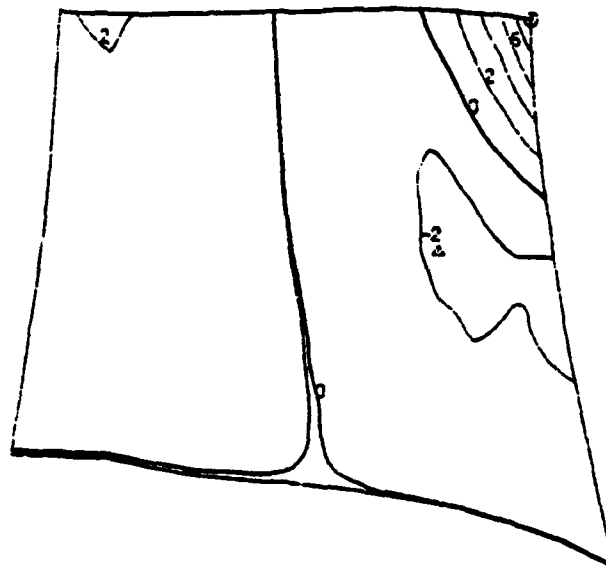
NORMAL MODE SHAPE   ISOPLETH INTERVAL= .5

VIEW 2   IDENT 1   SF= 5.00   RPM= 63000
MODE 3   FREQ(HZ)= 32440

C   CME BLADE - VIBRATION ANALYSIS
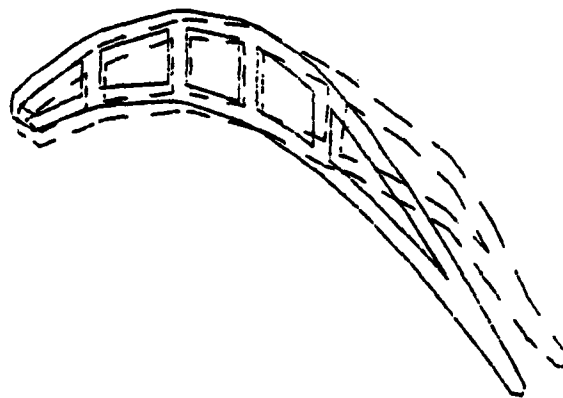

DEFORMATION, MAGNIFIED (IN)

VIEW 1   IDENT 1   SF= 5.00   RPM= 63000   STATION 4
MODE 3   FREQ(HZ)= 32440

Figure 61.   CME Blade Mode Shapes - Mode 3.

100

NORMAL MODE SHAPE

VIEW 2   IDENT 1   SF= 5.00   RPM= 63000
MODE 4   FREQ(HZ)=36135

C   CME BLADE - VIBRATION ANALYSIS

DEFORMATION, MAGNIFIED (IN)

VIEW 1   IDENT 1   SF= 5.00   RPM= 63000   STATION 4
MODE 4   FREQ(HZ)=36135

Figure 62.   CME Blade Mode Shape - Mode 4.
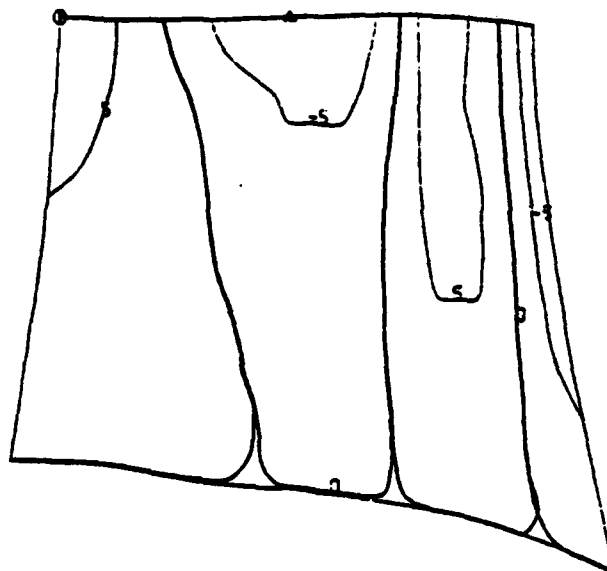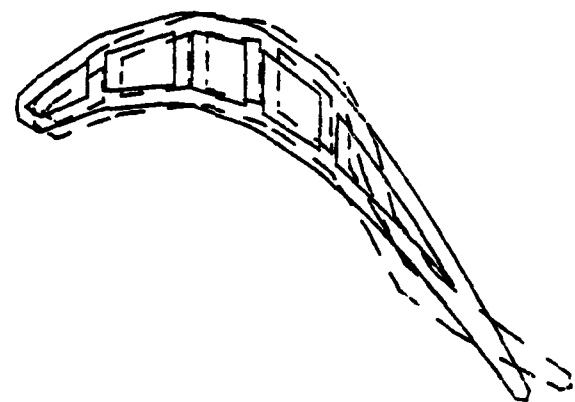
101

NORMAL MODE SHAPE   □ MAX   △ MIN
                    ISOPLETH INTERVAL= 5

VIEW 2   IDENT 1   SF= 5.00   RPM= 63000
MODE 5   FREQ(HZ)= 46022

C   CME BLADE - VIBRATION ANALYSIS

DEFORMATION. MAGNIFIED (IN)

VIEW 1   IDENT 1   SF= 5.00   RPM= 63000   STATION 4
MODE 5   FREQ(HZ)= 46022

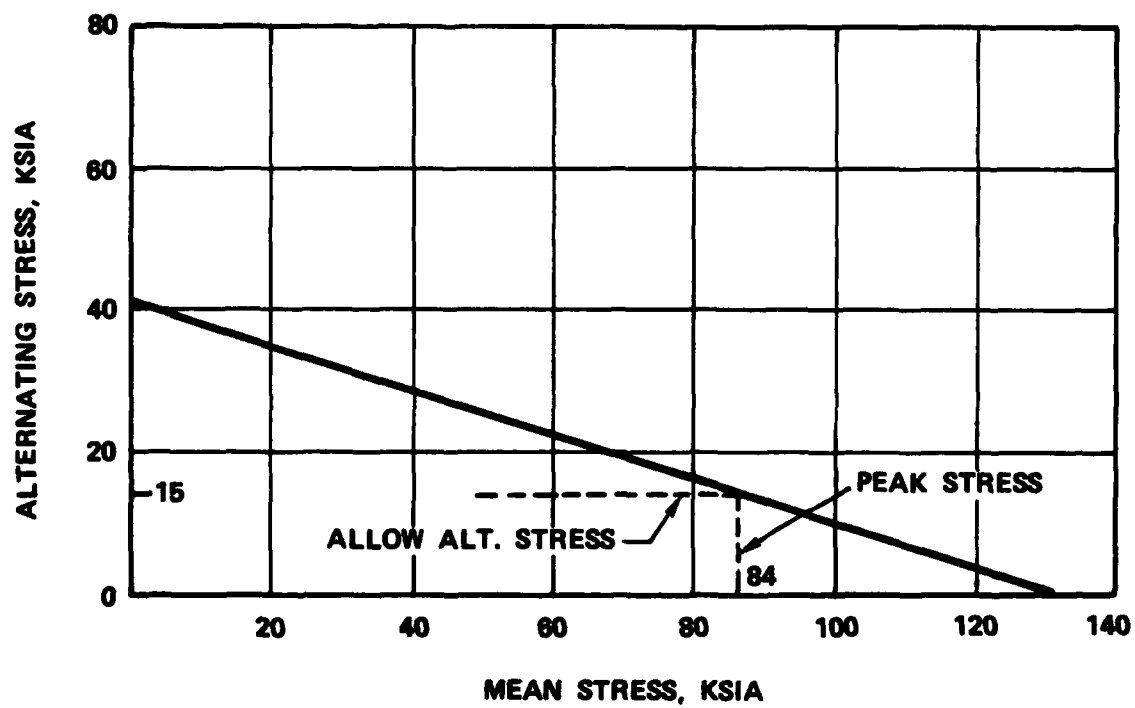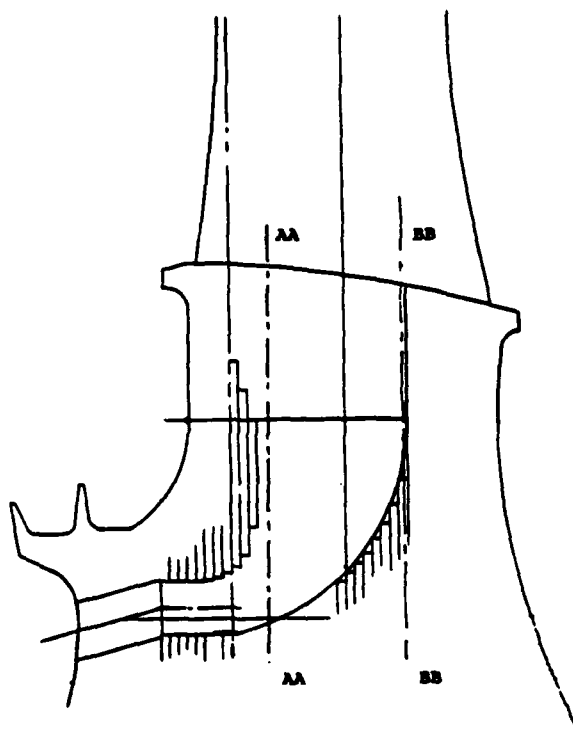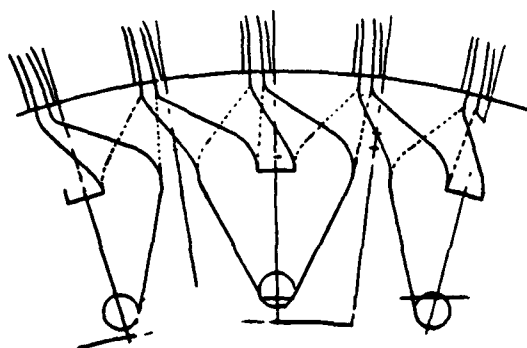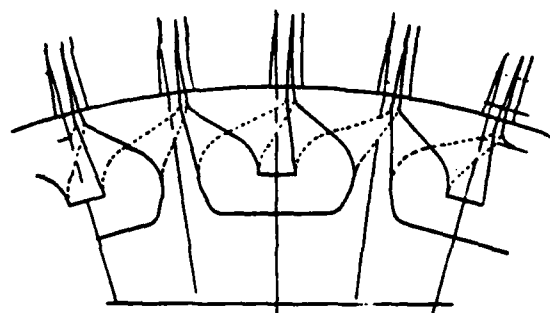**Figure 63. CME Blade Mode Shape - Mode 5.**

Figure 64. CME Blade - Goodman Diagram

103

(a) CME ROTOR DISC DESIGN COOLING PASSAGES.

(b) CME ROTOR DISC SECTION AA.

(c) CME ROTOR DISC SECTION BB.

Figure 65. Disk Design.

certain amount of useful redundancy in supplying the coolant to the blades. Airfoil loading is transferred smoothly to the forward and aft axisymmetric portions of the disk and then down to the lower hub region.

The entire blade and the central portion of the disk is fabricated from photo-etched Astroloy sheets of 0.015- and 0.020-inch thicknesses, with the latter predominating. Forward and aft of the laminated regions are end plates of Astroloy machined from forgings that will be separately bonded to the laminate stack. The forward cantilevered knife seal and coolant supply orifices are predominantly within the nonlaminated portion of the disk.

Thermal Analysis - Thermal and stress analyses of the turbine disk were accomplished at the maximum power design point. A two-dimensional thermal analysis of the disk was conducted using a model developed directly from the rotor finite-element stress model to ensure complete compatibility for thermal stress calculations.

Cooling flow has an assumed even distribution of radial flow throughout the disk internal cavity. Pipe flow correlations were used on the interior to determine the forced convection heat-transfer coefficients. In addition to forced convection, free convection due to rotational body forces on the fluid is substantial. The two effects have been superimposed upon one another and combined values of heat-transfer coefficients were predicted. In the extreme rim region, the additional heat-transfer surface area created by the complex laminate geometry has been accounted for with appropriate fin effectiveness applied. Cooling flow temperature rise due to solid body pumping was included.

The external heat-transfer coefficients for the rear of the disk were obtained from Program DSKFLO. Pipe flow correlations

were used for the bore and turbulent flat plate correlations were used on the platform. By eliminating the blade from the platform during thermal analysis, the predicted heat flow into the disk rim is at an upper bound, thus the thermal analysis should provide slightly conservative results.

On the disk, from the bore to the cantilevered seal knife edge, a relative velocity of $1/4 \ r_\omega$ was assumed, and $1/2 \ r_\omega$ was used from the knife edge up to the platform. The lower relative velocity between the bore and the knife accounts for an increase in the average masss tangential velocity due to the inducer injection of air into the cavity. A rotating disk correlation was used to determine the heat-transfer coefficients along the disk front.

Results of the steady-state thermal analysis are presented in Figure 66. Peak temperature at the rim is 1511°F and, due to the effective heat exchanger created by the rim geometry, there is a fairly steep gradient down to 1000°F at the cantilevered seal radius. The bulk average temperature of the disk is 960°F.

Stress Analysis and Structural Evaluation - The rotor two-dimensional stress analysis model is identical to the thermal model with the exception of the addition of elements that represent the airfoil. The airfoil elements were prescribed with appropriate thickness to accurately simulate the airfoil loading on the disk rim. An additional stress model with substantially more refinement in the step seal area was also made to study the stresses around that area in more detail. All stress analyses were accomplished using the two-dimensional elastic stress finite-element program ISOPDQ.

Results of the analysis include stress levels presented in Figures 67, 68, and 69 for maximum rotor speed (63,000 rpm) and uniform room-temperature conditions, and those presented in
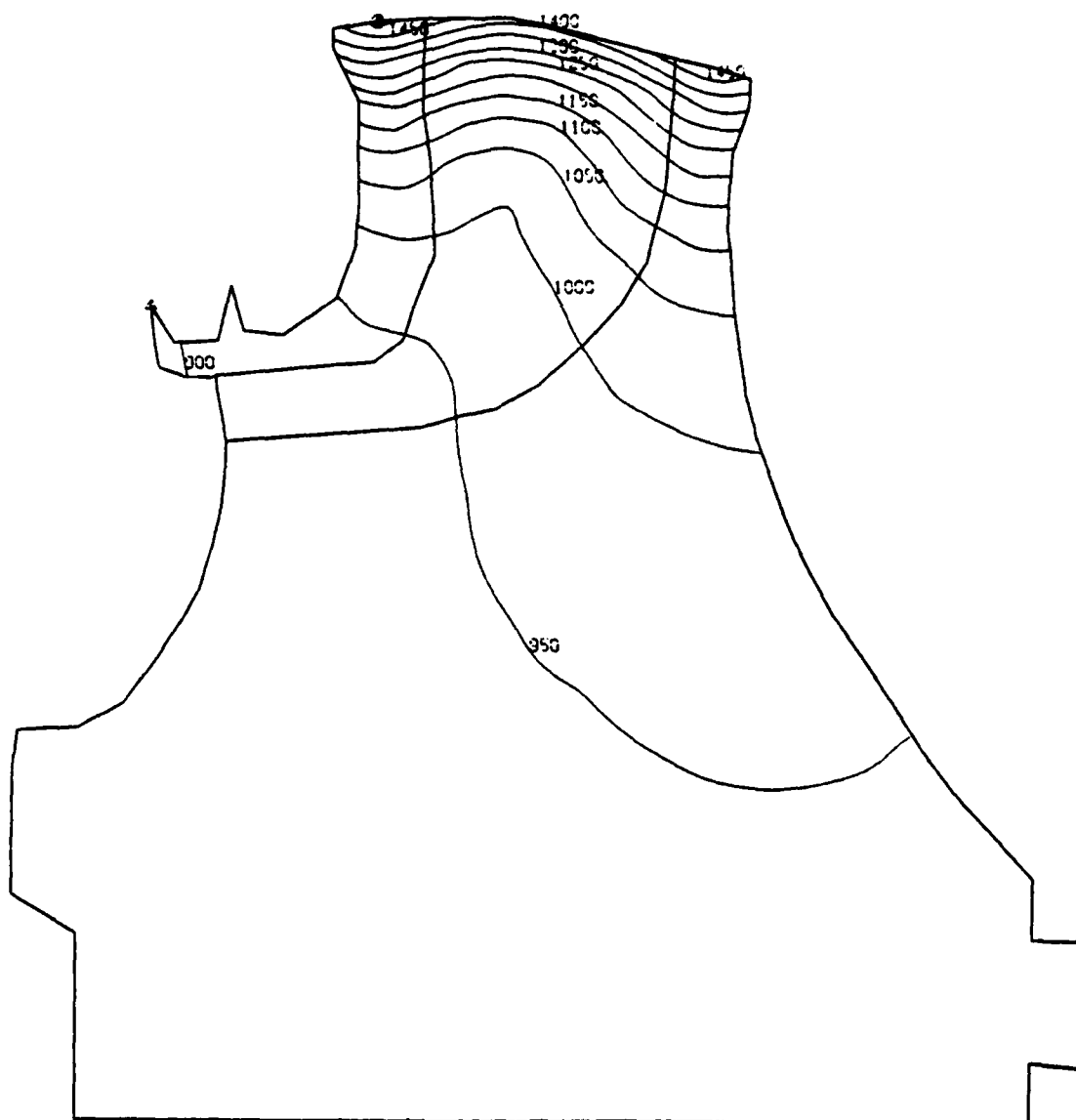
Figure 66. Temperature (°F) at Steady-State Maximum Power Condition.

SIGMA(E)

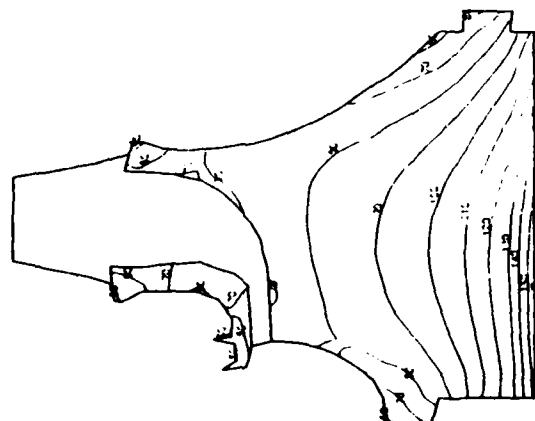Figure 69.

Rotor Effective Stresses,
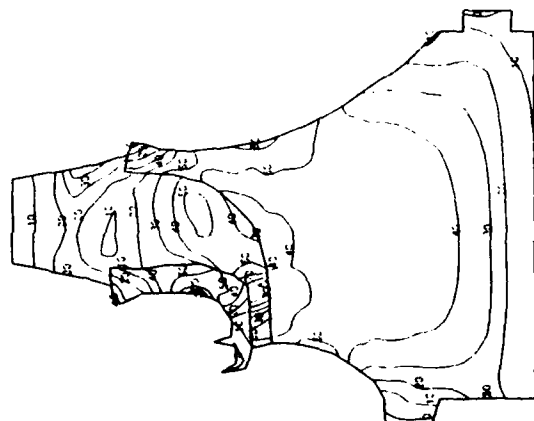KSI (Rotation Only).

SIGMA(R)

Figure 68.

Rotor Radial Stresses,
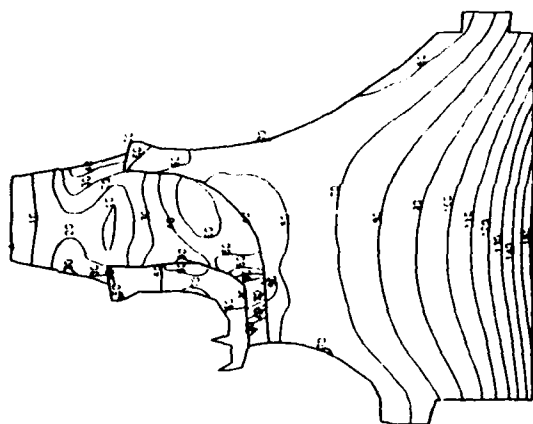KSI (Rotation Only).

SIGMA(T)

Figure 67.

Rotor Tangential Stresses,
KSI (Rotation Only).

108

Figures 70, 71, and 72 for the maximum power point. The areas of interest from this analysis are the cantilevered seal, the rim, and the peak stress region at the bore.

Special attention was given to the bending stresses caused by the cantilevered seal on the disk. A refined analysis did not indicate any stresses significantly higher in the seal and below the seal than those shown in Figures 69 and 72, which are effective stresses on the order of 60 ksi. These are well below levels that would be of concern if combined with the stress concentrating effect of the cooling-air inlet holes.

Stresses in the center of the web region between cooling passages are shown to be quite high at maximum power in Figure 72. The stress component is almost entirely radial and is split about evenly between rotational and thermally induced portions. Although the predicted value is below yield at the temperature in this region and is therefore not of great concern, subsequent to the analysis, design modifications to the web were made which thicken it and reduce the stress level. An estimated 20-percent reduction in radial stress has been made due to the thickness increase.

A significant result of the stress analysis work is the evaluation of disk tangential stresses as affected by the thermal gradient. The high metal temperatures at the outermost portion of the rim, along with the large cool mass below the cooling-air inlet hole, create the high compressive stresses shown at the rim. This is primarily a result of having very small amounts of hot axisymmetric material and is unlike stresses set up in a solid integral wheel with a similar temperature gradient. This can be seen by comparing tangential stresses at the bore as in Figures 67 and 70 which do not differ to any significant level as they might in a solid wheel. Another point to note is that the steepness of the gradient at the rim, resulting from highly
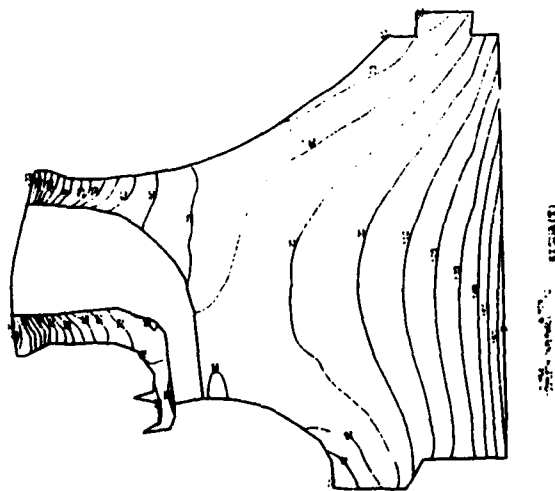
Figure 72.
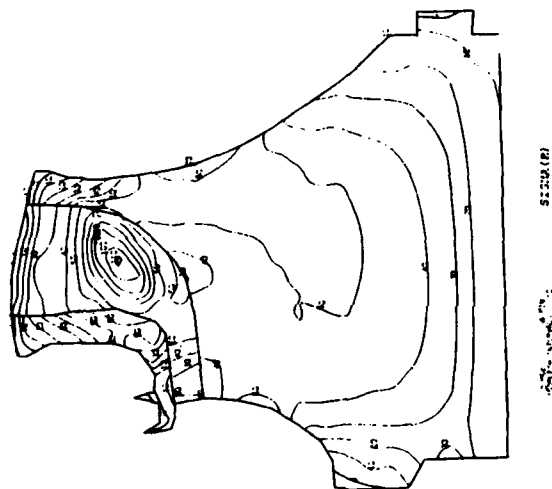Rotor Effective Stress
(KSI), with Temperatures
and Rotation.

Figure 71.
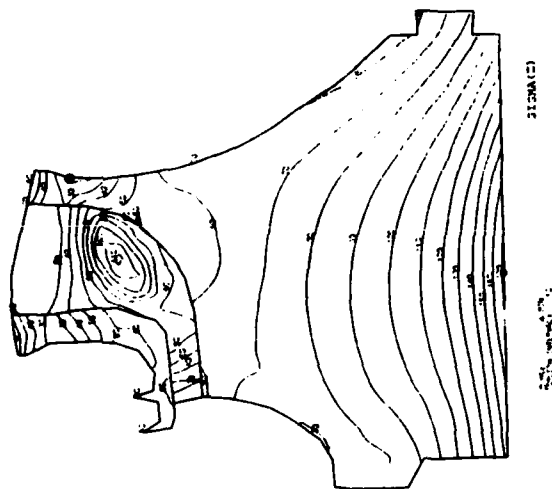Rotor Radial Stress (KSI),
with Temperatures and
Rotation.

Figure 70.
Rotor Tangential Stress
(KSI), with Temperatures and
Rotation.

110

effective cooling in this region, is less important than the maximum-to-minimum temperature difference in the wheel.

Although the effective stress at the rim remains positive in both cases run, Figures 69 and 72, the tangential component varies from a moderate positive value to a large negative value during an anticipated start to shutdown cycle. Since this rotor is intended for use in an expendable engine, where engine start cycle capability is not pertinent to the design evaluation, transient thermal stress analysis was not conducted. However, to illustrate conceptually the rim stress behavior during a cycle, Figure 73 was constructed showing the thermal and rotational component of the combined stress, which would have a 150 ksi range. With any significant stress concentration due to the airfoil cooling passages at the rim, a very limited low-cycle-fatigue capability would result.

At the bore of the turbine rotor, a peak elastic effective stress of 170 ksi is achieved at steady state during maximum power operating conditions. This stress level is quite common in high-performance rotors using forged alloys and would result in several thousand low-cycle-fatigue cycles if a detailed cyclic life analysis was performed.

The most pertinent method of evaluating the rotor disk design for this engine application is the prediction of rotor burst margin which is accomplished using the expression below.

$$BM = \sqrt{\frac{(B.F.)(U.T.S.)}{ATS}}$$

where   BM   = Burst margin expressed as a fractional margin over 100-percent design speed
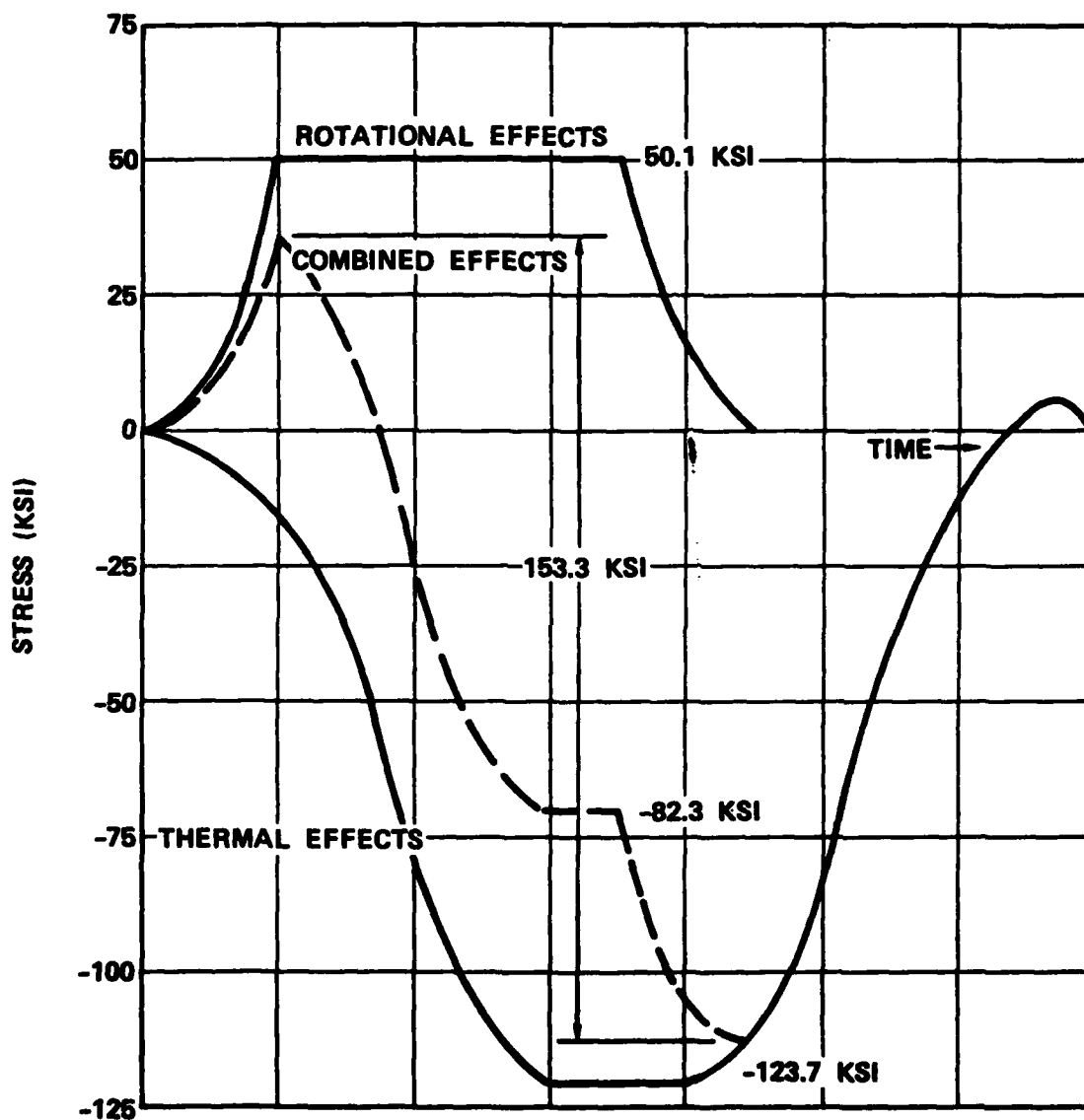
Figure 73. Conceptual Tangential Stress at the Disk Rim
During Startup and Shutdown.

BF   =   Burst factor or material utilization factor as a function of material and geometry. An empirical factor relating to load distribution in the structure

U.T.S.   =   Ultimate tensile strength of the alloy at the disk mass average temperature

ATS   =   Average tangential stress at 100-percent speed

A plot of burst margin against burst factor is presented in Figure 74 for this rotor. The anticipated burst factor and margin for this rotor are 0.80 and 1.18, respectively. A burst margin of greater than 1.15 is considered acceptable for an expendable engine.

PCM Tooling - The photochemical machining (PCM) tooling for the laminates was generated on a computer-graphics system which describes each Z-section or laminate interface using an X - Y digitized design system. The appropriate etch factors are applied to the laminate details and the coordinates are stored on magnetic tape for direct input to a Gerber Precision Plotter. The plotter accurately images each PCM tool on a photosensitive glass plate which becomes the tooling master. Mylar PCM tooling copies are made from the master for use in the photoetching process with the Astroloy sheet material. Figure 75 is a copy of laminate tool No. 21. Note the bonded wheel blank will be circular with no center bore initially and machining will be indexed from the two 0.250-inch diameter holes shown. This provides the maximum area in the disk region for ultrasonic inspection and mechanical property testing of the laminated rotor.
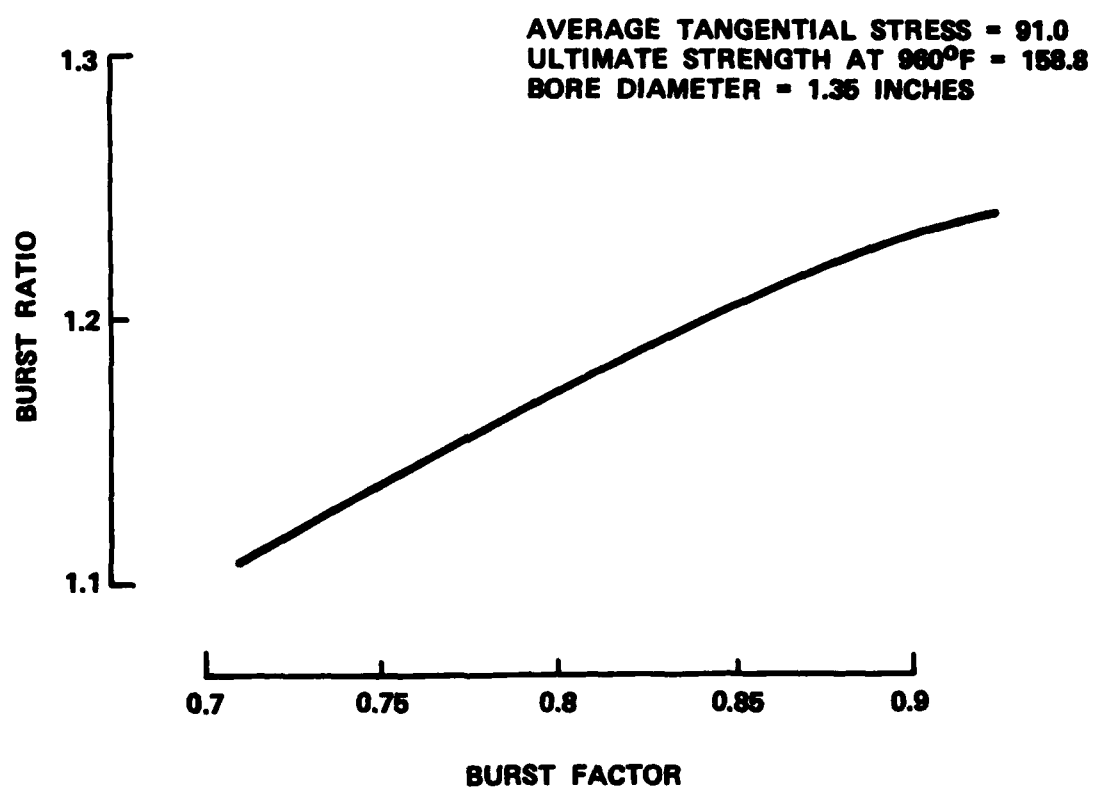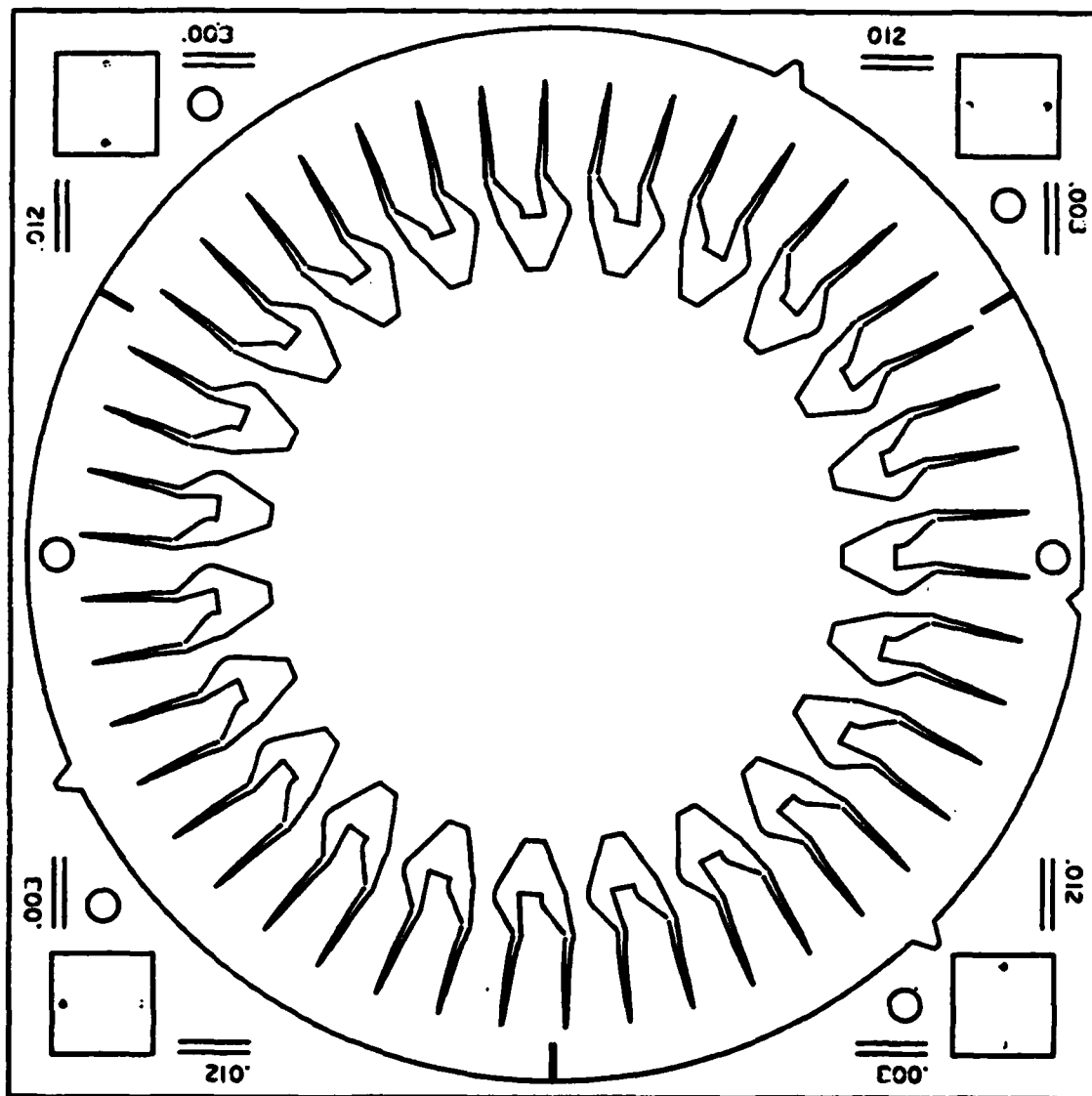
AVERAGE TANGENTIAL STRESS = 91.0
ULTIMATE STRENGTH AT 960°F = 158.8
BORE DIAMETER = 1.35 INCHES

Figure 74. CME Rotor Burst Ratio.

114

ENGR P/N 3552074-1
FILE NAME 58.2.3595.057.21.SHI.NC

DRN CULBERTSON 3-17-80
SCALE FULL   STK .020

3595057-21FS

Figure 75.   PCM Laminate Tool No. 21.

115

<u>Detail Assembly Drawing</u> - The small cruise-missile laminated turbine rotor detail assembly drawing is presented in Figure 76. The assembly identifies the individual laminates by number which will be manufactured using the PCM laminate process.

Figure 76. Small Cruise Missile Laminated Turbine Rotor Detail Assembly Drawing.
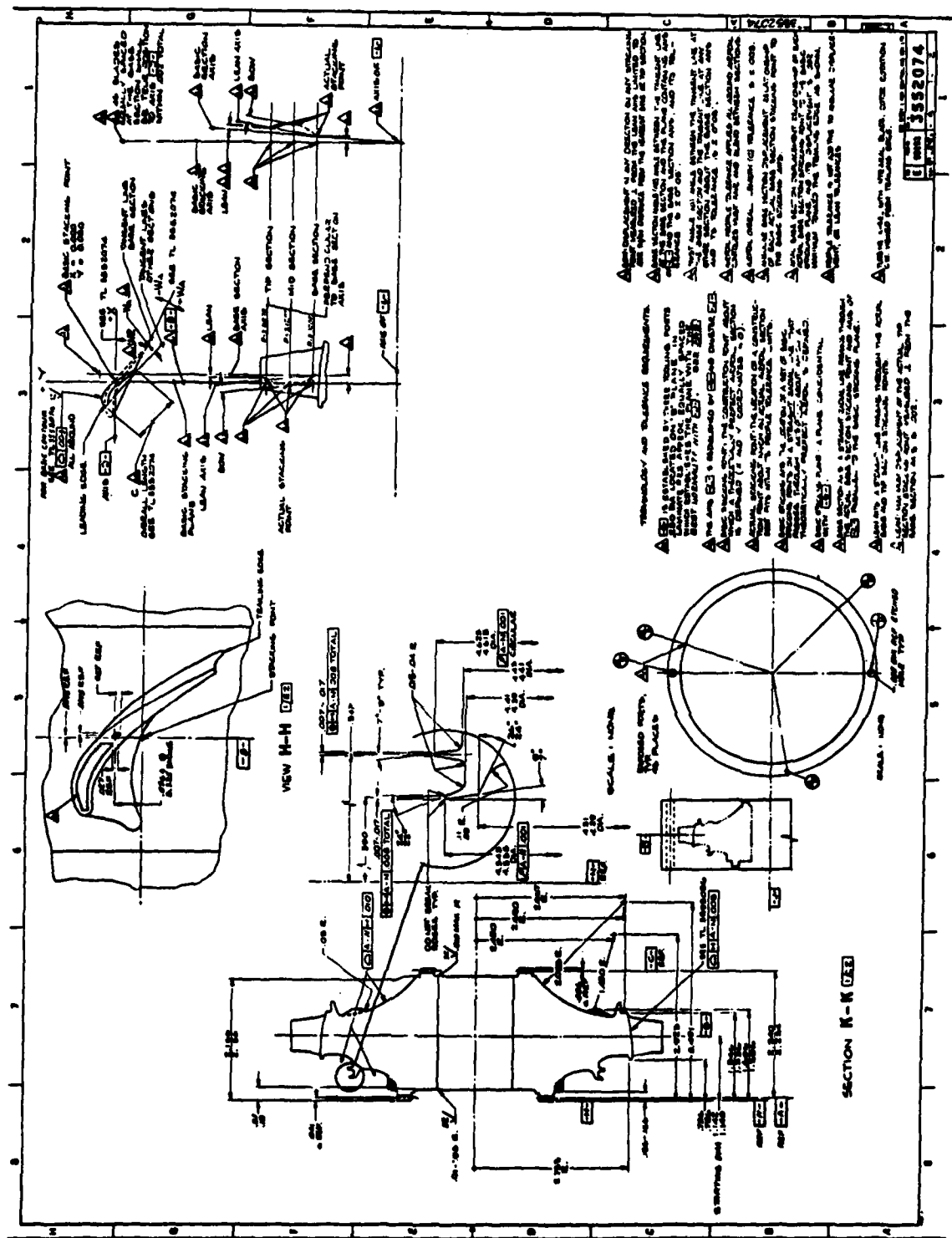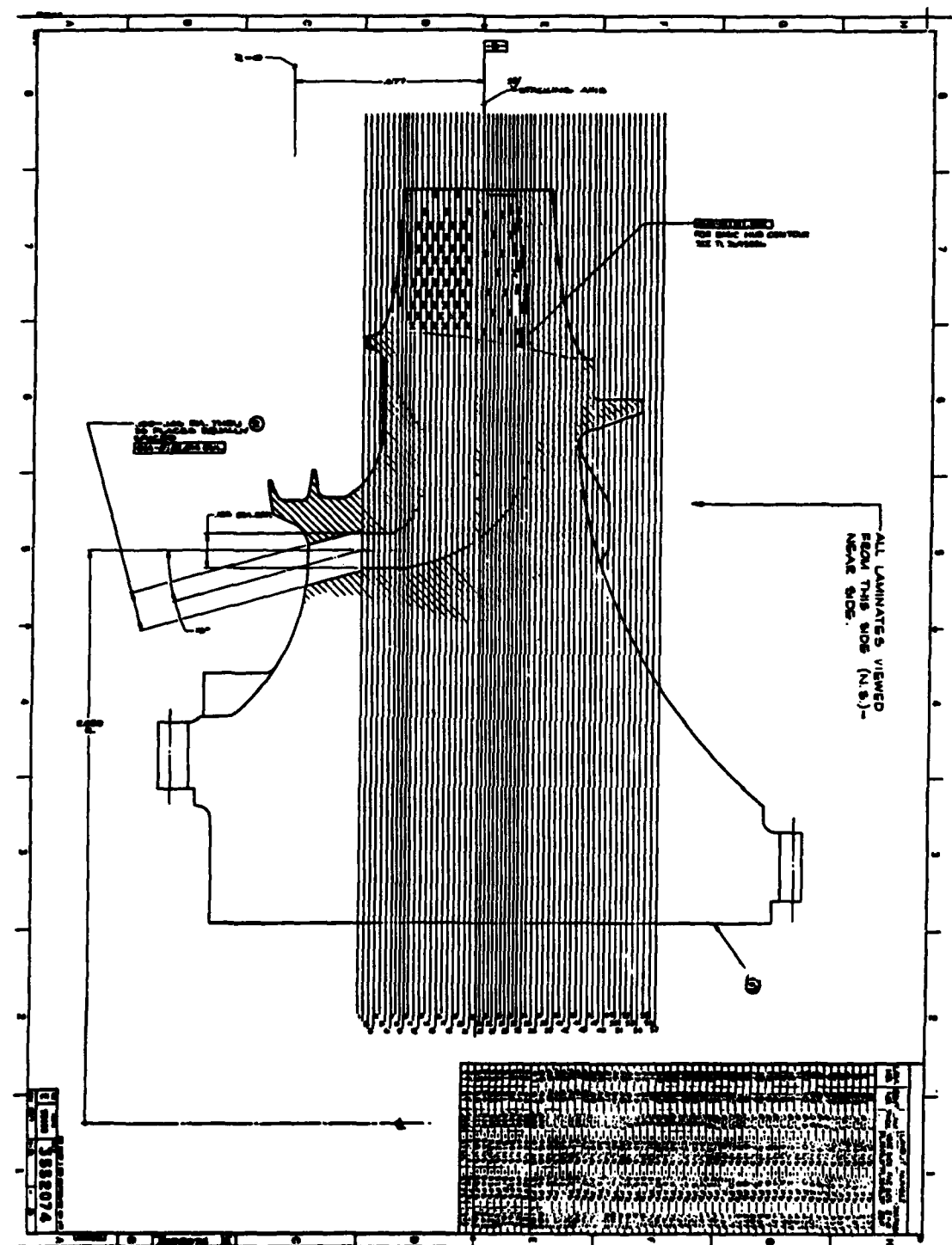
117

Figure 76. Small Cruise Missile Laminated Turbine Rotor Detail Assembly Drawing.

Figure 76. Small Cruise Missile Laminated Turbine
Rotor Detail Assembly Drawing.

CONCLUSION

The engine test demonstrated, in a propulsion engine environment, the mechanical integrity and durability of a small, integral, cooled, laminated, axial turbine. The accuracy and repeatability of the photoetch laminate process has been verified through the component tests performed and the measured heat-transfer performance of the turbine blade. The application of an advanced optical pyrometer system for blade metal temperature measurement has proven to be a simple and accurate development tool, which will see greater use in future test programs. Finally, the engine demonstration test has shown this unique, integral, rotor design approach to be particularly useful in applications such as cruise missiles where the benefits of the increased temperature capability, combined with the low-cost laminate manufacturing process, can be maximized.

A small, cooled, laminated rotor has been designed for cruise-missile application. This new turbine will be fabricated in the AFML Axial Laminated Fabrication Program. It is recommended that further testing be conducted on this advanced component including an aerodynamic performance test to establish the cooled and uncooled performance levels and a gas generator test to establish the durability at high temperature.

DATE
ILMED

8